FCTUC FACULDADE DE CIÊNCIAS E TECNOLOGIA
UNIVERSIDADE DE COIMBRA

DEPARTAMENTO DE ENGENHARIA MECÂNICA

Experimental Analysis of the Flow Over a 3D Ridge and the Fire Spreading Under Wind and Slope Conditions

Dissertation Presented for obtaining Master Degree in Mechanical Engineering in the specialty Energy and Environment

Author

Abdelrahman Wael Abdelwahab Abouali

Supervisor

Domingos Xavier Filomeno Carlos Viegas

Co-supervisor

Jorge Rafeal Nogueira Raposo

Jury

President	**Professor Doctor António Rui de Almeida Figueiredo** **Association Professor of University of Coimbra**
Members	**Professor Doctor Domingos Xavier Filomeno Carlos Viegas** **Full Professor of University of Coimbra**
	Professor Doctor Jorge Campos da Silva André **Assistant Professor of University of Coimbra**

Coimbra, September, 2016

To my loving parents…

“There are no limitations to the mind except those that we acknowledge.”

— Napoleon Hill

Acknowledgment

The research work presented on this master thesis has been carried out in the last six months at the Association for Development of Industrial Aerodynamics (ADAI), these six months boosted my technical skills and experience as it's the first time to do a research work for me, although it looks like a short period but it was the most inspiring and benefiting period in my engineering education time so far and it has contributed a lot to my personal development thanks to the wise guidance and support I had from my scientific advisor Professor Domingos Xavier Viegas which I wish to express a sincere gratitude to him for his trust, encouraging and freedom during my research that this work would never come out the same without them.

I would like also to thank ADAI chaired by Professor Domingos Xavier Viegas for their personal financial support to me on the last period of this research and the research financial support as an overall.

I am grateful to all ADAI team for their support and help to conduct the work done during this research and specially I am very thankful for Doctor Jorge Rafael Raposo for his support, encouraging and guidance with the laboratory techniques.

Finally, to my parents who are the main reason after god that I reached this point of my life and writing these words in the first place, to my brother, my friends and the beloved people in my life for their good wishes and encouraging.

Coimbra, September 2016

Resumo

São apresentados os resultados laboratoriais do estudo de investigação sobre a propagação do fogo na cumeada de uma colina 3D, com uma secção transversa triangular de altura decrescente sobre ação do vento.

Dois tipos de comportamento extremo do fogo foram observados nestas condições. O primeiro é o alargamento da frente de fogo, favorável ao declive da cumeada, que ocorre na face do sotavente da colina, imediatamente a seguir ao fogo passar a cumeada. O segundo fenómeno ocorre na face do barlavento da colina, em que o fogo sofre uma propagação lateral na direção descendente da colina, em casos de colinas com declives muito elevados ou com orientações do escoamento negativas em relação a esta.

O primeiro fenómeno resulta do efeito de um vórtice horizontal que se forma a jusante da cumeada e que direciona o escoamento na direção dos extremos laterais da colina. O segundo efeito é resultante escoamento imposto nessa direção.

Abstract

Results from a flow study and laboratory-scale investigation of a fire spreading over a 3D ridge have a triangular cross section and decreasing its height gradually under wind blowing condition. They show two fire extreme behaviors, one is a lateral spread happening on the leeward face just after the ridgeline in an up ridge direction only from the middle of the ridgeline and not to the other direction, this lateral rate of spread effected by the inclination of the ridge and the blowing wind velocity and direction. The other behavior is on the windward face where the fire spreads laterally to the down ridge direction in a case of high ridge inclinations or negative orientations. The lateral spread on the leeward face is happening as a result of a horizontal vortex takes place after the ridgeline and pushes the flow to the edges of the ridge, the lateral spread on the windward is a result of a flow draft happening on that direction.

Keywords

Extreme Fire Behavior, Fire Channelling, Lateral Fire Spread, Horizontal Vortices, Conical Vortices, 3D ridge

Index

Figures Index

1. Introduction

The wildfire behavior has been investigated by many researches on the past decade due to the increased events and accidents of the wildfire in many areas and countries around the world for reasons will not be discussed here since it's not the study concern, however, these accidents are causing many life and resources losses. Our concern here on this study is the extreme wildfire behavior, one of the common situations that making the fire behavior becomes extreme is when the fire across a complex topography with influence of a blowing wind where the fire starts to spread in directions other than the blowing wind direction and that's what makes it extreme. Many numerical and experimental studies was carried out to analyze the fire behavior on the complex topographies and one of these topographies are the ridges, previous studies on this topography showed that if we have a blowing wind perpendicular to a ridge, an extreme behavior will happen on the leeward face of the ridge where if we have a fire propagating on the windward face in a direction up slope and when the fire just cross the ridgeline it will start to spread laterally parallel it. This phenomenon is referred as the 'fire channelling', McRae (2004) who's first noticed it which he referred to as 'lee-slope channelling'. A previous experimental study by Raposo et al. (2015) has been conducted on a 2D ridge and it demonstrated that the interaction between the fire and the blowing wind over this complex terrain can give a rise to dynamic mechanisms that can enlarge a fire front near the top of the crest. However, the study on this work in a continuing to that study where the fire enlargement on the leeward face drove us the main motivation to study it aslo over a 3D ridge, which is a more complex topography than the 2D ridge.

On this study we are experiment the fire behavior over the 3D ridge on a laboratory scale with a blowing wind, this configuration is very common on the nature and it can be seen as the ends of any ridge where the slope is decreasing gradually between the ridge and the ground. Since the fire behavior over the ridge is a result of the interaction between the complex flow around the ridge and the fire, so an experimental and numerical simulation study of the flow around the ridge is carried out also to explain the fire behavior.

The main objectives of this work are addressed on the following points:

- Developing an automate methodology (program) to measure the rate of spread of the fire front from an infrared records taken during the experiments.
- Studying the fire behavior over the 3D ridge experimentally under wind condition with different parameters, namely: wind velocity, wind direction, inclination and ignition point.
- Studying the flow around the 3D ridge experimentally in a wind tunnel and through a CFD numerical simulation

The thesis structure will start with the developed program snice it's the main tool used in analyzing the fire tests, then the wind tunnel tests are presented to give us an understanding of the flow around the ridge followed by the CFD simulation to give us a visualize idea about the flow and deeper understanding and then finally the fire tests followed by a conclusion.

2. State of Art

Previous studies on the 2D ridge terrain showed that if we have a blowing wind perpendicular to the ridge, an extreme behavior will happen on the leeward face of the ridge where if we have a fire propagats on the windward face to up slope and just after the fire cross the ridgeline it will start to spread laterally parallel it. This phenomenon referred as 'fire channelling', McRae (2004) who's first noticed it which he referred to as 'lee-slope channelling'. Sharples et al. (2012) has previously determined that several environmental conditions are necessary for fire channelling, he determined that the leeward slope angle of the ridge should be greater than ~25° and the angle between the topographic aspect and synoptic wind direction should be within ~40° of each other, also the synoptic wind speed should be greater than, 25–30 km/h, which allows a flow separation in the lee of the ridge to take place.

A previous experimental study by Raposo et al. (2015) have been conducted on a 2D ridge model tested on a combustion wind tunnel and demonstrated that the interaction of the fire and the blowing wind over this complex terrain can give a rise to dynamic mechanisms that can enlarge a fire front near the top of the crest, the study showed that the lateral spread is happening from the middle of the ridgeline in two direction left and right, for the symmetry of the behavior in the two directions (right and the left) of the ridge, the study confirmed that there is an overall good symmetry conditions between the two of them.

For the flow over the ridges there is no a lot of studies unfortunately for the 3D ridge but we do have for the 2D ridge configuration. In a study of by Schlichting (1968) showed that the flow will develop along the windward face as a turbulent boundary layer with increasing in the velocity from the bottom to its top. At the ridgeline, depending on the radius of curvature, the Reynolds number of the flow and its turbulent intensity the flow may separate forming a horizontal axis vortex (cylindrical) and reattaching downslope on the leeward face. The average shape and extension of this separation zone is very much dependent on the incident flow properties and the ridge geometry. If the radius of curvature of the ridge is very small, we are in the presence of a sharp ridge, like in the case of a bluff body. In this configuration, flow separation will certainly occur, because the flow velocity at the edge of a convex dihedral becomes very large and the flow will not be able to overcome the pressure increase that occurs after the ridgeline, causing separation regardless of the Reynolds number. However, in the nature these situations are common, so we took into consideration in our study here this condition in order to avoid dependence on flow Reynolds number and to minimize scale effects (Meroney 1990).

The complex flow produced around two-dimensional hills immersed in a turbulent boundary layer has been studied by Ferreira et al. (1995), among others. Even in the simple cases of sinusoidal or triangular cross-sections, the flow topology in the absence of fire is not simple and there is not a uniquely defined reference velocity to characterize this flow. In numerical or experimental studies in which the imposed flow is either uniform or has a well-defined boundary layer profile, it is quite easy to define a

characteristic flow or wind velocity, but this is not the case in full-scale situations for which other parameters may be required to characterize the flow.

Simpson et al. (2013) demonstrated that the lateral spread results are owed to the interaction between the fire's plume and the horizontal vorticity due to flow separation near the top of the ridge. This interaction generates vertical vorticity on the fire's flanks, which in turn generates a lateral flow in the immediate lee of the ridge. For this reason, this phenomenon is appropriately designated by Simpson et al. (2013) as 'vorticity driven lateral spread'. The physical process associated with the lateral enlargement of the fire and the fast spread of the fire across the leeward slope can be explained partially by the analysis of the vorticity balance of the flow near the ridgeline. The turbulent boundary-layer flow over the windward face of the hill accumulates vorticity vy that gives rise to a large recirculation vortex after flow separation at the ridge. This separated vortex contributes to enhancing convective heat transfer in the upslope direction on the lee side of the ridge, intensifying the rate of combustion. The ascending flow produced by the fire generates vertical vorticity vz, as well as longitudinal vorticity vx parallel to the wind direction. These two vorticity components combine to produce a net pyrogenic vorticity vp, which acts to drive the rapid lateral fire spread.

3. A Developed program for measuring the rate of spread (ROS)

Measuring the rate of the spread (ROS) of a fire spreading in a prescribed direction is the main key in analyzing the behavior of this fire, either the fire is for experimental purposes (laboratory scale) or a real wildfire, usually it's required also to analyze the spreading of the fire along many directions to understand the differences in the fire behavior between these directions, however, we developed a new automated method (program) that satisfying the following requirements:

- Automated, to reduce the human errors as much as possible during the process and to make it fast.
- Accurate and reliable, giving the user the ability to get the ROS along any direction or generally between any two points fire have passed by them.

To satisfy these requirements a program has been made using the MATLAB® software and its toolbox Computer Vision Toolbox®, which is one of the MATLAB ® toolboxes. The main program tasks are addressed in order on the following:

- Calibrating the camera to create a 3D scene realizing the position of the camera and the surfaces where the fire is propagating.
- Create an X-Y plane using the camera calibration on the surface where the fire is propagating to measure the real distances being passed by the fire form the taken images of the fire
- Open the taken images (frames) of the fire propagation and ask the user to detect where is the fire front by drawing small segments of lines manually over the image.
- Building a net of lines either parallel to each other or with angle between them forming half a circle according the user choice or the nature of the fire propagation, then, finding the intersection between these lines and the lines forming the fire front on each frame, the ROS will be calculated along these lines as we will see how later. However, this step can be skipped if the user chooses to draw the lines manually. See Fig 3-3
- Calculating the ROS along the lines and give the user the ability to choose an output as shown on sec. 3.3.

3.1. The calibration process

It is the main process on the program to perform all the other calculations and functions, there is a built in function in the MATLAB® doing this calibration. However, the calibration is made using a printed checkboard pattern on a board (see Fig 3-1) and the process starts by taking about 20 image of it while it's being placed in different random locations in the space around the fire surface where we need to calculate the ROS, these

locations must include a location where the checkboard is placed adjusted to the fire surface. The program apply an algorithm to these images to estimates the camera parameters by detecting the corners of the checkboard squares that its size was already given to the program, one of these camera parameters is the extrinsic parameters which are the 3D rotation of the camera and its translation relatively to the checkboard for each location the board has pictured on it, briefly this rotation and translation is to make the camera perpendicular to the plane where the board is located, after that, by using the extrinsic parameters for image where the checkboard was on the fire it becomes possible to realize for each pixel on the image its location on the real axis (X,Y). The algorithm generally is more complicated; we have addressed only a short brief about how it's working here and for more information please check the MATLAB® help about these MATLAB functions:

"generateCheckerboardPoints", "estimateCameraParameters" and "detectCheckerboardPoints"

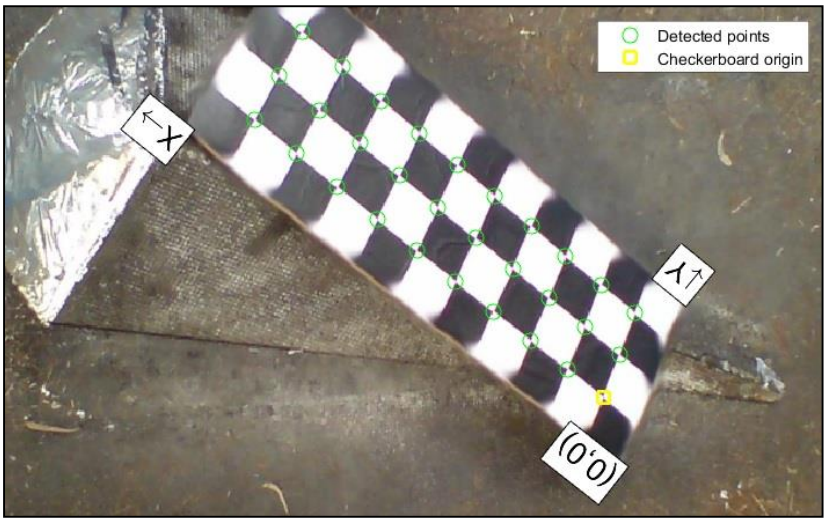

Fig 3-1 Image taken during one of the performed tests on this work and it shows the checkboard used on the calibration, also it shows the program detection of the square corners

3.2. The fire Rate of spread calculation

The ROS can be calculated by the program as an average ROS or dynamic ROS along a predefined direction by the user. For the average ROS, it was defined according to Viegas 2006 where the ROS was estimated as the slope of a linear fitted line on a plot of the passed distances (D) by the fire versus the times consumed to pass them (t), we are aware that in some cases the fire spread is not steady but we assumed that the ROS is constant along the spread direction following also Viegas 2006. For the dynamic ROS, the ROS was defined with the same method of the slope but the line is fitted between each two following points on the D-t plot where it's representing the average ROS that the fire translated with between the two time steps (frames), using this option the user can define the ROS dynamically with time along the direction and as much frames will be considered as much the user will have a more described ROS along the direction.

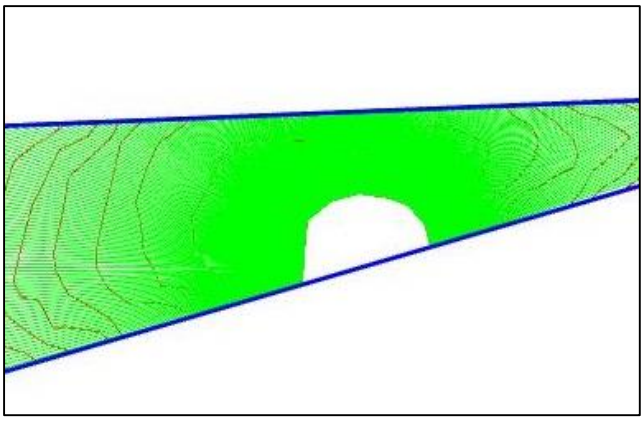

Fig 3-3 A 300 lines net where the ROS will be calculated through these lines and on this case it has a circular distribution

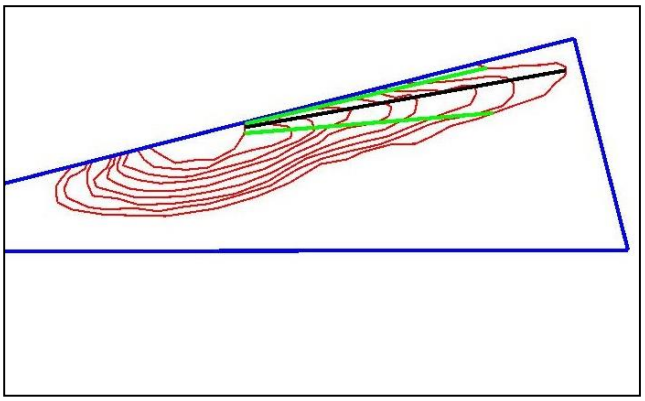

Fig 3-2 An example of the area where the average ROS where calculated defined by the green lines, on the image is from 0 to 10 degree and the black line is the maximum on this area

3.3. Program inputs and outputs

Inputs

- The fire images or the frames taken during the fire evolution.
- The calibration images (must be more than 10 images) and the size of the checkboard squares.
- The time laps between the frames.
- The size and the shape of the fuel bed
- The number of lines in case the user wants to build the lines net.
- The location of the fire front on each frame.

Outputs

The program allows the user to choose between the following outputs:

- The average ROS by one of the following methods:
  - The area between two angles, this option is in a case of building circular distribution lines net where the angles are measured in a CCW direction, the program takes the mean of the average ROS values of the lines having an angle between these two angles. See Fig 3-2
  - The area between two lines the user draws them, this option is in case of building a lines net either parallel or circular, the program takes the mean of the average ROS values of the lines lying between these two lines.
  - Along one line only drawn manually by the user.
- The dynamic ROS, the user can get it along a line prescribed by one of the following methods:
  - By determining a line of the lines net through its rank
  - By drawing a line manually on the propagation map of the fire front or one of the fire images.

- Measuring distances, where the user can measure a distance between any two points either on the fire images or the propagation map.
- The propagation map of the fire front, which is the fire front line on each frame representing the evolution of the fire. See Fig 3-5
- A 3D representation of the dynamic ROS values and its X-Y location on the fuel bed an iso-surface, so the user can visualize how the fire spreading behavior over the whole domain area. (Fig 3-4)
- All the values (ROS's, distances …) that were calculated during the program run will be saved on an excel sheet automatically and also saving figures showing the locations where the ROS either dynamic or average have been calculated on both the propagation map and the fire image.

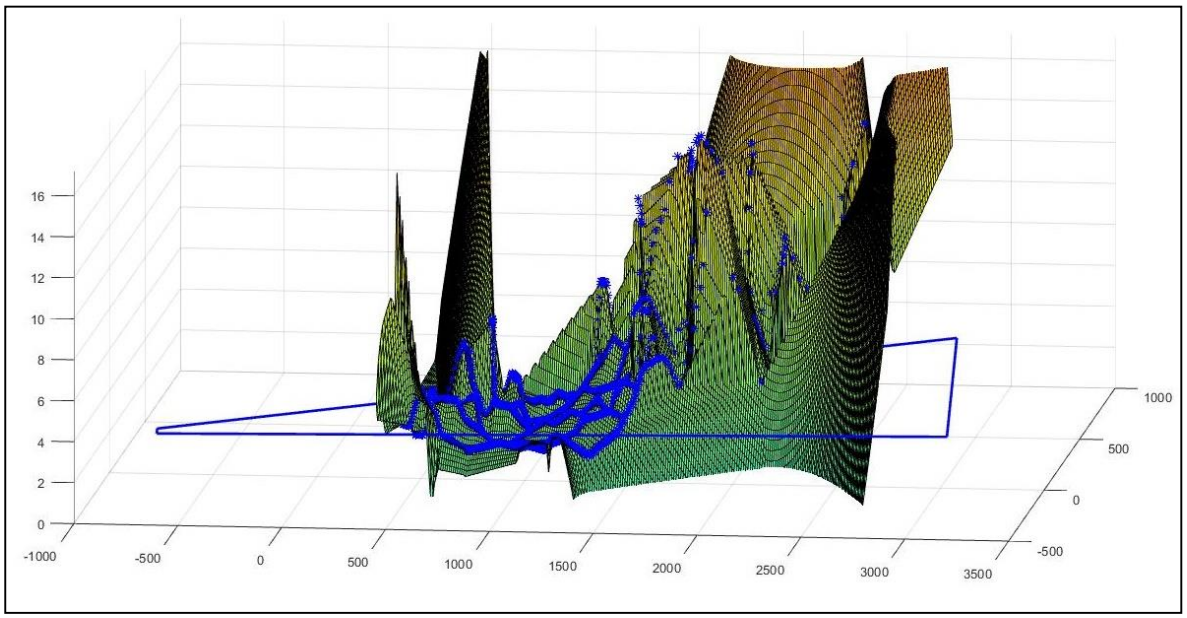

Fig 3-4 the iso surface ROS values representation with their X-Y position on the fuel bed

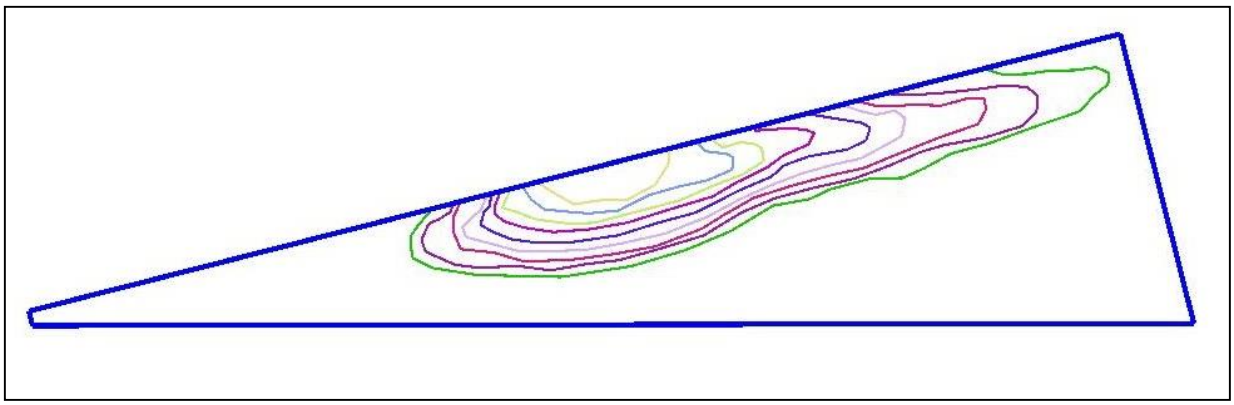

Fig 3-5 the propagation map of the fire front for one of the tests performed on this work and the iso surface shown above is for the same test

3.4. Program Validation

To validate the program, a manual method was considered to calculate the ROS of the fire and calculating the same ROS by the program during one of the performed tests on this work, the idea was to measure the time taken by the fire to pass an already marked distances on the fuel bed that we know, to mark the distances we used freezed wool strings to make it viewable on the infrared image, the strings ware distributed on the leeward face of the triangle ridge forming 5 distances, see Fig 3-6 showing the distance between the strings, its position of the fuel bed and their indexes, the inclination of the ridge was 35-deg and the wind was perpendicular to the ridgeline with a velocity of 2 m/s.

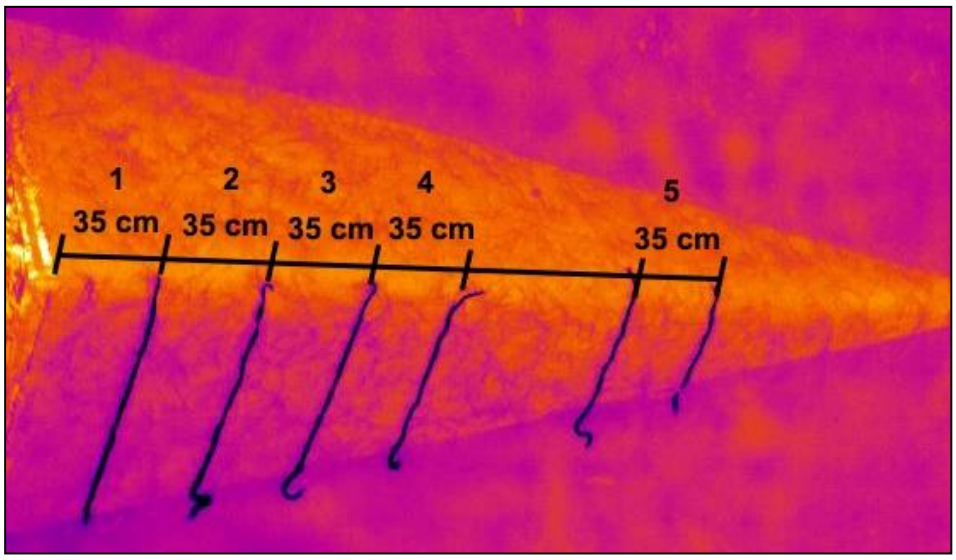

Fig 3-6 infrared image of the ridge and the strings are shown placed on the leeward face, we can see the five distances between the strings and their index

The behavior of the fire on this test was already known where the fire ignition was on the middle of the windward face and the fire will start to propagate up slope, after the fire will cross the ridgeline from its middle between distance 4 and 5 it will start to propagate latterly in a direction parallel to the ridgeline left and right where it will cross the strings. We have faced difficulties on detecting manually (by eye) when exactly the fire front will cross the string to take the time lap, this detection of coarse is much more accurate by using the infrared images, as a result, by comparing the time taken manually to pass some distance and the time form the infrared video to pass the same distance we found a big difference. However, we considered only comparing the distances between the strings calculated by the program and the correct values that we know already. Since the detection of the string position on the image by the program is made manually so we considered 5 different measures for each distance and on the following table we are presenting the error we had on each distance:

Distance index	1	2	3	4	5
Error (%)	1.7	8.5	8.7	2.0	2.9

The average error of these errors is **4.8 %**, this error is a combination of three errors: the calibration errors, manual detection of the string position by the program and the position of the strings on the fuel bed itself since we couldn't fix the string on an exact location due to the nature of the steel structure and the fuel. However, another measurement ware taken also which is the length of the ridgeline, on the following table the errors of five measurements were taken for this length by the program:

measure index	1	2	3	4	5
Error (%)	1.6	1.9	0.9	0.9	0.7

Form this we have an average error of **1.2%**, indeed this error is also combined error between the calibration errors and the manual detection of the bed edges. another measures also were taken for the width of the bed and the average error was **4.8%**.

To conclude, the program gives good results since the errors are relatively low and from the above results we can consider an error margin not exceeding **5%** as the maximum error we can get on any of the program results.

4. Wind Tunnel Tests

As we mentioned before that in order to understand the fire behavior over this terrain configuration we have to understand first the aerodynamics over this configuration and for this purpose we carried out a group of tests in the wind tunnel of (LAI) "Laboratório de Aerodynamica Industrial", the wind tunnel have a working section of 5m length by 5m width and 3m height, for testing, wooden models with smooth surface have been prepared and it has the same design of the models that will be used on the fire tests later but it's only down sized by 1:4 ratio to fit in the working section of the tunnel, so it's size will be 1 m for the ridgeline length by 0.25m for the width, see Fig 4-1, the model was fixed inside the working section where its center is always at 2.4 m distance from the wind entrance section (Fig 4-2), The considered parameters (Fig 4-5) on the tests are:

- Wind velocity (U): 2, 5 and 7 m/s
- Inclination of the ridge (α): 25, 35 and 45 degrees
- Orientation of the ridge or wind direction (φ): -20, -10, 0, 10 and 20 degrees, the angles are measured as the zero is when the ridgeline is perpendicular to the wind direction, the minus direction is by tilting the model on CW direction and the positive is the CCW direction

A combination of these parameters was made to form thirteen tests addressed in the following table:

Test Ref.	Wind speed (U) (m/s)	Inclination (α)	Orientation (φ)
3D1	7	45	0
3D2	5		
3D3	2		
3D4	7	25	
3D5	5		
3D6	2		
3D7	7	35	
3D8	5		
3D9	2		
3D10	5	35	20
3D11	5		10
3D12	5		-20
3D13	5		-10

Table. Wind Tunnel Tests and Their Parameters

4.1. Testing Methodology

The followed methodology to study the flow around this body (configuration) is to measure one of the basic quantities of the flow which is the pressure on the surface of the body, to measure this pressure the common method of static tubes was followed. On this method a slender, flexible, plastic tube used to obtain the pressure at a point on the surface, this tube is aligned parallel to the incoming flow to minimize disturbance to the flow, the pressure is measured by several tappings made on the same radial plane downstream of the geometry to avoid the effect of local pressure gradients. A total number of 38 tapping are distributed along four lines over the model, the location of the lines and the tappings on one face is shown on the following figure (Fig 4-1) mentioning that the distribution is identical on the leeward and windward faces. Preparing the tappings and the tubes have been made according to the LAI experience on these kind of tests and also considering the instructions of "Springer Handbook of Experimental Fluid Mechanics". The four lines will be mentioned during the discussion by their rank, starting from the 1st line it has 14 points along the two faces, then the 2nd line has 10 points, then the 3rd line has 8 points and finally the 4th line has 6 points. The points indexes numbering along each line is on the wind direction always, so the first point is on the windward face on the bottom and the last point is also the last point near the ground but on the leeward face.

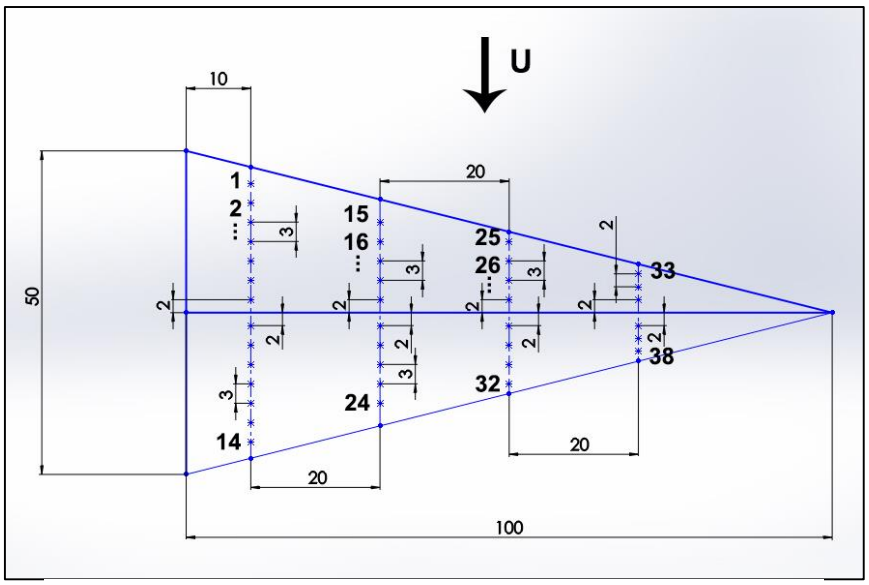

Fig 4-1 Distribution of the tapping's locations on the ridge faces

For simplicity during the discussions on this work, a number of directions will be agreed on to be mentioned with these names: for the direction where we are heading toward the leg of the triangle will be called up ridge and the opposite direction as we are heading toward the sharp angle of the triangle will be down ridge. Also we have an up slope direction where it's from the bottom of the model and heading toward the ridgeline and the opposite direction will be down slope. Also two points will be clarified, the ridge tip and the ridge top corner where the tip is at the sharp angle of the triangle and the top corner is at the 90-deg angel. See Fig 4-3.

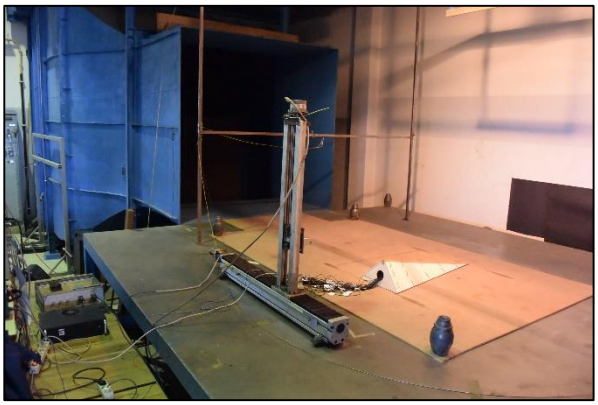

Fig 4-2 Fig. Image showing the installation of the model in wind tunnel

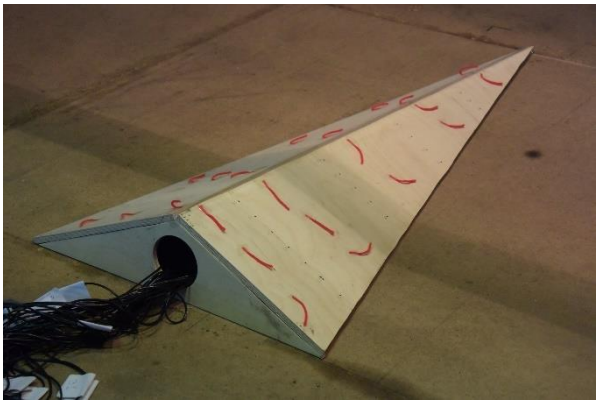

Fig 4-3 Image showing a close up look to the model where we can see the four lines of the points

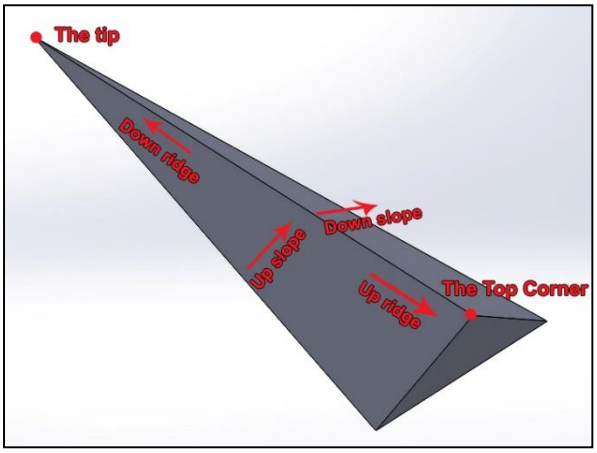

Fig 4-4 The used directions during the discussions

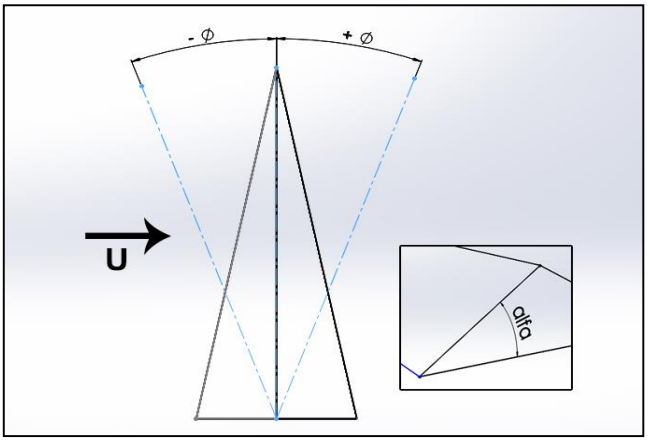

Fig 4-5 Angles of the ridge and the wind direction

The equipment used to measure the pressure on these tappings are: a program made by "Test Point" software, a pressure transducer and a Scanivalve, this equipment and the method are the same that used on the common practice by LAI researchers. The Scanivalve sated to scan each tube for a period of 30 seconds to get the average readings that will be measured by the pressure transducer from that tube during this period, by taking this average we avoid misreadings. To ensure a correct connection and true reading of the tubes a pry-test trials have been carried out.

The readings that being obtained by the measurement system are the pressure on the point minus the free stream pressure, however, to make these results capable to be compared to each other a dimensionless form have been used which is the pressure coefficient C_p as known on the common practice.

$$C_p = \frac{(P - P_\infty)}{\frac{1}{2}\,\rho\, {U_\infty}^2}$$

Where:

U_∞: free stream velocity ρ: air density

P: the point pressure P_∞: free stream pressure

Now we can see that the result given by the program is the numerator on of the pressure coefficient relation. The wind velocity has been measured by a pitot tube attached at the center of the wind entrance section, the two pressures of the pitot tube are measured by the Scanivalve also by connecting plastic tubes between it and the Scanivalve, so the static and total pressures of the pitot tube are being measured in the beginning of each test then we can calculate the wind velocity from this relation:

$$U = \sqrt{\frac{2(P_t - P_s)}{\rho}}$$

Where:

U: wind velocity ρ: air density

P_s: Static pressure P_t: Total pressure

The air density considered to be constant on all the tests and has a value of: **1.2 kg/m^3**

A study of the Reynolds number has been made to compare the Reynold number between the wind tunnel tests and the fire tests later since the used model has different size and the tested velocities are different also.

$$R = \frac{V * h}{\nu}$$

Where:

V: wind velocity h: characteristic height

ν: kinematic viscosity

The Reynolds number for the wind tunnel tests is in average **57400** and for the fire tests the Reynolds number is in average **90560,** these have calculated considering the characteristic height as the highest point on the model and the velocity is 5 m/s for the wind tunnel tests as average (we have 2, 5 and 7 m/s) and 2 m/s for the fire tests as an average also (we have 1, 2 and 3 m/s), the kinematic viscosity was constant for 300 k temperature.

4.2. Results and discussion

We have tested our model with three different velocities for each of the three inclinations to demonstrate that the pressure coefficient results are independent of the wind velocity, on the following figure (Fig 4-6) a representation of the 2nd line results for the three inclinations (25, 35 and 45 degrees) with three different wind velocities which is 2, 5 and 7 m/s:

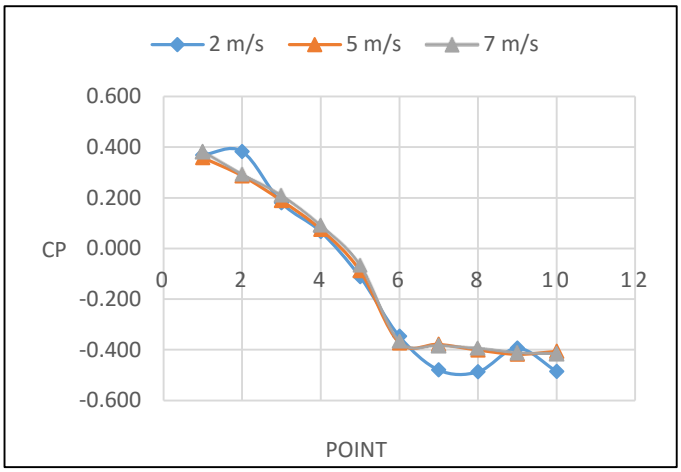

a. 25-deg inclination

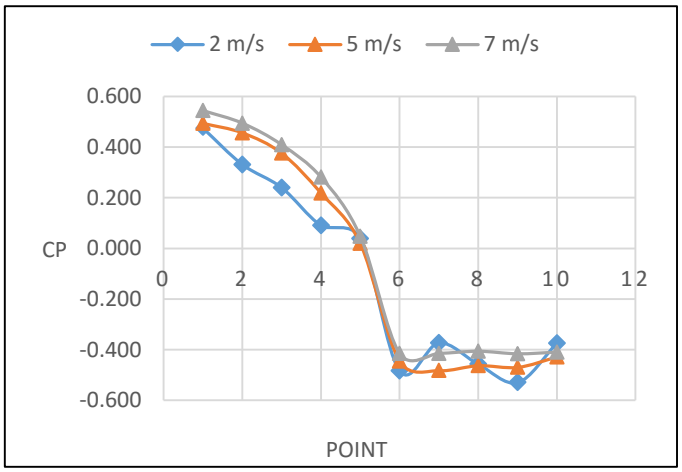

b. 35-deg inclination

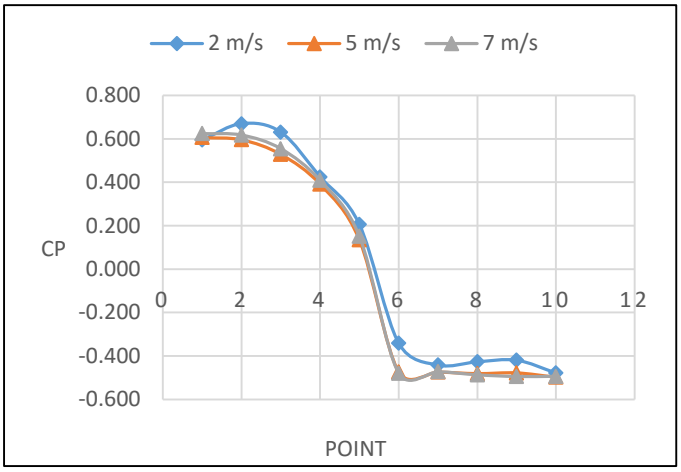

c. 45-deg inclination

Fig 4-6 Comparison between different velocities results on the second line points for different inclinations

From Fig 4-6 we can see that for 2m/s wind velocity we don't have a match between its values and the 5 and 7 m/s velocities where both of them are giving the same almost the values except a small difference on the leeward face for 35-deg inclination. We can study the match in the results between 5 and 7 m/s by dividing the results of 7 by the 5 m/s we will find a match by 102% for 45-deg inclination, 97.8% for 35-deg and 97.5% for 25-deg which give us an overall match between the two results of **99.2%.** However, this result is expected since we know from the common practice on this tunnel that the velocities lower than 5 m/s is not valid usually (don't give a velocity independent Cp results) because of the sizing effect and the Reynold numbers. As a result, we will consider the results of 5 m/s velocity on the following discussions.

4.2.1. The Inclination Effect

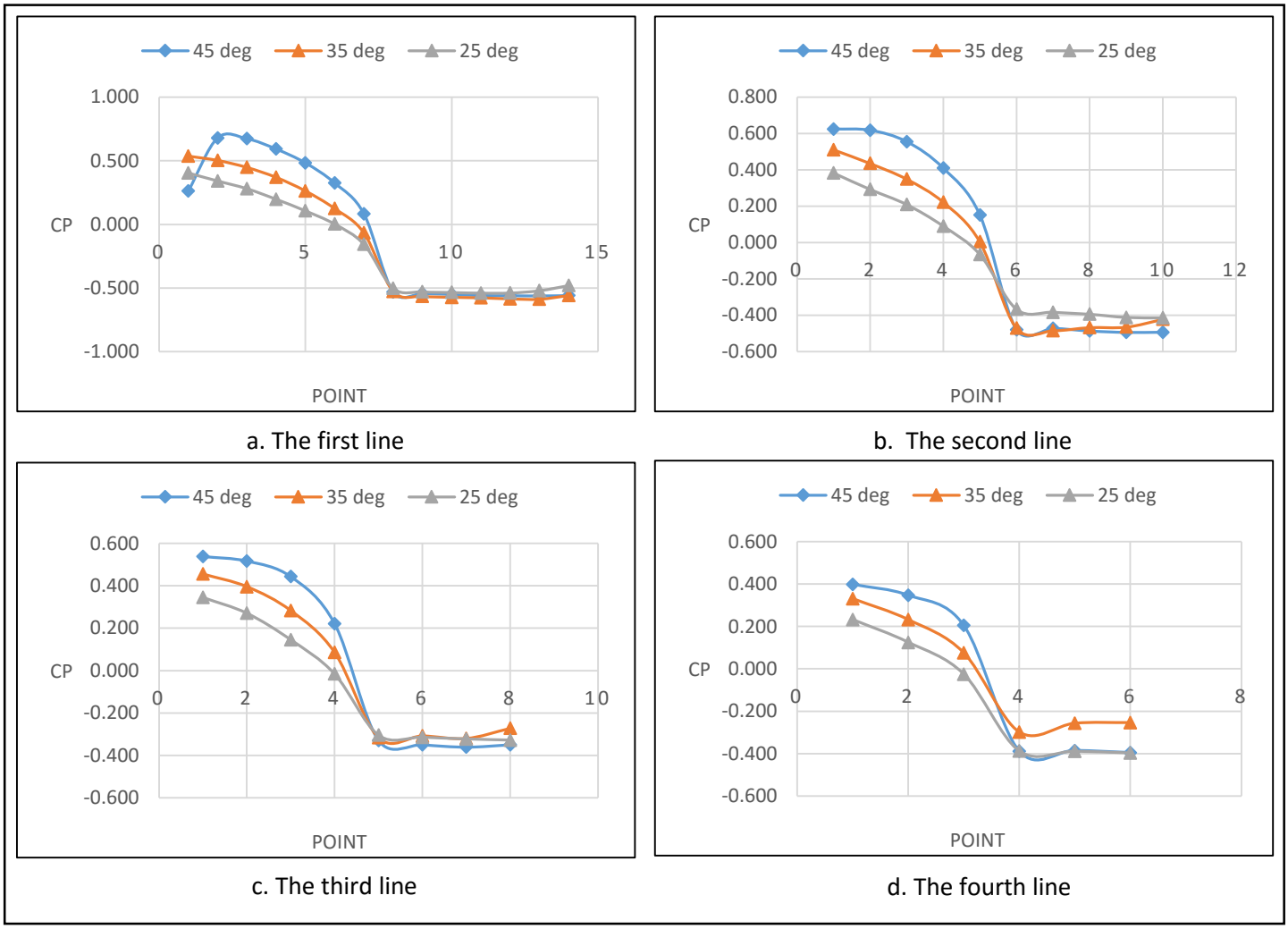

a. The first line

b. The second line

c. The third line

d. The fourth line

Fig 4-9 comparison between the different inclinations results for the four lines with velocity 5 m/s

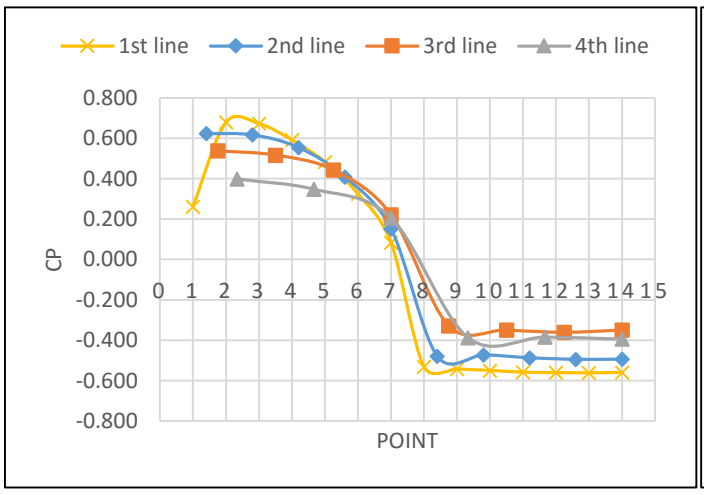

Fig 4-7 The four lines for 45-deg inclination

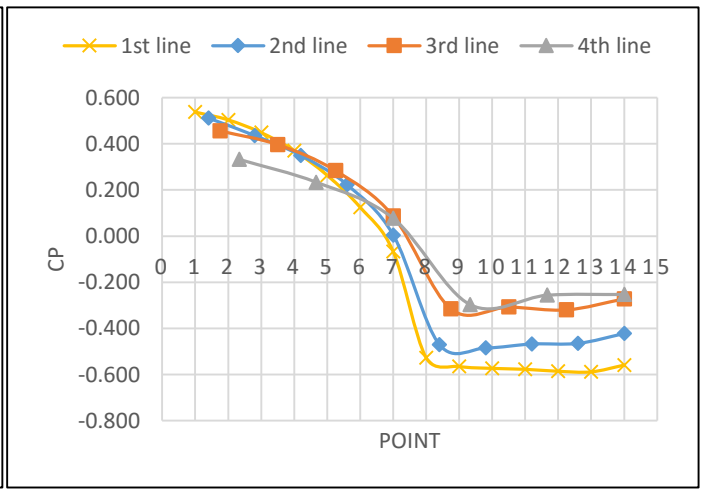

Fig 4-8 The four lines for 35-deg inclination

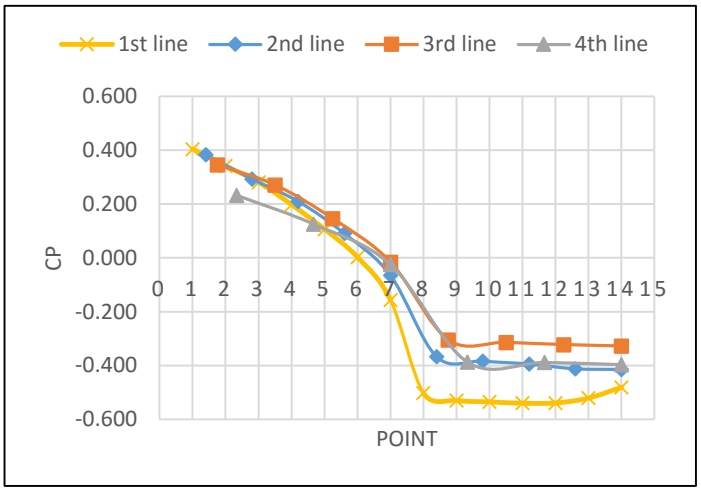

Fig 4-10 The four lines for 25 deg. inclination

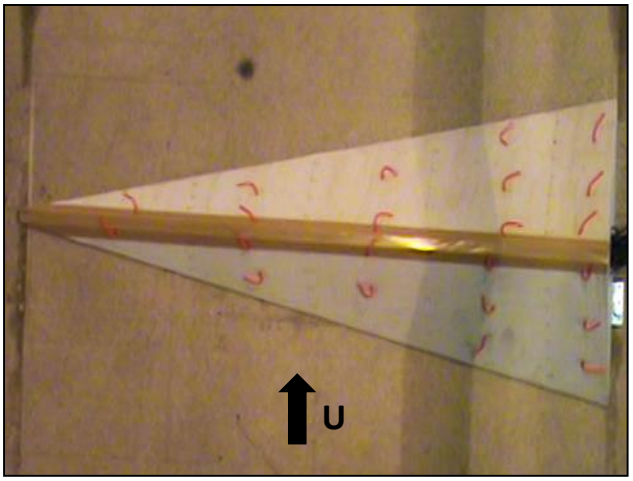

Fig 4-13 flow visualization for 45-deg inclination

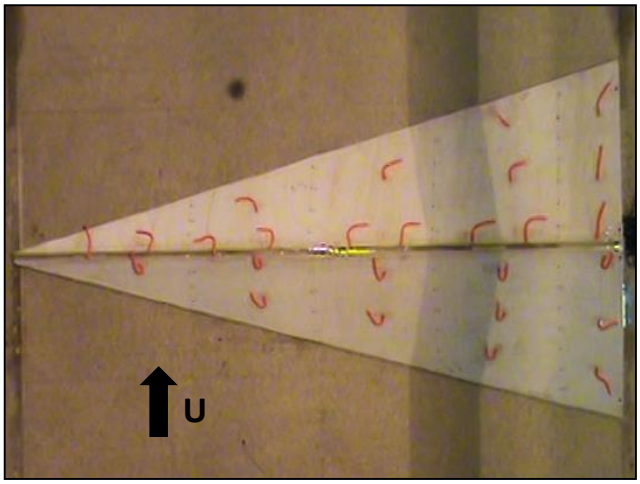

Fig 4-12 flow visualization for 35 deg. inclination

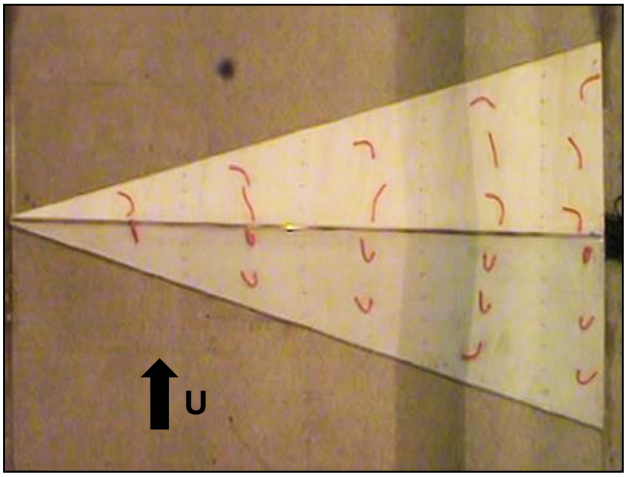

Fig 4-11 flow visualization for 25 deg. inclination

From Fig 4-8 and Fig 4-9 we can see that we have almost an identical flow behavior for the four lines where we have a positive pressure coefficient on the windward face which and a negative pressure coefficient on the leeward face which is an indicator of a circulation zone on the leeward face. For the velocity of the flow we can see that the lowest velocity is at the first point of each line where it's near the ground on the windward face and then the velocity starts to increase along the face until it reaches the ridgeline, then the flow gets caught on the leeward circulation where it gives almost a constant negative pressure value for the points on each line on the leeward face.

In a comparison between the three inclinations we find that as we increase the inclination the flow has lower velocity over the windward face but for the leeward face we have almost matched values except for the fourth line where there is a small difference between the three inclinations.

For the four lines on each inclination we can find a comparison between them on Fig 4-7, Fig 4-8 and Fig 4-10 , we can notice that at the beginning of the face where the flow will start accelerates up slope we have the highest velocity at the first line and decreasing until the fourth line, as we go farther up slope and before the ridgeline we can see that the highest velocity is for the fourth line and decreasing to the first line, so the behavior is getting reversed comparing the velocity along the four lines in the beginning and the end of the windward face.

For the leeward face we can see as mentioned before that we have constant negative values along each line, but in a comparison between the lines we find that the fourth line has the lowest pressure coefficient always on the three inclinations, then the value increase on the up ridge direction until we reach the first line, this flow behavior with a consideration of the existence of the circulation zone and also the slope of the ridge we can deduce that there is a conical vortex happening on the leeward wake. The conical vortices are existing on many configurations but the most famous cases are the delta wing and the roof tops when flow attacks it with oblique angle, a study by H. Kawai (1996) on characteristics of the conical vortices on a flat roof in oblique flow shows that by analyzing the pressure coefficients that the pressure coefficient is proportional to the diameter of the vortex, that's confirming the existence of the conical vortex on our configuration, the 3D ridge.

About the flow visualization we can see on Fig 4-13, Fig 4-12 and Fig 4-11 that the strings on the windward face is positioned toward up slope direction which is an expected behavior, but for the leeward face, generally, there is a strong turbulence zone since the strings was fluctuating a lot and even changing the direction some times which is a behavior has been noticed on the three inclinations. An important behavior also is noticeable on the line of strings attached on the leeward face just after the ridgeline directly, if we divided this line from the middle of the ridgeline to two halves we will find the strings on the upper ridge half is directed almost parallel to the ridgeline and toward up ridge, the other half is directed parallel to the ridgeline also but toward down ridge, see Fig 4-12, this behavior is seen clear on the 45 and 35 degree inclination but not very strong on the 25 degree, we have increased the number of the strings on the 35 degree to make more clear visualization of it as we see on Fig 4-12, these strings demonstrating that there is a strong flow draft on these two directions after the ridgeline. This behavior of the flow will be discussed again on the fire tests section and will see its effect on the fire propagation where it's the reason of the extreme fire behavior (the fire channelling).

4.2.2. The Orientation Effect

To study the effect of changing the wind direction relatively to the ridgeline a comparison has been made between the pressure coefficient results of the four bed orientations, we have -20, -10, 10 and 20 degrees adding to them the basic orientation (0 degrees) where the ridge is not tilted and it's perpendicular to the wind direction, on the following figures we will find this comparison for the four lines:

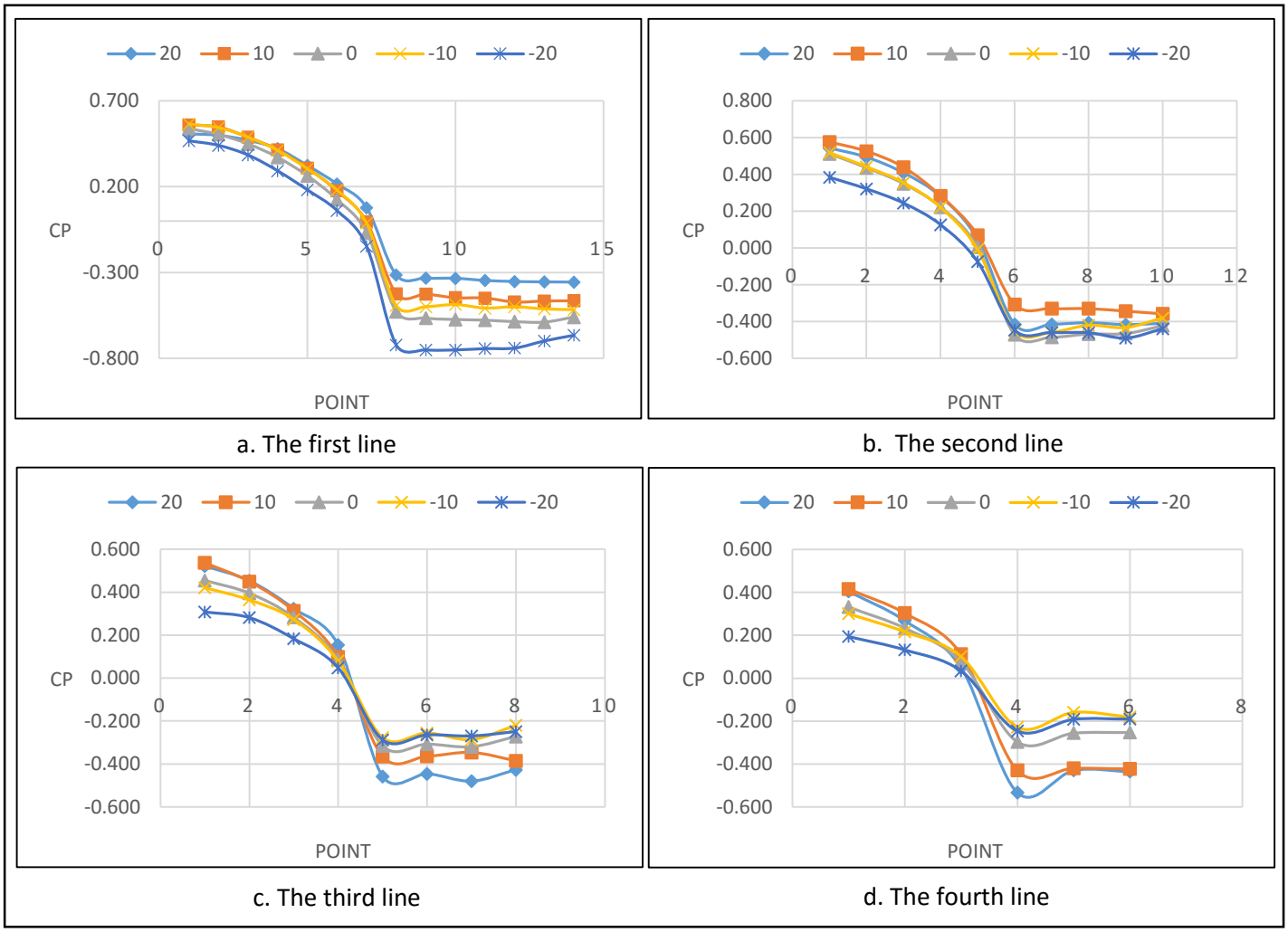

Fig 4-14 comparison between the different orientation results for the four lines with velocity 5 m/s and 35-deg inclination

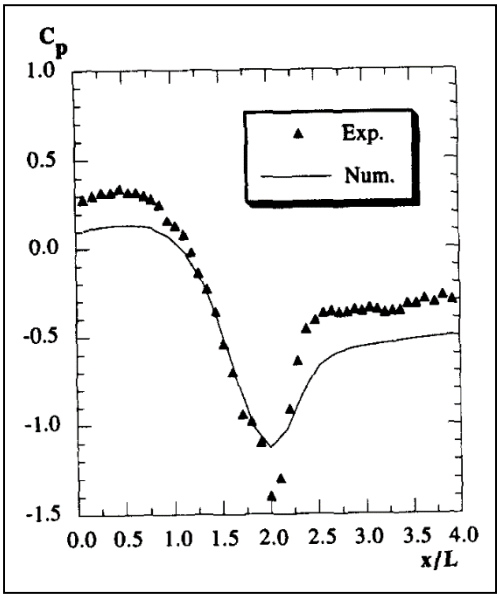

Fig 4-15 Pressure coefficient results from a study by Ferreira AD (1995) on a 2D ridge with sinusoidal cross section

From Fig 4-14 as an overall we can notice small differences on the flow behavior on the windward face between the lines with the different orientations, but by analyzing these differences we can find along the first line that the pressure is almost the same and as we go down ridge line after line we can notice a slight difference is appearing, so by looking to the third and fourth lines we find for the positive orientations (10 and 20 degrees) that their pressure coefficients is higher than the not-tilted ridge coefficients (0 degrees), while the pressure coefficients of the negative orientations (-10 and -20 degrees) are getting lower than the not-tilted ridge values. This behavior means the velocity magnitude along these line is higher on the negative orientations and lower on the positive ones. Also the net velocity component direction is getting change when tilting the ridge near these third and fourth lines.

However, by studying the flow directions from Fig 4-16 we can see for the windward face with the negative orientations the strings that on the down ridge part near the fourth line are directed a little toward down ridge parallel to the ridgeline where it is perpendicular to it toward up slope direction on the no-tilting case (Fig 4-12), it's noticeable also for -20 degree orientation specifically this change in direction is bigger than the -10 degree and not only the strings that on the down ridge part but it's almost all the strings on the windward face, so we can deduce that as we increase the angle of orientation on the negative direction (CW) the net velocity component will change to be more parallel to the ridgeline toward down ridge. On the same matter, for the positive orientations we can see that the velocity component is perpendicular to the ridgeline as the no-tilted case and even for the 20-deg (Fig 4-16-d) we will find the component is tilted to the other direction, up ridge, a little. About these velocity component direction change on the down ridge part of the windward face, we could also find the same behavior on the not tilted ridge with 45-degree inclination (Fig 4-13) where the strings are also tilted a little to be more parallel to the ridgeline and generally as we decrease the inclination of the ridge this velocity component direction will get beck to be perpendicular to the ridgeline. If we connected this visualization results to the results of the pressure coefficients that being deduced before from Fig 4-14 we can find that not only the flow changes its velocity component directing but it also increases its magnitude by tilting the ridge on the negative direction and decrease on the positive direction.

To conclude, this behavior of the velocity component direction change is mainly because the combined effect of the two slopes: the ridgeline slope and the face slope, as known the flow is taking the path where it will dissipate less energy, so the wind here has the tendency to slip on the windward face toward down ridge direction, this tendency increase if we tilted the bed on the negative direction and decrease on the positive direction even it disappears on the 20 degrees, also as we increase the inclination of the ridge the flow increases this tendency to slid on the windward face as it dissipate less energy than going up slope. This behavior will be mentioned on the rest of the work as the **"sliding wind"** on the windward face.

For the flow on the leeward face we can find form Fig 4-14 a change on the conical vortex intensity as the pressure changes, these changes are not easy to be interpreted from the wind tunnel tests so it will be discussed on the CFD simulation section. However, from (Fig 4-16) we can see the flow draft after the ridgeline is still exist on all the orientations.

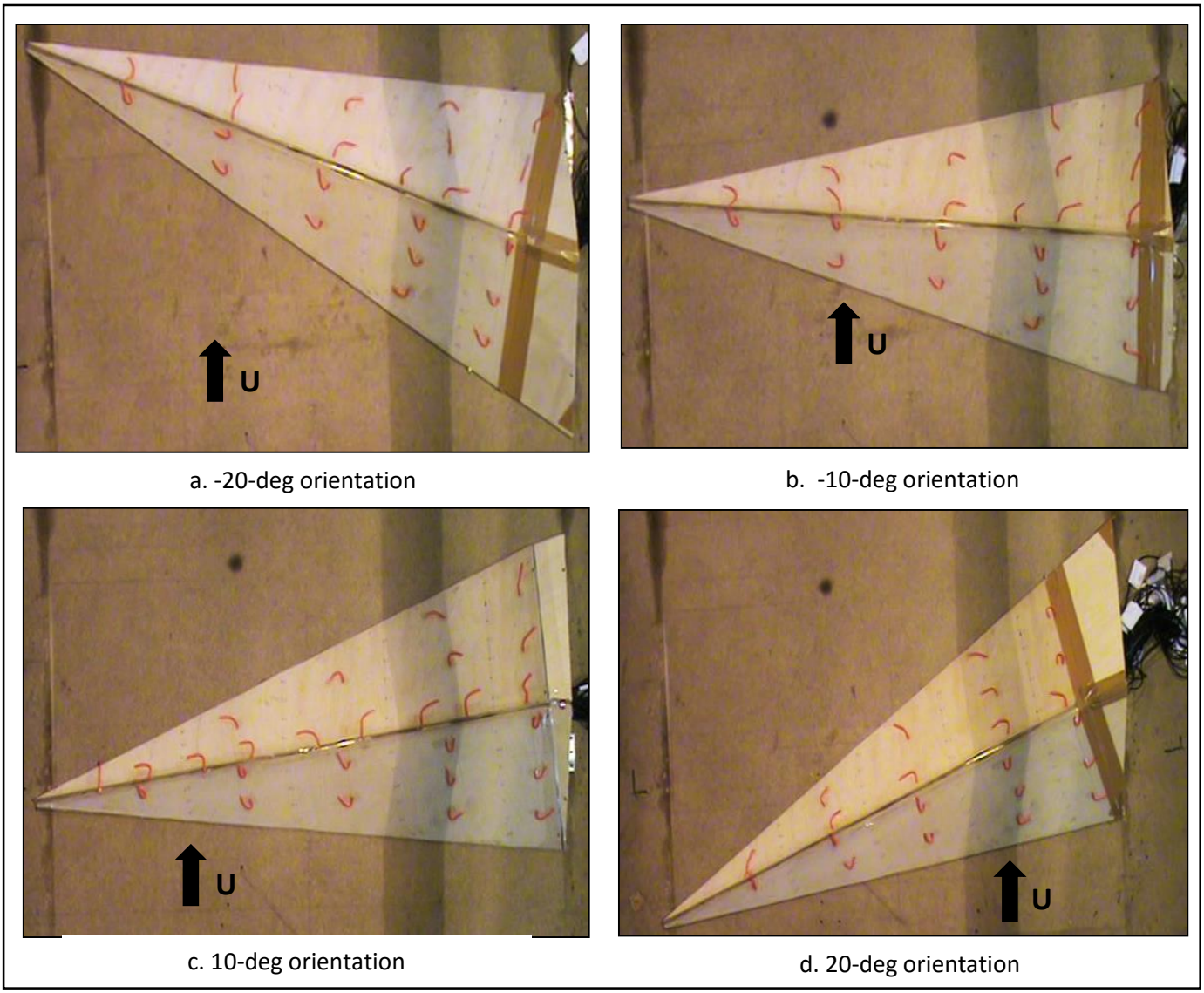

a. -20-deg orientation

b. -10-deg orientation

c. 10-deg orientation

d. 20-deg orientation

Fig 4-16 flow visualization for the different orientation results for the four lines with velocity 5 m/s and 35-deg inclination

Fig 4-17 flow visualization for different tests for the 2D ridge ware conducted on the same wind tunnel

A behavior was noticed also on the flow draft that exist just after the ridgeline and parallel to it where this draft is not very strong in the middle of the ridgeline where it will start while it get stronger as we approach more the edges of the ridge from both sides, the behavior wasn't noticed only on the 3D ridge, but it was also noticed in some wind tunnel tests were conducted by the same authors on the simple 2D ridge with the same used test characteristics on the 3D ridge, we can see a flow visualization on Fig 4-17 showing this behavior and also for the 3D ridge we can see it on Fig 4-12, on the static images of the strings shown here the behavior sometimes is not very clear but with a video camera we can see the fluctuations of the strings are less and they more directed parallel to the ridgeline as we approach the edge of the ridge.

A study by Ferreira AD (1995) on a 2D ridge with sinusoidal cross section shows that the area just after the ridgeline is having a relatively low pressure as we can see on Fig 4-15, the study is including wind tunnel tests and simulation, both of them showed the same result. However, on the CFD numerical simulation that will be discussed on the next section showed also a low pressure area

4.3. Conclusion

The flow around the triangle ridge is a complex flow especially on the leeward face, however we can conclude the flow behavior on the following points:

- Starting with the windward face we can find the flow accelerates as we are heading up slope along all the face, with different inclinations in an overall the wind velocity is higher as we lower the inclination of the ridge.
- The flow on the leeward face has a circulation zone generally and we deduced that there is a conical vortex generated form the tip of the ridge and its diameter is getting wider as we are heading up ridge, the vortex intensity doesn't change a lot with changing the inclination but it changes with the orientation of the ridge and these changes will be clarified more by the CFD simulation.
- On the leeward face we also noticed that there is a flow draft just after the ridgeline and directed parallel to it, the direction of this draft is toward up ridge on the upper half of the ridgeline and it's directed toward down ridge (the other direction) on the lower half, we have assumed that this is a horizontal vortex happening directly after the ridgeline and we noticed also for this vortex that it's increasing its intensity as we are approaching the edge of the ridge either form up or down. This assumption will be discussed more on the final conclusion of this work.
- Finally, a behavior on the windward face that we have called the "sliding wind", this behavior is happening on the lower half of the ridge where the net velocity component changes its direction instead of being perpendicular to the ridgeline, it becomes more parallel to it, the sliding wind effect is more intense on the higher inclinations and it starts to disappear as we lower the inclination until we reach 25-deg where it disappears, with changing the orientations it gets more intense on the negative orientations and almost disappear with the positive orientations.

5. CFD Numerical Simulation

On the past section we saw that the results of the wind tunnel tests showed a complex flow around the 3D ridge, this complexity drove us the motivation to do some numerical simulations so we can visualize the flow around the ridge and get a deeper understanding of the flow characteristics the ridge as we will see on the next section.

The simulation has been made by a commercial software, Autodesk® CFD, the software is one of the Autodesk® Simulations software package which is a general-purpose multi-physics finite element analysis software package initially developed by ALGOR Incorporated and acquired by Autodesk later. It is intended for use with Microsoft Windows and Linux operating systems. For more about the software you can check the Autodesk® CFD simulation software website.

5.1. The Simulation Setup

5.1.1. The Domain

The used domain was constant for all the configurations and simulations, the defined domain is a box has the dimensions: 1.5 m height by 2.5 m length by 2 m width, the model dimensions used on the simulation are the same one that used on the wind tunnel tests which are 1m as the length of the ridgeline and 0.25 m as the leg of the triangle face. The domain was made with this dimensions based on the size of the model, where the height of the domain is roughly 10 times the height of the model and 10 times the model's height also as a length after the model and 5 times before it. So on this the model have been placed where its center line is 1 m away from the entrance of the flow and on the middle way of the domain width. See Fig 5-1

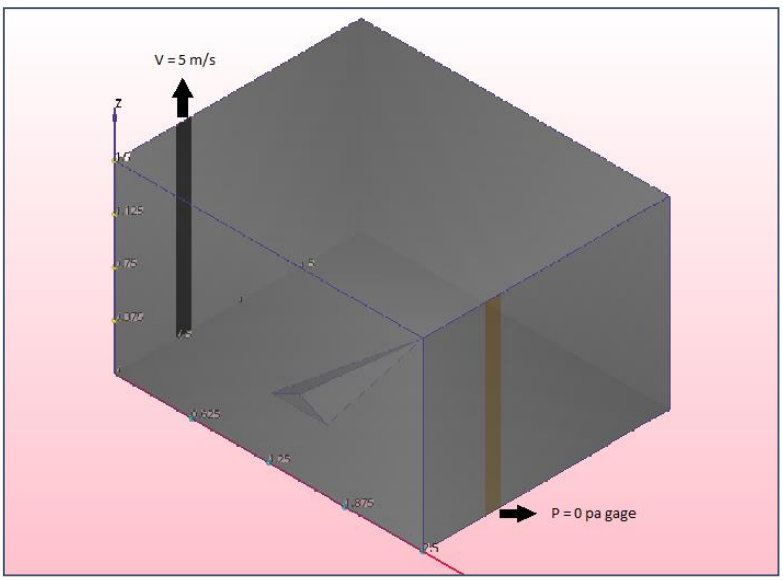

Fig 5-1 Image showing the position of the model inside the domain and the boundary conditions

5.1.2. Boundary conditions

We have two boundary conditions entered to the software setup, the first is the entrance of the flow where the velocity have been specified by 5 m/s, the second condition is the flow exit where the pressure have been specified by 0 pa Gage. On Fig 5-1 you can see the two faces where the conditions have been placed. There is also the condition of zero velocity across the walls which defined automatically by the software.

5.1.3. Mesh size

The software creates a mesh size automatically based on the geometry where the mesh is automatically concentrated in regions of high curvature and rapid size variation. The mesh size is represented by an index and it can be refined of course, the mesh size used for the simulations has an index of 0.2 and an average number of nodes 300,000 node changing from simulation to another depending on the configuration. In order to refine the mesh more but on the same time to reduce the total number of nodes and the calculation time, a region around the model was created where the flow is complex and has high turbulence, this region has a finer mesh and a height roughly 3 times the model height with the same domain width but the length is starting in the mid-way between the entrance and the model, see Fig 5-2, this mesh has an index of 0.015 on this region where the total number of nodes will be about 1 million nodes on the whole domain and it's connected to the basic mesh (0.2) by a way that ensures a proper element transitions. In some simulation a smaller region was even considered beside the above mentioned region, the smaller region height is just above the ridge and it's starting in the half of the windward face covering the leeward face and the weak area just after it, this region has mesh with index 0.008 and gives a total number of nodes about 1.2 million nodes, the region is shown also in Fig 5-2

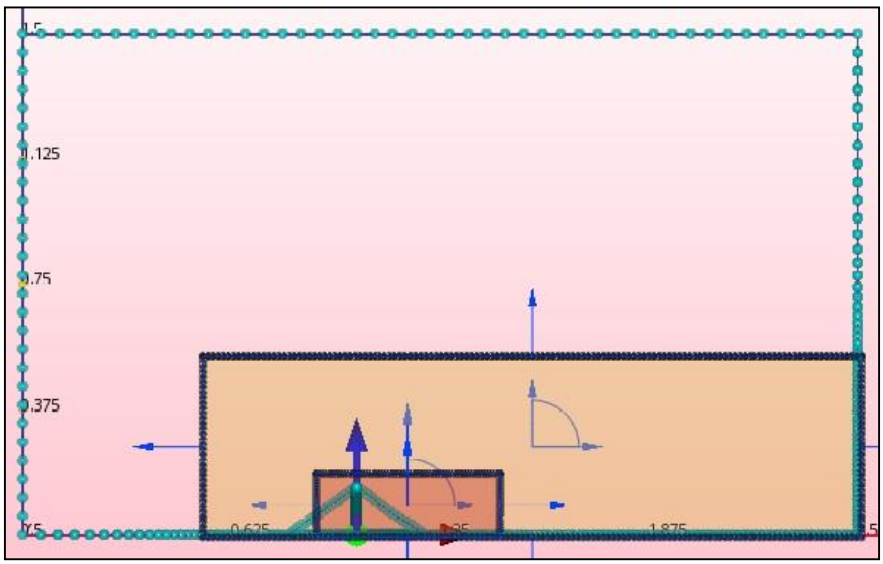

Fig 5-2 Image showing the position of the two region in the domain where the mesh is finer

5.1.4. Turbulence model

The results going to be presented on this work are made by the Two Equation Turbulence Model k- ε and the SST k-omega model, a study have been made to compare how the different models are responding, the considered models are: the RNG, the SST k-omega and the k- ε turbulence models. The turbulence models and the used equations will not be discussed here since the itself simulation is not the main objective of this study, the comparison between the results of these models is on Fig 5-3 with the wind tunnel tests results. We can see the pressure coefficient results along four line as on the wind tunnel tests, all the simulations have the same mesh on this comparison, the 0.015 mesh, in an overall we can say that there is no an exact match we can find but as we can see the SSD k-omega model gives the closest value to the wind tunnel tests. Both k- ε and SSD k-omega models will be used on the presented results on this work.

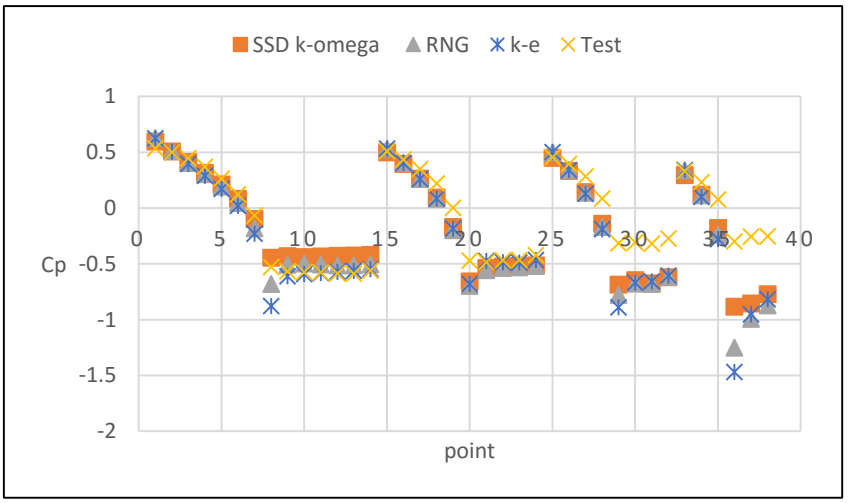

Fig 5-3 comparison between different turbulence models and the wind tunnel results

5.1.5. Considered Fluid Physics

The solution mode is steady state and the flow is incompressible without heat exchange, the flow entrance has a uniform profile and the boundary layer effect is being developed as the flow approaching the model and considered during the solution.

5.2. Mesh refining study

The study is based on comparing the simulation pressure coefficient results with the wind tunnel results, so 38 points were detected on the two faces of the model with the same distribution made on the wind tunnel tests, see Fig 4-1 showing the positions of these points. The considered meshes are: 0.05, 0.03, 0.02, 0. 2 with a region 0.02 around the model and 0.02 with region 0.015, another study with the SSD k-omega turbulence model using a mesh 0.2 with two regions, a region with 0.015 mesh and a smaller region with 0.008 mesh, see Fig 5-2, the following figures (Fig 5-4) showing this comparison:

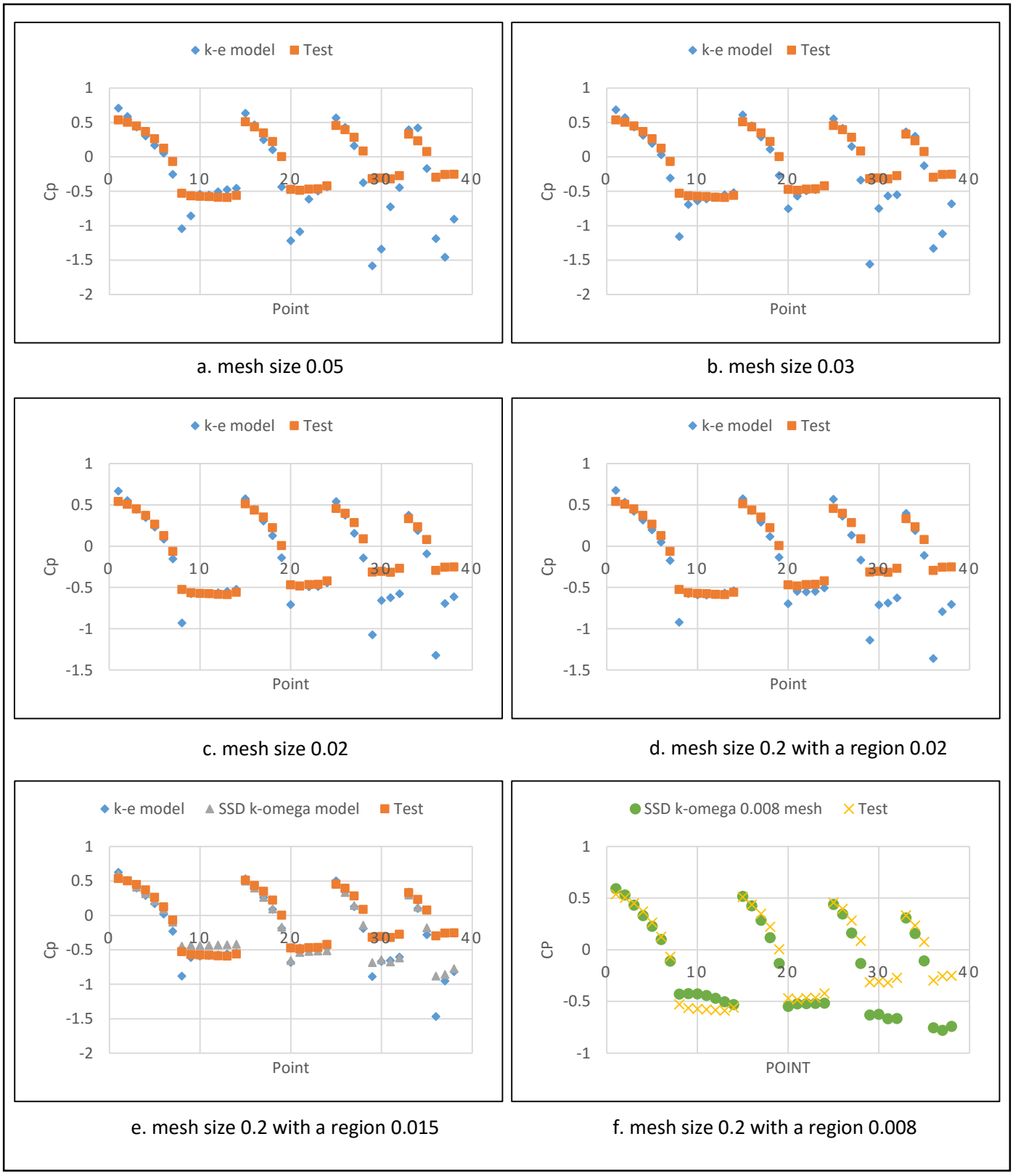

Fig 5-4 Comparison between the pressure coefficient results along the second line of the different meshes and the wind tunnel tests

On Fig 5-4 we can see a representation of the pressure coefficients at the 38 points where the first 14 points are for the first line, then the next 10, 8 and 6 points are for the 2nd,3rd and 4th lines respectively. Starting with the coarser mesh 0.05 we can see there is a big difference between the simulation and the test results specially on the leeward face. As we are refining the mesh more for the 0.03 and 0.02 meshes we can see the results are converging more to the test results but we still need to refine more, so the regions mentioned before will be used with finer meshes. The next refined mesh had index 0.2 for the basic mesh on the whole domain and 0.02 mesh on the region and we can see for this mesh that the results are very similar to the 0.02 mesh without using a region and even more converged at some points. A more refined mesh had 0.015 in the region, we can see from Fig 5-4-e that the results are very converged to the test results except for the leeward face on the third and fourth lines but if we used the SSD k-omega model with the same mesh we will find it more converged. The most refined mesh was the 0.008 mesh which has two regions and by using also the SSD k-omega model we can see as overall the results are the most converged. On the following Fig 5-5 we can have an idea about how the mesh is getting refined on the face of the model.

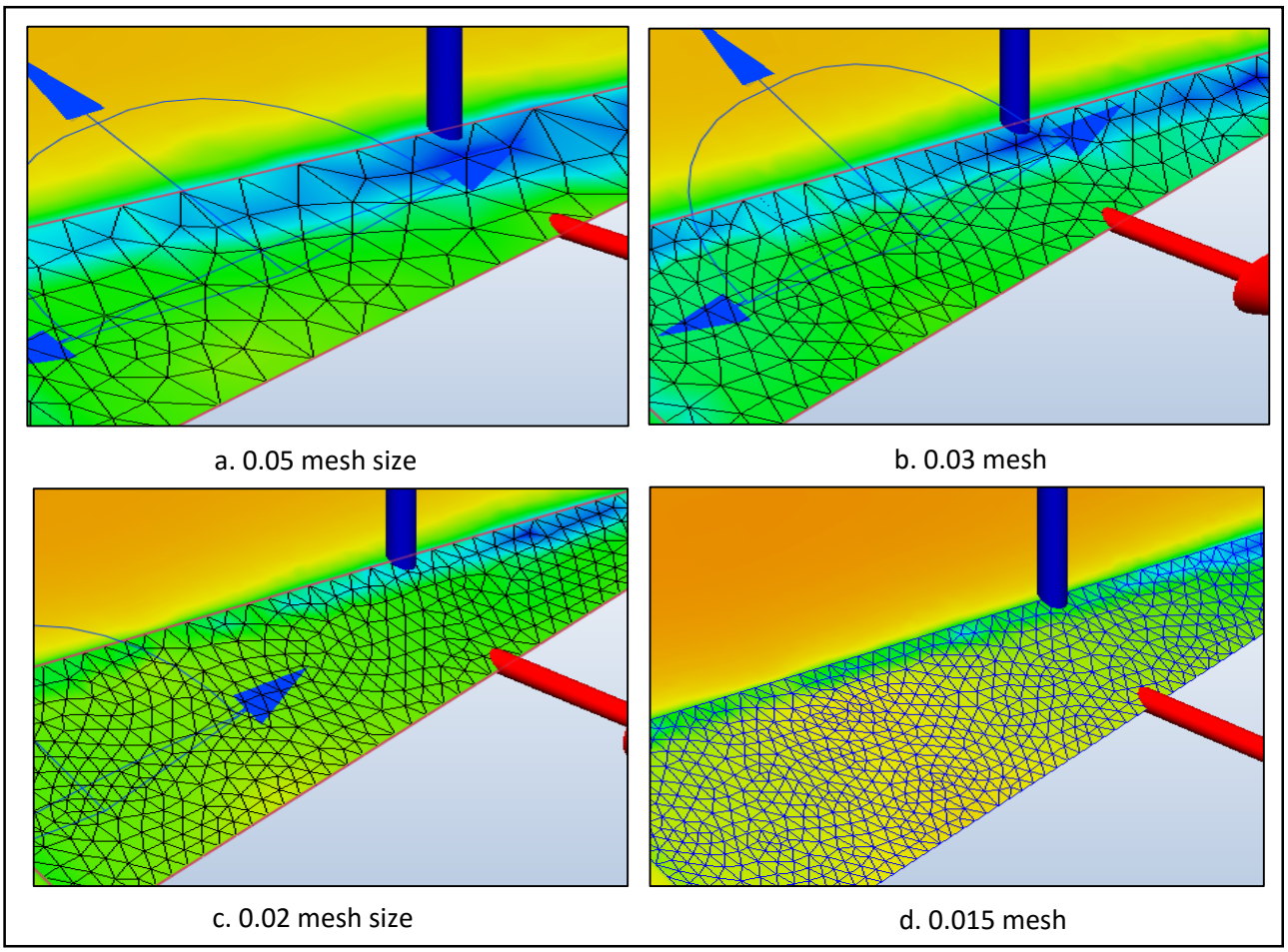

Fig 5-5 The different mesh sizes and distribution on the leeward face of the model

5.3. Comparison Between the Simulation and the Wind Tunnel Results

On Fig 5-6 we can see a comparison between the pressure coefficient results of the wind tunnel and the simulation where the SSD k-omega turbulence model where used with the mesh 0.008 that contains two regions, the comparison is for the same three ridge inclinations that was used on the wind tunnel tests (45, 35 and 25-deg), we can see the difference between the two results is changing with the inclination, on the 35-deg we have the best convergence but for 45-deg we can find the results are lower a little and for 25-deg are higher. However, there is not a big difference in the flow behavior around the ridge except for the third and fourth lines on the leeward face where it shows always lower values than the test results, considering that the conical vortex is generated in some area between these lines so we can deduce that the simulation is solving this vortex on its beginning as it has higher velocity or intensity than the wind tunnel.

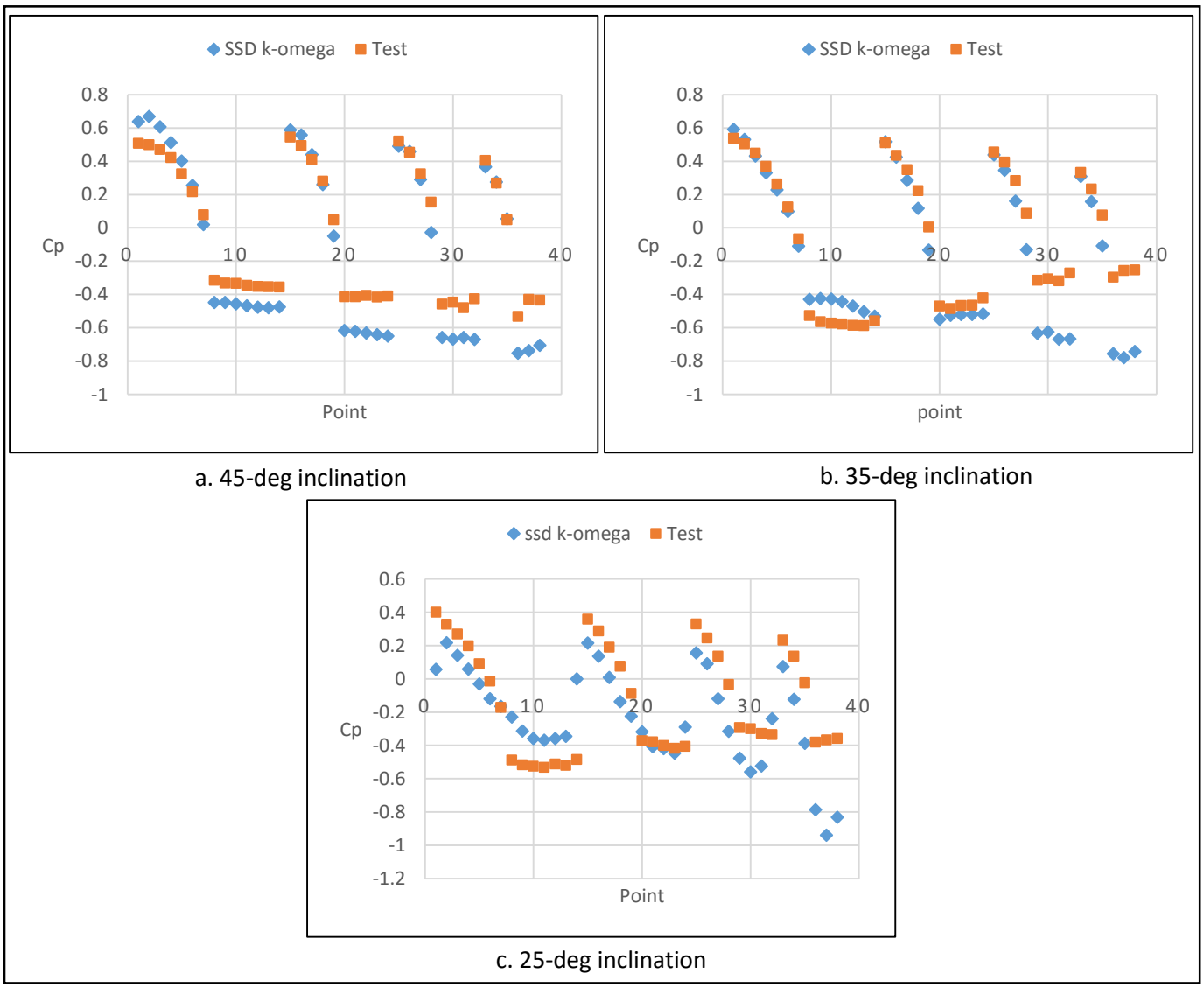

Fig 5-6 Comparison between the simulation and wind tunnel results with 0.008 mesh for different inclinations

5.4. Simulation Results and Discussion

We will present the results of the simulation as velocity and pressure coefficient profiles on planes in different locations, also the stream traces and iso volumes for some results. The presented results for the three inclinations (45, 35 and 25) are forming a group where the solution made by the SSD k-omega model with the 0.008 mesh. The second group will be for a different orientations of the ridge (-20, -10, 10 ,20) with 35-deg inclination, this group is solved by the k- ε model with the 0.015 mesh.

5.4.1. Different inclinations

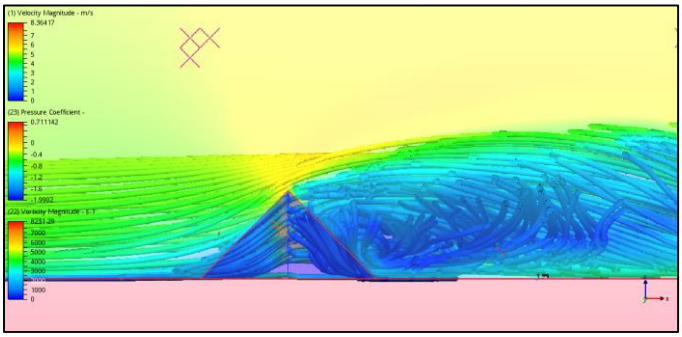

a. 45-deg inclination, velocity magnitude with the traces

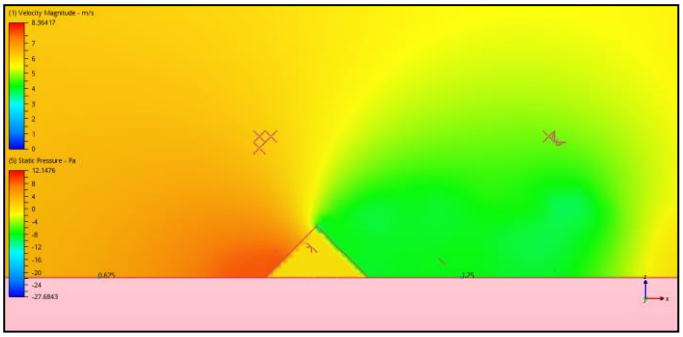

d. 45-deg inclination, Cp

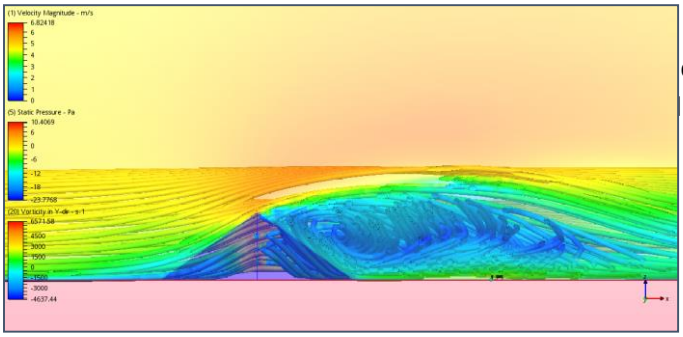

b. 35-deg inclination, velocity magnitude with the traces

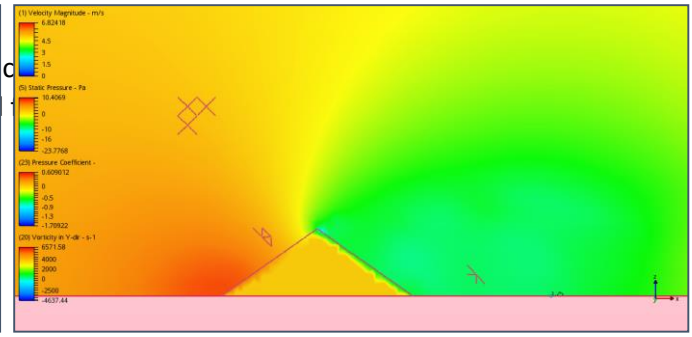

e. 35-deg inclination, Cp

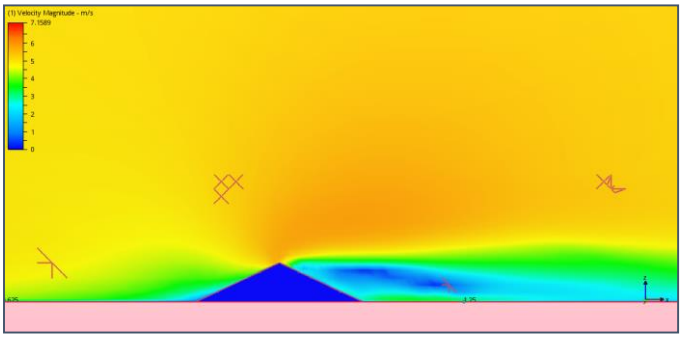

c. 25-deg inclination, velocity magnitude

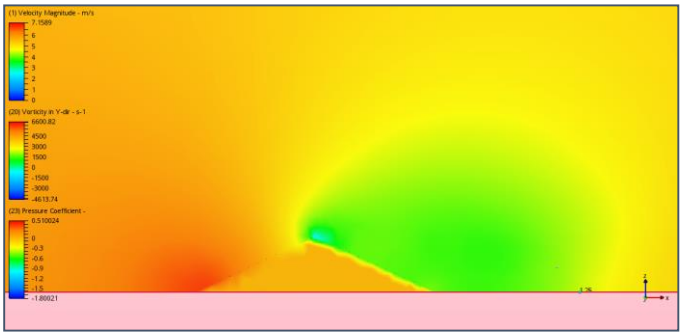

f. 25-deg inclination, Cp

Fig 5-7 The velocity and pressure coefficient profile on a plane in the middle of the model for different inclinations

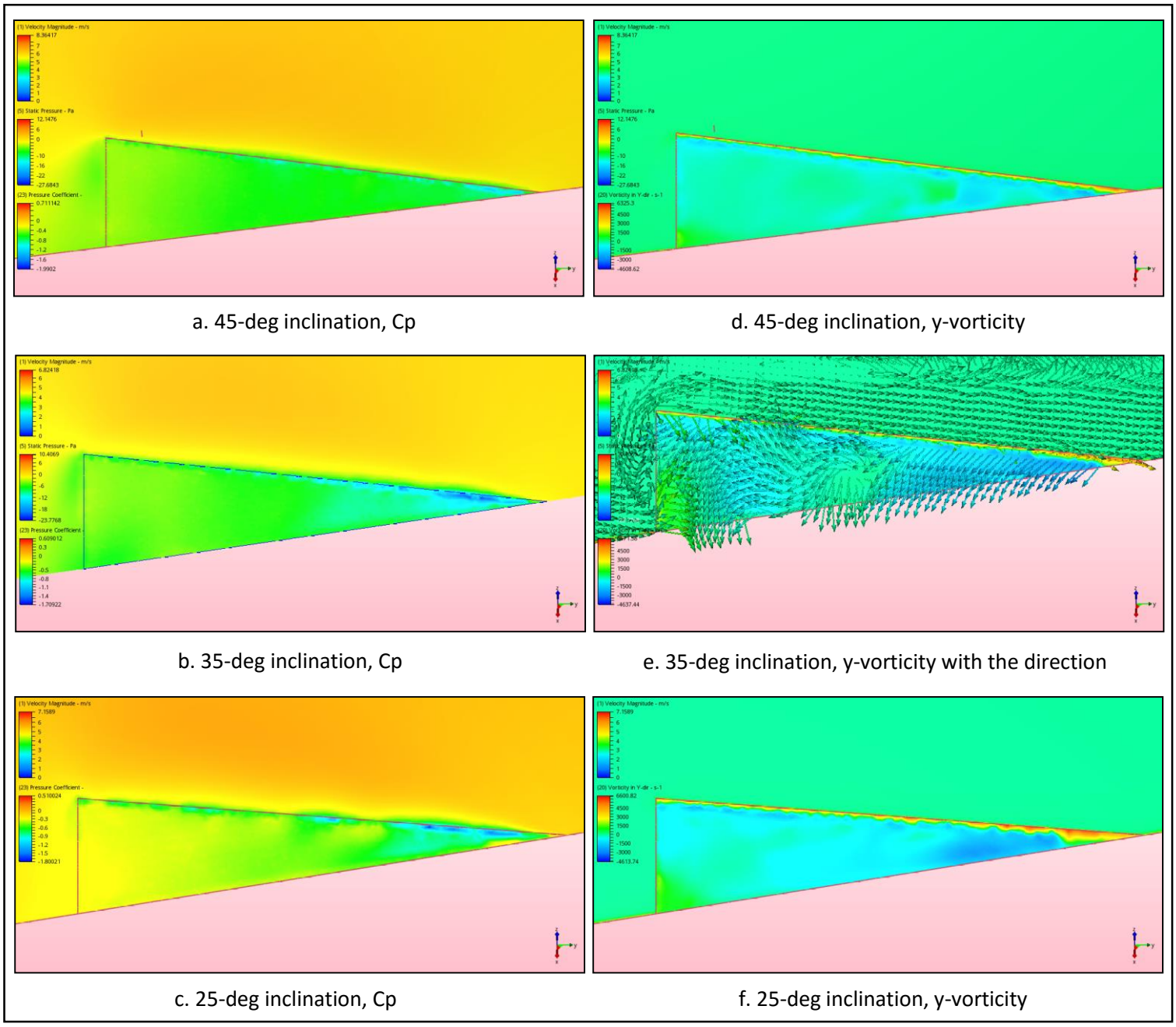

a. 45-deg inclination, Cp

d. 45-deg inclination, y-vorticity

b. 35-deg inclination, Cp

e. 35-deg inclination, y-vorticity with the direction

c. 25-deg inclination, Cp

f. 25-deg inclination, y-vorticity

Fig 5-8 The pressure coefficient and the vorticity magnitude on y-direction profiles on a plane adjusted to the leeward face of the model for different inclinations

From Fig 5-7 we can see that as we increase the inclination the weak area after the ridge increase its size, the maximum velocity on this mid-plane doesn't vary a lot where it shows 8.3, 6.8 and 7.1 m/s for the 45, 35, 25 degree inclinations respectively. For the pressure coefficient, we have positive values on the windward face and negative on the leeward, form Fig 5-8 we can see the distribution of the pressure coefficient on the leeward face and we can see that for all the inclinations we have a small area parallel to the ridgeline and along it where we have the lowest pressure on this face, this is an important result since we had on the wind tunnel test a flow draft on this area and has a direction parallel to the ridgeline, now on the simulation we see that this area have also a relatively low pressure. For the vorticity, we can see on Fig 5-8 the distribution of

the vorticity magnitude in y-direction over the leeward face where we can see the highest y-vorticity on this face is happening just after the ridgeline where it's the same area of the low pressure, in an overall evaluation for the y-vorticity, on Fig 5-10 we can its distribution on the ridge and around it where it appears that the vorticity generally has the highest values near the ridgeline either form the leeward or the windward side and regardless the inclination it has a direction down ridge on the windward and up ridge on the leeward face.

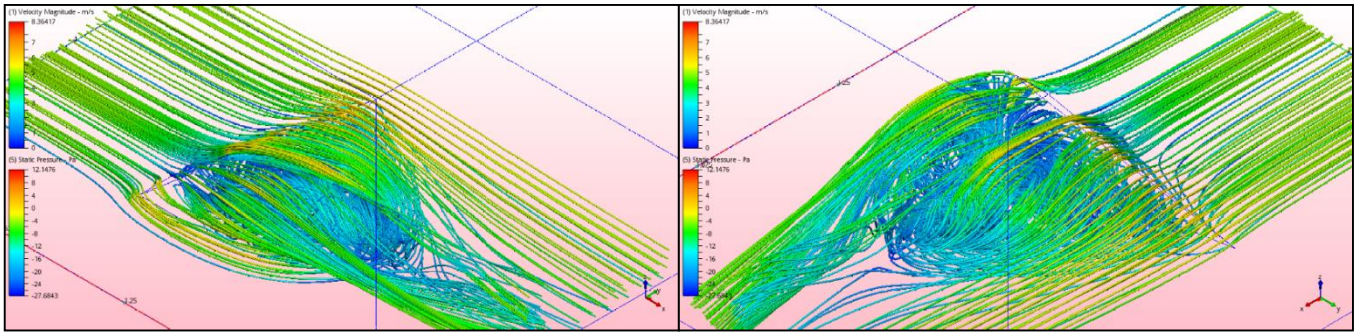

a. 45-deg inclination

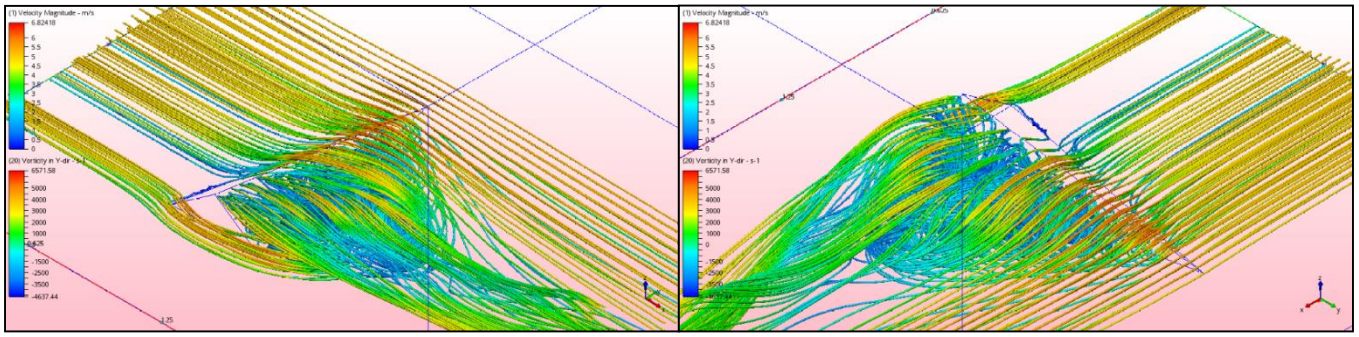

b. 35-deg inclination

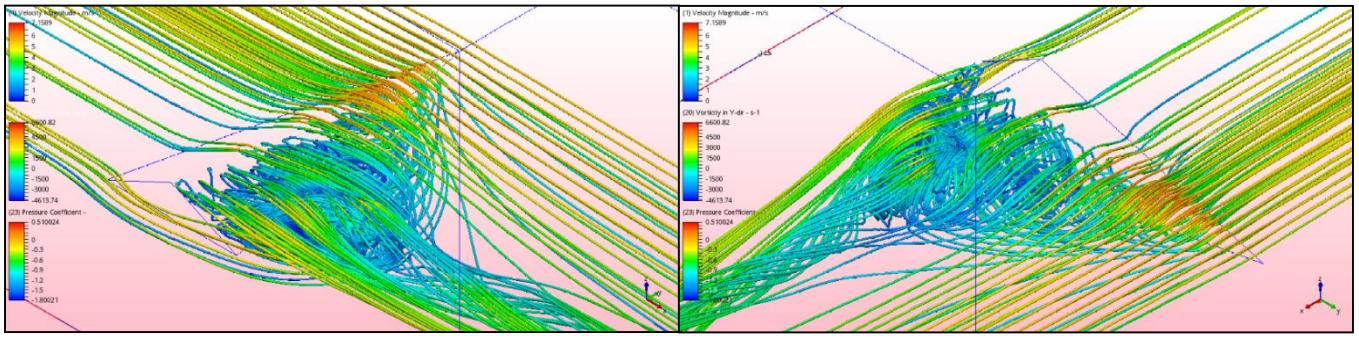

c. 25-deg inclination

Fig 5-9 The stream traces showing the conical vortex colored by the velocity magnitude from two views for different inclinations

The vorticity representation on Fig 5-10 also show a stagnation point on the windward face on the three inclinations near the up ridge and the area where we have the conical vortex. For a vertical plane that having the same angle of the ground edge of the ridge in the leeward face, we can see the velocity profiles on it in Fig 5-11, we can assume that this plane is containing the conical vortex core and we can see the velocity profiles of this vortex in a cross section of it, we can see the vortex core have the lowest velocities (the dark blue color).

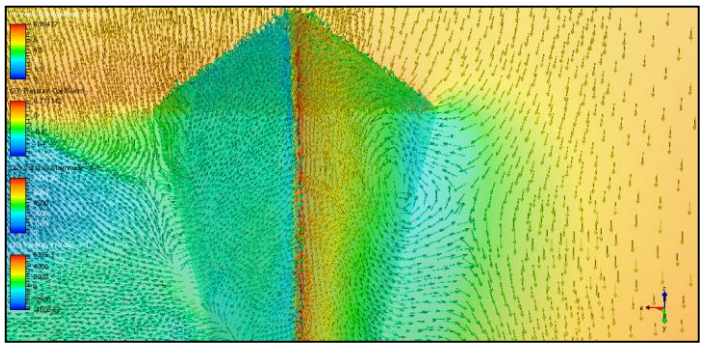

a. 45-deg inclination

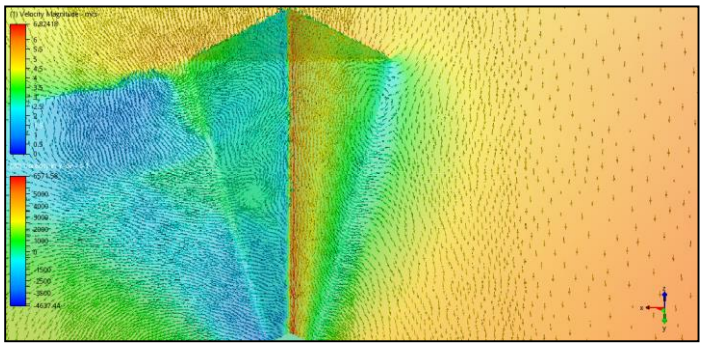

b. 35-deg inclination

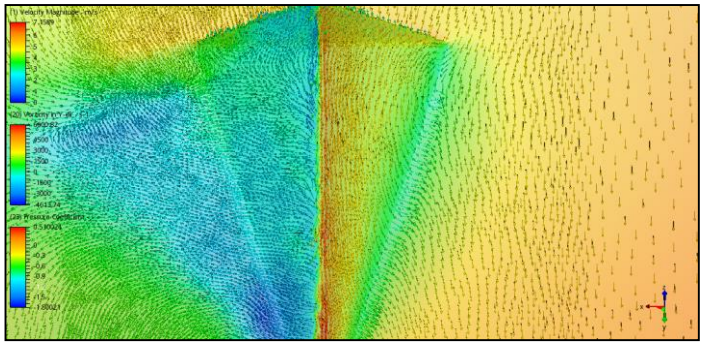

c. 25-deg inclination

Fig 5-10 The vorticity direction and its magnitude in the y-direction around the model for different inclinations

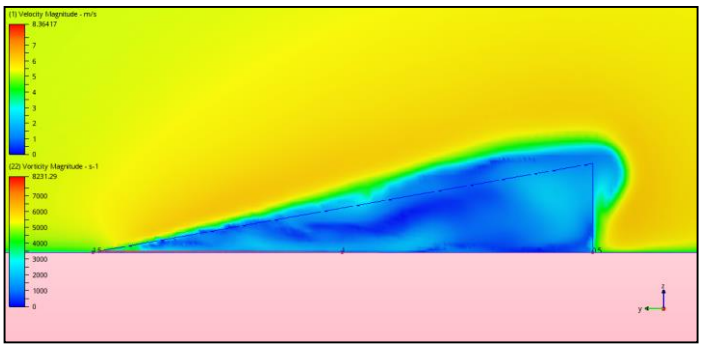

a. 45-deg inclination

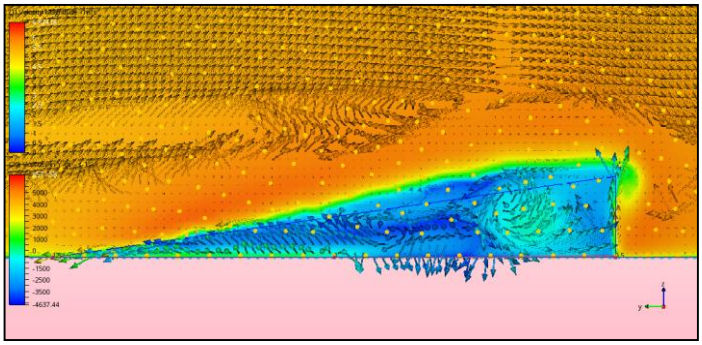

b. 35-deg inclination with the vorticity direction

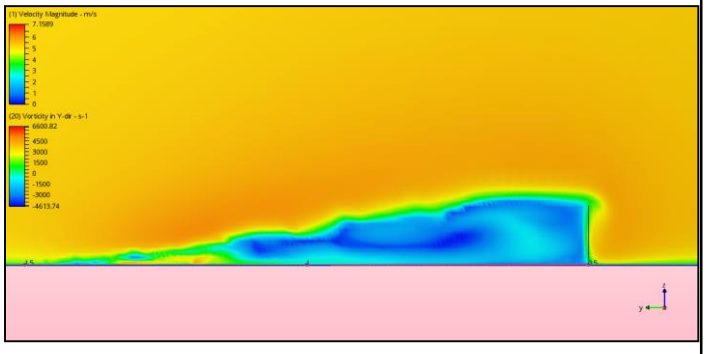

c. 25-deg inclination

Fig 5-11The velocity profile on a vertical plane containing the ground edge of the model in the leeward face for different inclinations

It's noticeable that the conical vortex doesn't continue its spreading since it gets interrupted by a flow coming around the ridge from the windward side where the both flows are getting united and exiting the vortex as we see on Fig 5-9, it's also shown on the vorticity profile on Fig 5-11 (b), we can notice also that the vortex is not generated exactly from the tip of the ridge but it will start forming at a distance roughly 10 to 15 % of the ridgeline length.

On Fig 5-14 we can see the distribution of the total vorticity magnitude and on Fig 5-15 we can see the its magnitude on the x-direction and its showing the heist values are for the conical vortex, in both figures we can see how the flow is exiting the vortex with the other flow coming around the ridge. An iso-volume representation of the Cp with values between -0.5 and the lowest value -1.8 on Fig 5-13, it's clearly that the lowest Cp values goes for the core of the vortex and the area just after the ridgeline, on Fig 5-12 we can see also a closer look to this area after the ridgeline and the low pressure on it.

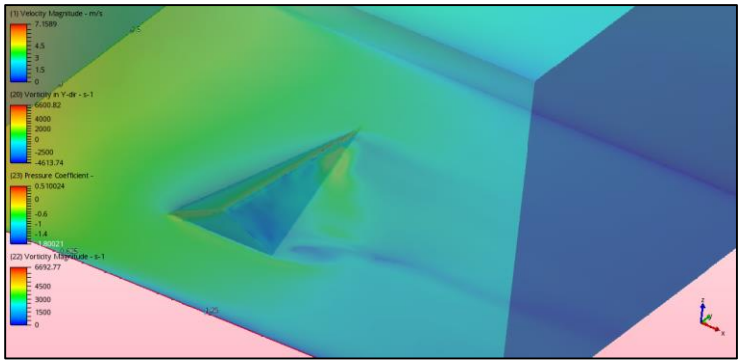

Fig 5-14The vorticity magnitude around the ridge with 25-deg inclination

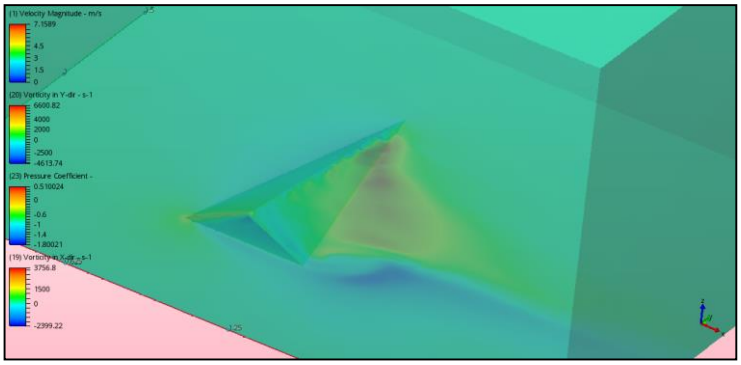

Fig 5-15 The vorticity magnitude in x-direction around the ridge with 25-deg inclination

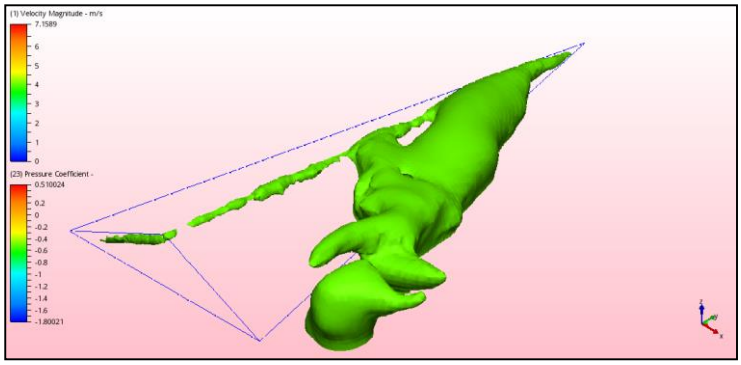

Fig 5-13 An iso-volume for the Cp values from -0.5 to the lowest -1.8 with 25-deg inclination

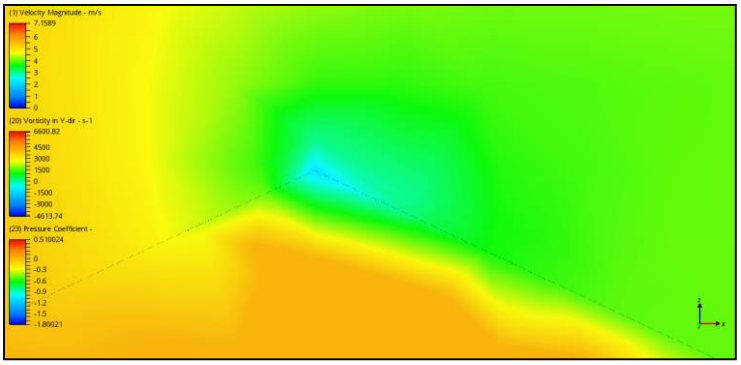

Fig 5-12 The Cp distribution on the mid-plane with a closer look to the area around the ridgeline (25-deg)

5.4.2. Different orientations

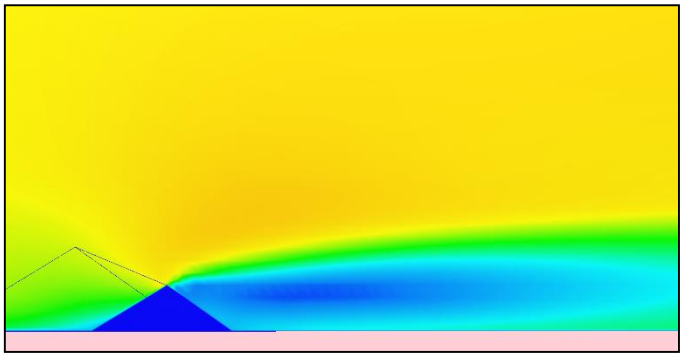

a. -20-deg orientation

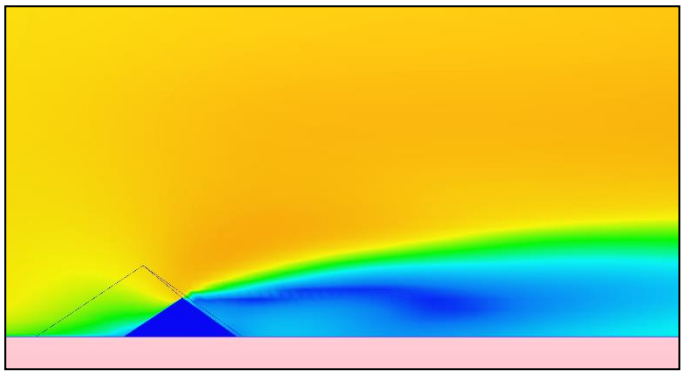

b. -10-deg orientation

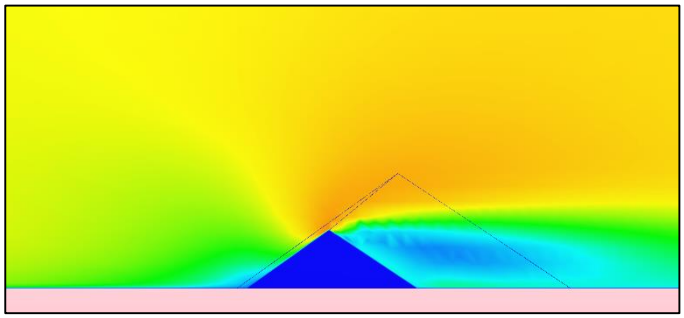

c. 10-deg orientation

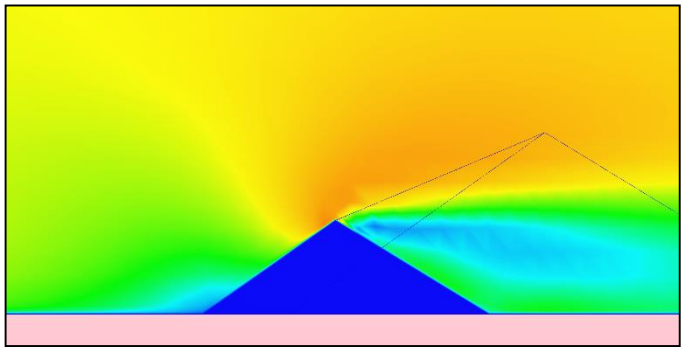

d. 20-deg orientation

Fig 5-17The velocity profile on a plane in the middle of the model for different orientations

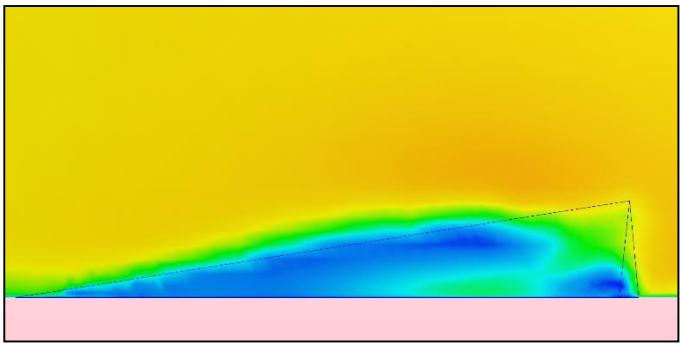

a. -20-deg orientation

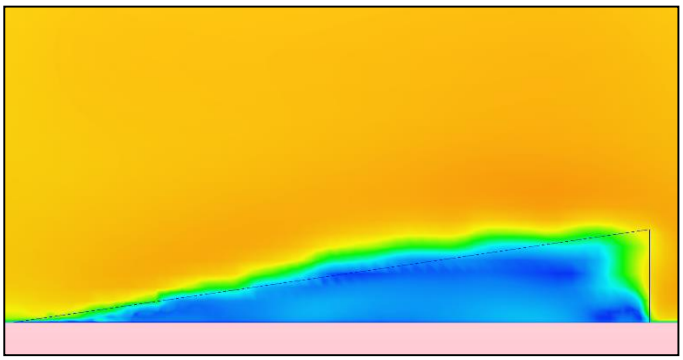

b. -10-deg orientation

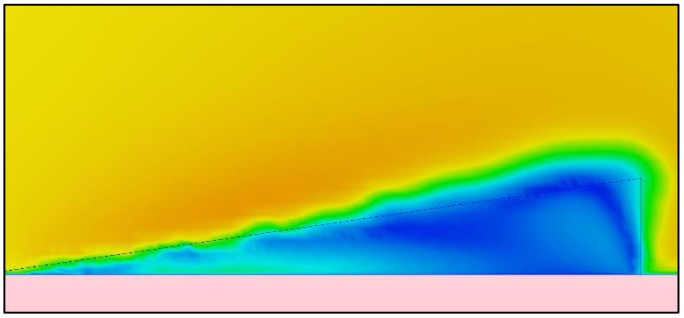

c. 10-deg orientation

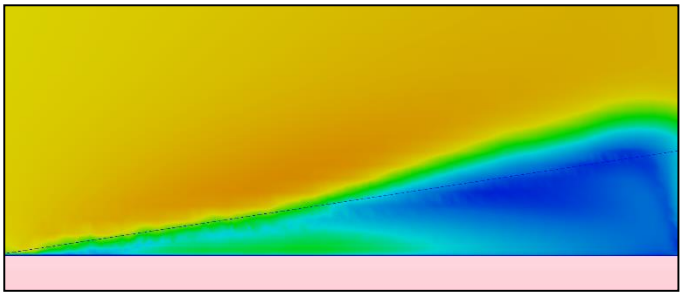

d. 20-deg orientation

Fig 5-16The velocity profile on a vertical plane containing the ground edge of the model in the leeward face for different orientations

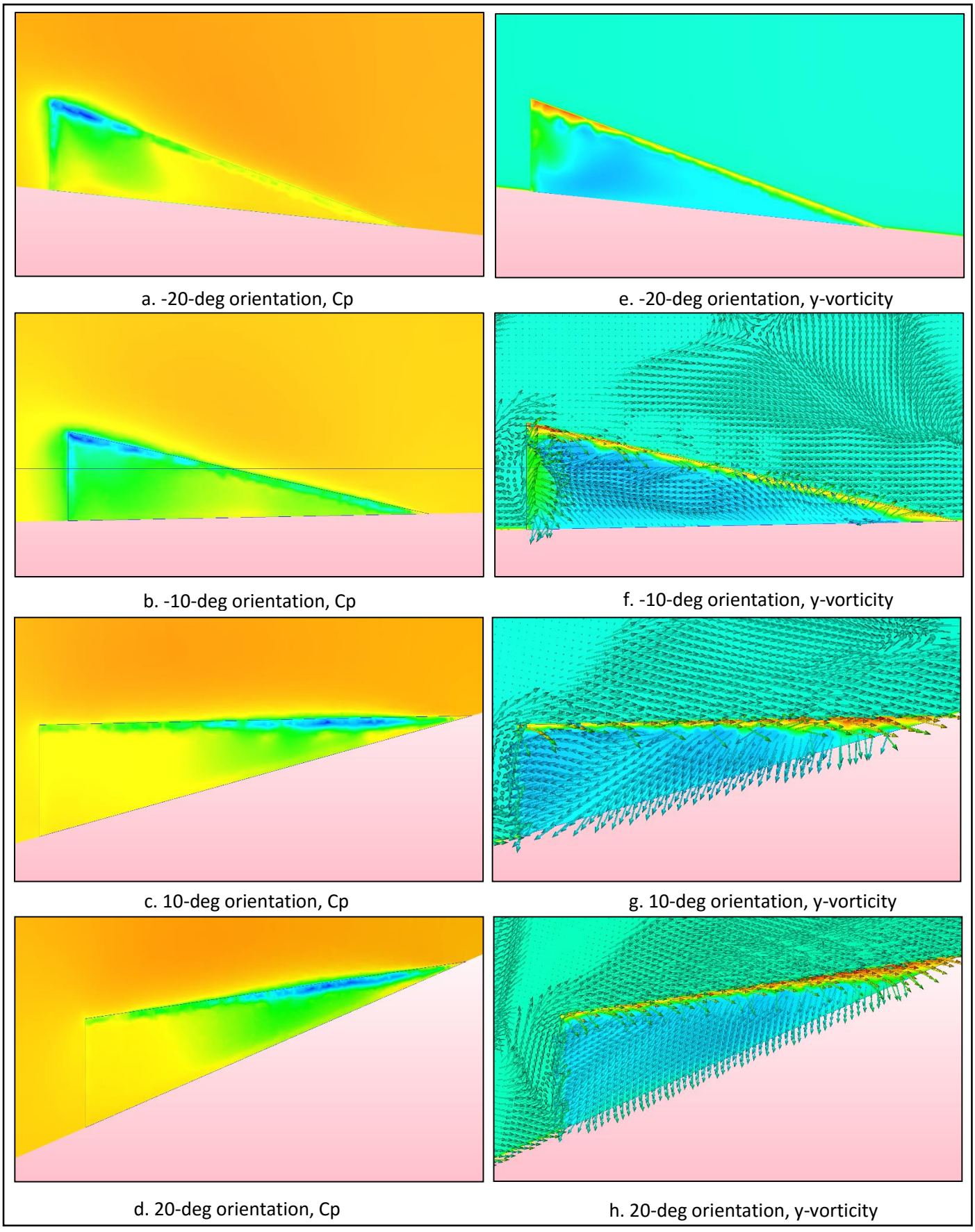

a. -20-deg orientation, Cp

e. -20-deg orientation, y-vorticity

b. -10-deg orientation, Cp

f. -10-deg orientation, y-vorticity

c. 10-deg orientation, Cp

g. 10-deg orientation, y-vorticity

d. 20-deg orientation, Cp

h. 20-deg orientation, y-vorticity

Fig 5-18The pressure coefficient and the vorticity magnitude on y-direction profiles on a plane adjusted to the leeward face of the model for different orientations

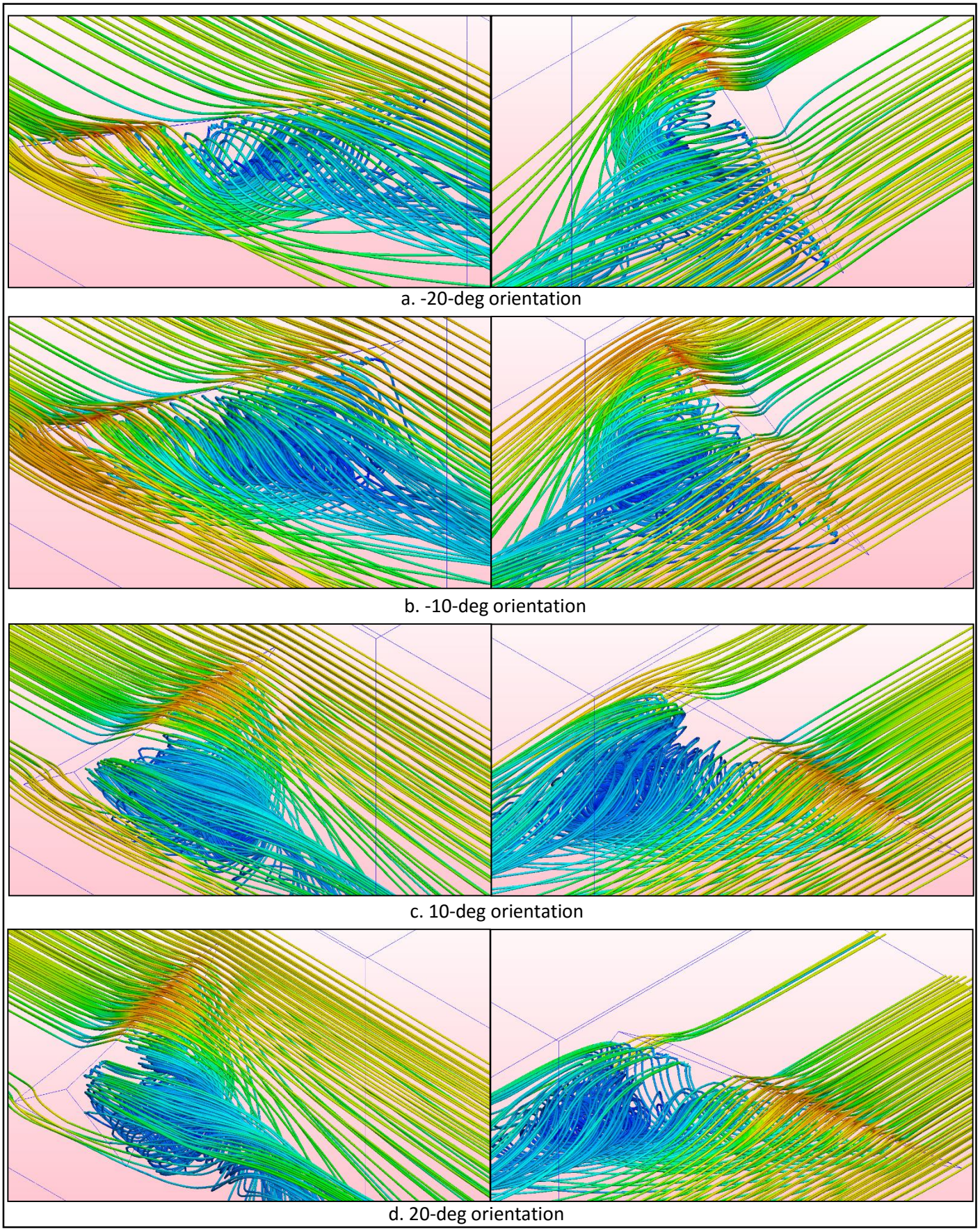

a. -20-deg orientation

b. -10-deg orientation

c. 10-deg orientation

d. 20-deg orientation

Fig 5-19The stream traces showing the conical vortex colored by the velocity magnitude from two views for different orientations

From Fig 5-16 we can see how changing the orientation of the bed can dramatically change the velocity profile in the mid-plane which is in fact a result of the changes in the conical vortex. In a comparison with the no-oriented case for the conical vortex, we can see on Fig 5-19 that with the negative orientations starting with the -20-deg orientation (a) that the conical vortex doesn't exist and another vortex is formed from the top corner of the ridge as the flow hits this corner first and it propagates in the reverse direction of the normal conical vortex, for -10-deg orientation (b) we can see that the conical vortex still exist but it meets the other vortex formed from the top corner of the ridge also and then the flow exit almost at the middle of the ridge, this actually forming a structure very similar to the cylindrical vortex in a case of the simple 2D ridge. For the positive orientations (c, d) we can see that the conical vortex is exist and it's along all the ridge not like with the no-orienting case where it meets a flow coming around the ridge and both of them exit the structure in some point before the end of the ridge, however, the vortex has bigger diameter with the 10-deg and even bigger with the 20-deg, also we can see that the conical vortex starts farther from the ridge tip than the no-orienting case.

For the pressure distribution over the leeward face we can see form Fig 5-18 that on the area just after the ridgeline we can find a low pressure area also as without orientation but the area where the flow will hit the ridge first has the lowest pressure, in the case of negative orientation we will find it near the top corner of the ridge and in case of the positive orientation it's near the tip of the ridge.

For the vorticity in y-direction over the leeward face we still find that the highest values are always near the ridgeline but it varies a little with the different orientations.

5.5. Conclusion

- For the conical vortex, the vortex changes its diameter where it gets bigger with increasing the inclination and generally the weak zone is longer, with changing the orientation we found for the negative direction that the conical vortex disappears and another vortex formed form the top corner of the ridge, with the positive orientations the conical vortex is exist and its dimeter increase a little comparing to the no-oriented case, also its start point is getting shifted farther from the tip of the ridge.
- For the area just after the ridgeline on the leeward face we saw that it has always a low pressure on the leeward face, and in an iso-volume representation we found that the lowest pressure on the whole domain is on this area and the core of the conical vortex. On this area also we saw vary high vorticity magnitude on the y-direction.

6. Fire Tests

The fire tests are the main tests on this study. As mentioned before the objective of these tests is to experiment the behavior of the fire spreading across the 3D ridge with a low radius of curvature ridgeline and under wind condition.

For this purpose, a structure has been made of steel and it consists of two triangle shape surfaces connected together by hinges so it can be adapted to any angle of inclination, the two surfaces are identical and have a right triangle geometry its dimensions are 4 m for the hypotenuse and 1 m for the leg, the sharp angle of the triangle wasn't made during difficulties in constructing such a very sharp steel structure, as a results of that the ridge or the hypotenuse has a length of 3.8 m only where the left 0.2 m were cut off. To simulate the atmospheric flow, the ridge model has been placed inside the combustion wind tunnel TC3 of the Fire Research Laboratory of the University of Coimbra (LEIF) in Lousa, Portugal, the tunnel has a working section of 6 m width by 8 m length with a maximum flow velocity of 8 m/s and has walls on the sides of 2 m height to guide the flow (Fig 6-4). Since the model has been made where it can be adjusted to any angle so it's open from the triangle leg side, this will create a circulation and vortices on this area and it will affect the fire spread, to avoid this effect and to make the structure simulating the 3D ridge in the nature more accurately a rounded end structure has been added to the model from that side (Fig 6-1) to make the flow pass around the model more smoothly, of course this rounded end was different from inclination to another.

The governing parameters of the tests: (Fig 6-2)

- Wind velocity (U): 0, 1, 2 and 3 m/s
- Inclination of the ridge (α): 10, 20, 25, 35 and 45 degrees
- Orientation of the ridge relative the wind direction (φ): -20, -10, 0, 10 and 20 degrees, the angles are measured as the 0 is when the model is perpendicular to the wind direction, the minus orientations are when the model being tilted in a CW direction and the positives are the CCW direction.
- Ignition point: three ignition points are being considered (A, B, and C) all of them are on the windward face. The ignition points are defined by two variables: the distance from the ground measured on the surface of the model which we can call it the height and the other is the longitude distance measured along the ridge line. For the height: a line joining between the sharp angle corner of the triangle and a point at a height of 0.25m from the ground on leg of the triangle in which the ignition point will be always on this line regarding the longitude distance. The longitude distance of the three points are: (A) is in the middle of the ridge, (B) is at 0.3 m measured from top corner of the ridge and (C) is also at 0.3 m but from the ridge tip.

To experiment the behavior of the fire with these different parameters a combination has been made between them to give us 32 different tests addressed on the following table with their parameters and references.

Test ref.	Wind velocity (U)	Inclination (α)	Orientation (φ)	Ignition point
3D1	0	25	0	A
3D2	1			
3D3	2			
3D4	3			
3D5	0	35		
3D6	1			
3D7	2			
3D8	3			
3D9	0	45		
3D10	1			
3D11	2			
3D12	3			
3D13	0	35	-10	
2D14	2			
3D15	0		-20	
3D16	2			
3D17	0		10	
3D18	2			
3D19	0		20	
3D20	2			
3D21	0		0	B
3D22	2			
3D23	0			C
3D24	2			
3D25	0	20		A
3D26	1			
3D27	2			
3D28	3			
3D29	0	10		
3D30	1			
3D31	2			
3D32	3			

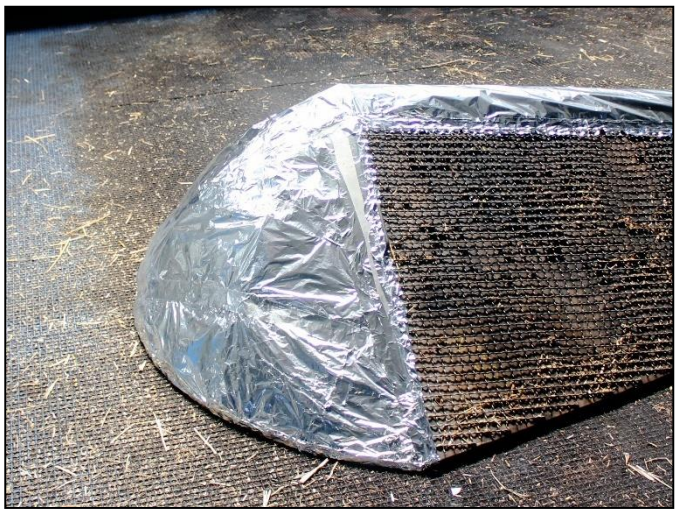

Fig 6-1The steel model and the rounded end attached to it

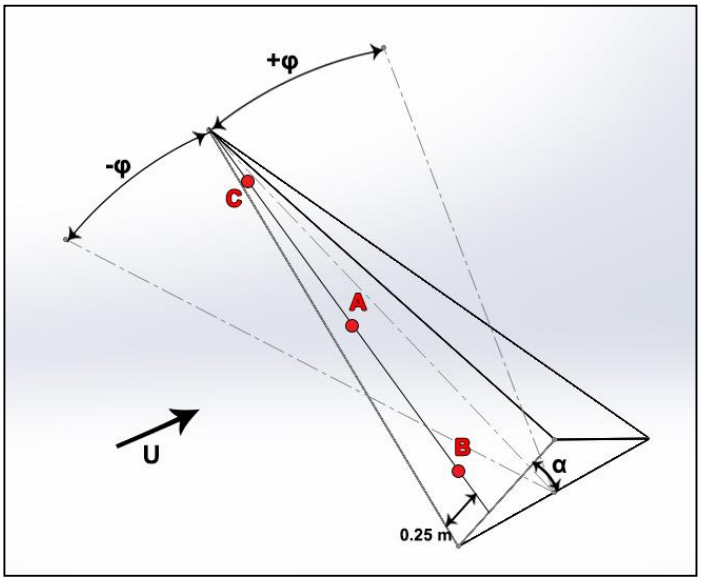

Fig 6-2The ridge angles and the ignition points location

6.1. Testing Methodology

The steel model was placed in the combustion wind tunnel where its center is in the center of the tunnel regardless the configuration being tested. Both faces of the model are covered by a fuel to form a fuel bed where the used fuel is dried Pine Needles (Fig 6-3) as as a potential forest fuel able to support the spread of a surface fire, the fuel bed assumed to be homogenous and has uniform properties in the entire area of interest. The used fuel load is 0.6 kg/m^2 on a dry basis and the average depth of the fuel bed was 5 cm, to make the fuel load in a dry basis and to avoid the moisture content changing effects, before starting each experiments session the moisture content was analyzed and based on its percenter the fuel load was compensated according to the following relation:

$$Total\ weight = dry\ weight * (1 + m_f)$$

Where: m_f is the fuel moisture

Fig 6-4 image showing the combustion wind tunnel and the model placed in its center, also the cameras are positioned on the left of the tunnel

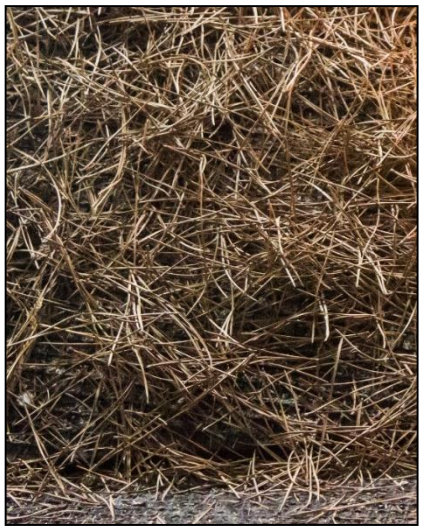

Fig 6-3 The pine needles fuel bed

The basic parameter to describe the spreading behavior of the fire is the fire rate of spread (ROS, R) and to measure this ROS the experiments were recorded by a fixed infrared camera placed at the highest possible elevation beside the wind tunnel (Fig 6-4), then frames where taken from the infrared record with a constant time laps between the frames for each test to be analyzed by the developed program that was discussed before on this work. In addition to the infrared camera a fixed video camera and a remote camera were used also to picture any interesting behavior happening.

The ROS's ware defined as an average ROS and also as a dynamic ROS through three directions (Fig 4-4) on each face (the windward and leeward faces) which are:

On the windward face:

- Up slope: a line perpendicular to the ridgeline and passing by the ignition point A in up slope direction
- Up ridge: a parallel line to the ridgeline and on an average distance of 10 cm from it toward the up ridge direction.
- Down ridge: a parallel line to the ridgeline and on an average distance of 10 cm from it toward the down ridge direction.

On the leeward face:

- Down slope: a line perpendicular to the ridgeline and on the same plane of ignition point A in the down slope direction
- Up ridge: a parallel line to the ridgeline and passing by the most advanced points of the fire fronts (peaks) toward the up ridge direction if existed.
- Down ridge: a parallel line to the ridgeline and on an average distance of 10 cm from it toward the down ridge direction or passing by the peaks if existed.

For the average ROS, it was defined according to Viegas (2006) by the distances passed by the fire each given time step along a predefined direction where the ROS was estimated as the slope of a straight line fitted on the plot of these distances (D) versus the time consumed to pass them (t), in some cases the fire spread was not steady but we assumed that the ROS was constant along each spread direction that was considered during the test. For the dynamic ROS, the ROS was defined with the same method of slope but between each two following points on the D-t plot where it's representing the average ROS that the fire transported with between the two time steps (frames).

For the tests where the ignition was on A, the analysis of the ROS on the leeward face was made by one of the average ROS calculation methods provided by the program which is building net of straight lines with angle between them form half a circle, the lines are starting from the middle of the ridgeline (see Fig 3-3), the ROS was calculated through each line of them, this was made to define the average ROS not only through a single line on the required direction but it will be the average of the ROS's of a the group of lines lying in an area prescribed by two angles where these angle were measured from the center of the ridgeline and in CCW direction, however, the average ROS in down slope direction on the leeward face was the average of ROS's of the lines having an angle between 80° and 100°, for the up ridge direction it was the average between 0° and 10°, and the last direction, down ridge, was the average between 165° and 180°. See Fig 6-5 .

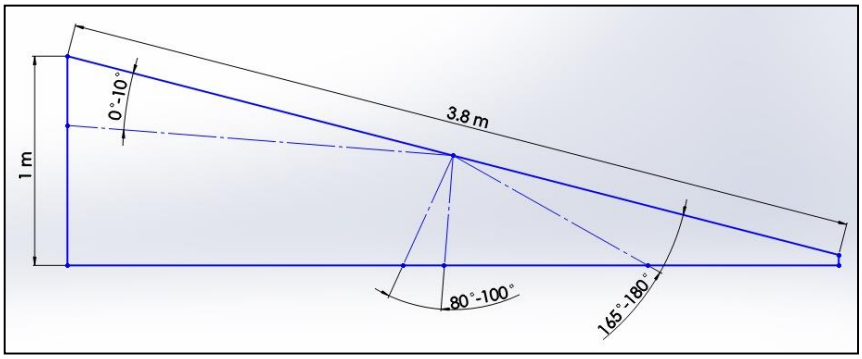

Fig 6-5 The areas were the average ROS is calculated on the leeward face

In order to minimize the effect of small variations on the fuel bed properties, namely moisture content, following Viegas and Neto (1991), we used the non-dimensional ROS (NDROS) in presenting the results and it's given by:

$$R' = \frac{R}{R_o}$$

Where R_o is the basic ROS with no-slope and no-wind conditions and it was measured for each experiments session by burning the same load of fuel 0.6 kg/m^2 in a flat bed of 1 m^2 area (Fig 6-7), the R_o was measured by tightening a strings at each 0.1 m along the bed and when the fire cross the string a time lap were taken to calculate later the slope of a fitted line between the distances and the time which is the basic ROS (R_o).

Also to minimize these effect on the passed distances by the fire during the dynamic ROS plots representation, a distance dimensionless form (D') was considered where it's the passed distance with the basic ROS (R_o) during a time unit.

$$D' = R_o * t_o$$

Fig 6-7 The 1 m2 area table where the Ro was defined

Fig 6-6A typical fire spread behavior on the leeward face (ref. 3D7)

To grantee that the results of the tests (ROS's) are correct and the fire behavior wasn't effected by some random local behaviors either on the aerodynamics or the fire dynamics, all the tests have been repeated two times (phases) and the results were compared to each other, for the tests where we had a big difference on the results between the two phases (more than 30%), the tests were repeated in a third phase to know which one of the first two phases was correct. All the presented results on the next section are the most correct results based on the comparison between the three phases.

All the used symbols on the results and discussion section are addressed on the following table:

Symbol	Definition
R(ROS)	The Rate of spread
R_0	Basic rate of spread without wind or slope conditions
R'(NDROS)	Non dimensional rate of spared
D	The distance passed by the fire along a prescribed direction
D'	Non dimensional distance passed by the fire along a prescribed direction
t	The time that the fire takes to pass a distance
U	Wind velocity

6.2. Results and Discussion

The results and their discussions of the tests are divided on three groups, the first group of tests were with changing the inclination and wind velocity (test ref.: 3D1 to 3D12 and 3D25 to 3D32), the second group is the tests where the orientation was changed (test ref.: 3D13 to 3D20), and the last group is the tests where the ignition point was changed (test ref.: 3D21 to 3D24).

We should notice also that since we have 32 fire front propagation map for the 32 test it's difficult s to address all of them on the discussion so they are all addressed on appendex1, however during the discussion some of them will be addressed as they have important behavior to mention.

6.2.1. First Group of tests

For each inclination we tested three different velocities (1,2 and 3 m/s) as mentioned before in addition to a test without wind to see the effect of the slope only and compare it to the combined effect of wind and slope.

6.2.1.1. The Leeward Face

Up ridge direction

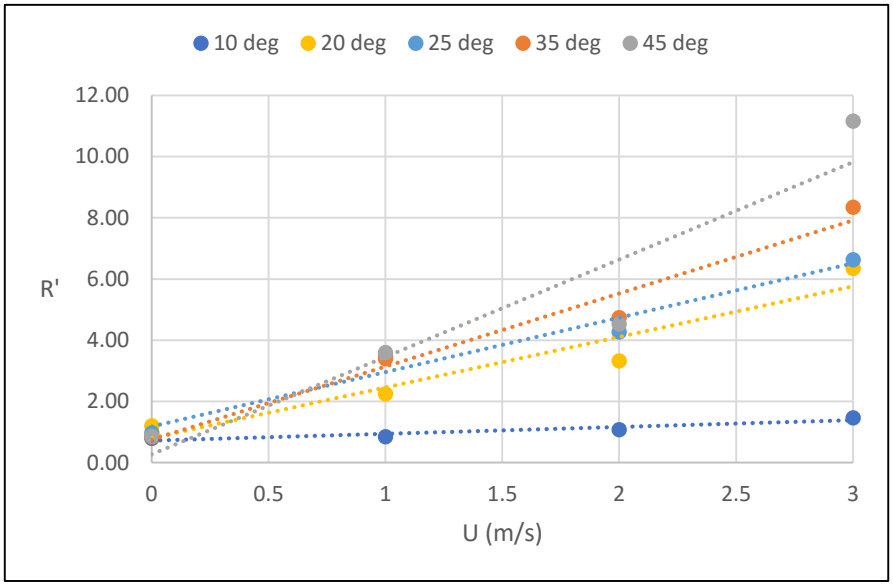

Fig 6-8The average NDROS for the different inclinations with different wind velocities in the up ridge direction on the leeward face

Form Fig 6-8 we can see the average NDROS for the different inclinations considered in our tests with the three different velocities we have and of course the case where no-wind condition (0 m/s), starting with no-wind case we can see that the values are very close to each other so the variation on the ROS is not very large with the slope effect only comparing to the variation of the ROS after adding the wind effect. For the three wind velocities we can see from the linear fitted line between the velocities for each inclination that the slope increase with increasing the inclination, so it's very clear that the inclination of the ridge changes the ROS dramatically, if we compared at 3 m/s the 45-deg inclination with the 10-deg inclination we will find it more than five times the ROS of the 10-deg. Relatively we can see a big difference between the 10-degree inclination and just the next one 20-deg which is due to the extreme behavior of the lateral spread on the leeward face (the fire channelling) where it didn't happen on the 10-deg but higher than that starting from 20-deg it always happened on the up ridge direction. We will Discuss the lateral spread on a dependent point later. However, if we studied the slope of the lines for the inclinations where there is a lateral spread happened (20, 25, 35 and 45) we can find the slopes are: 1.65, 1.77, 2.38 and 3.18 respectively, if we looked to the increasing in the slope as percentage we will find the increasing between 20-deg and 25-deg is about 7% and between 25-deg and 35-deg is about 34% and finally between 35-deg and 45-deg is about 33%.

For the dynamic ROS it's presented on the following three kind of plots, D'-t plot for each inclination with the different velocities, R'-t for each inclination with the different velocities and D'-t plot for each velocity with the different inclinations.

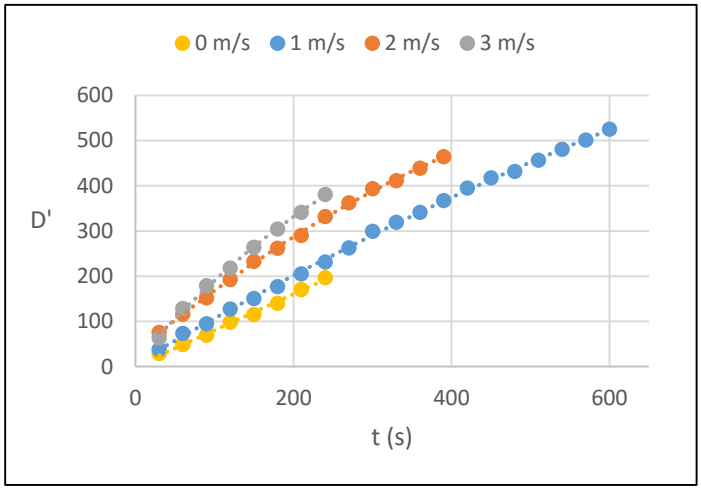

a. 10-degree inclination

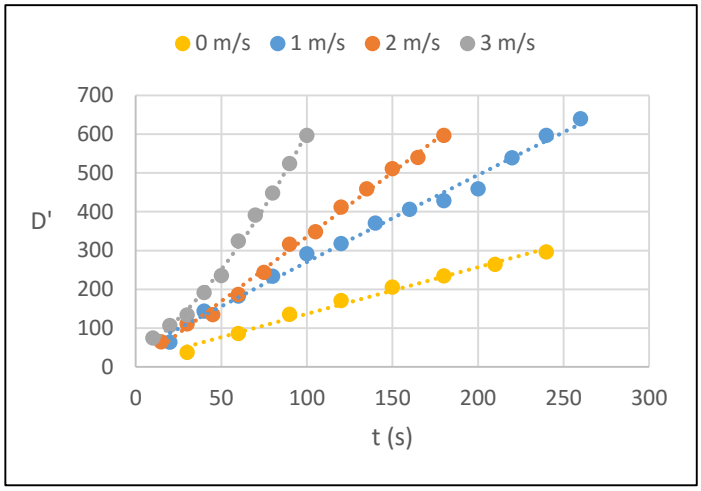

b. 20-degree inclination

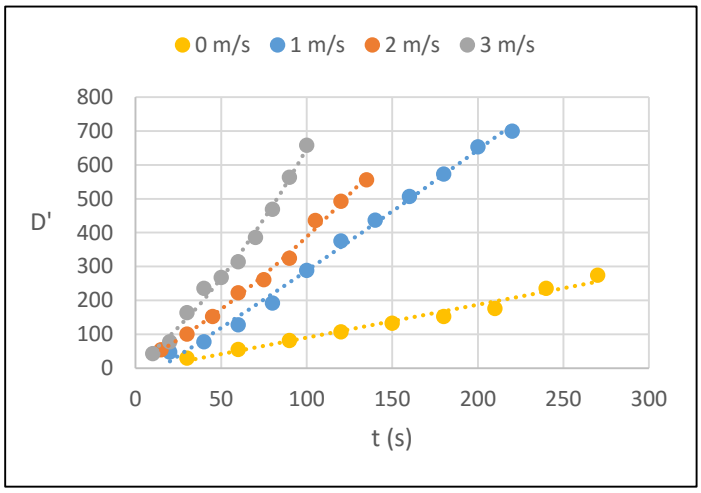

c. 25-degree inclination

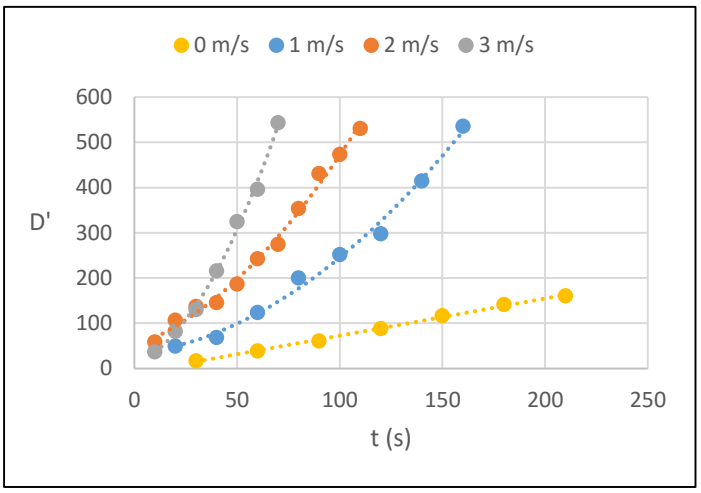

d. 35-degree inclination

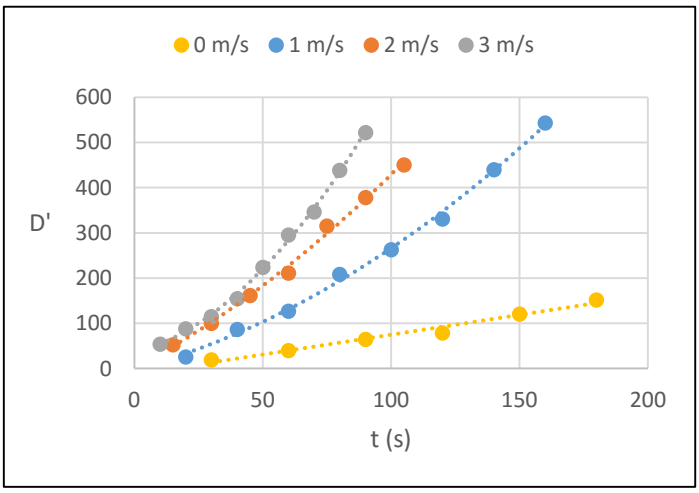

d. 45-degree inclination

Fig 6-9the non-dimensional distance versus the time representing the dynamic spread of the fire in the up ridge direction for different inclinations

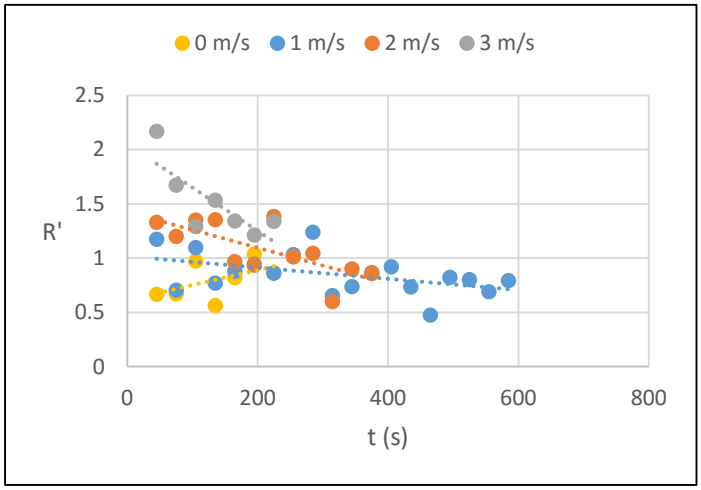

a. 10-degree inclination

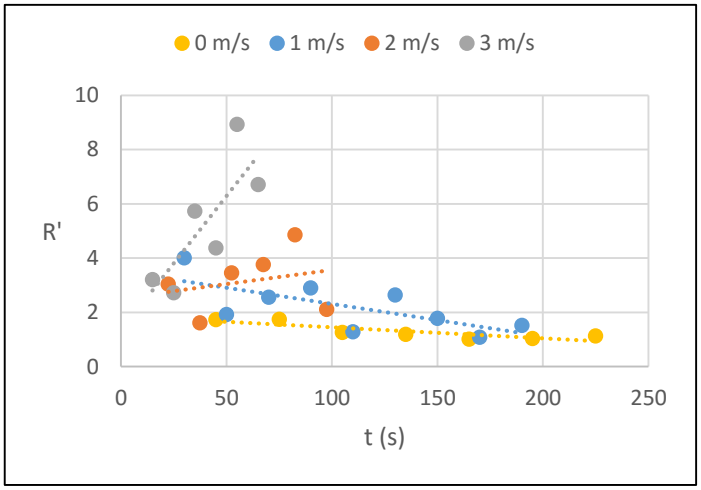

b. 20-degree inclination

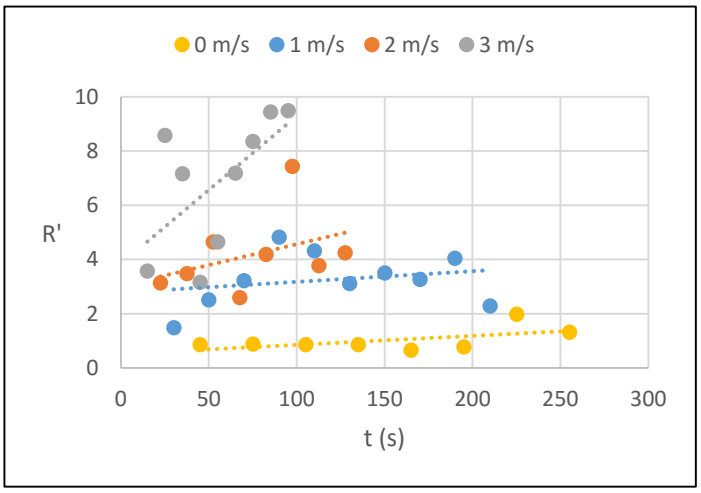

c. 25-degree inclination

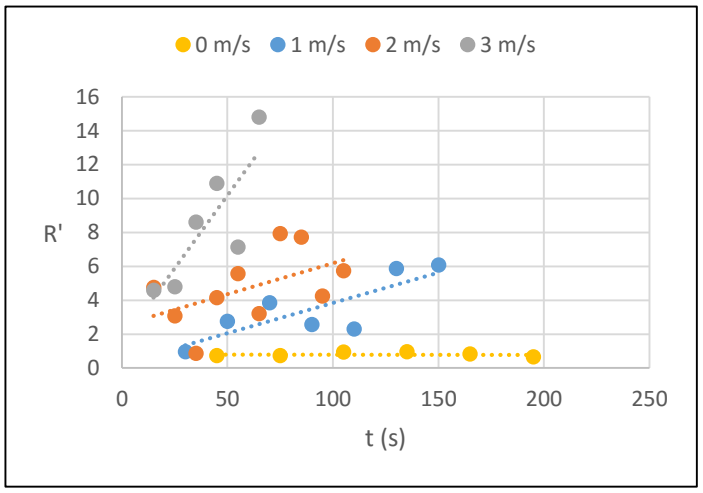

d. 35-degree inclination

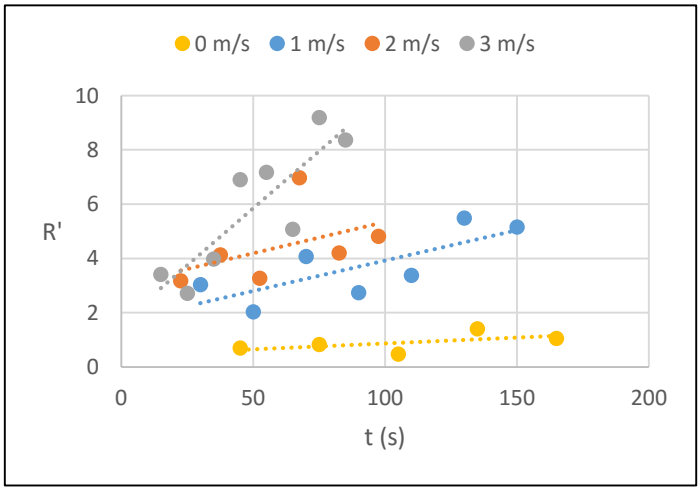

d. 45-degree inclination

Fig 6-10the NDROS versus the time representing the dynamic ROS of the fire in the up ridge direction for different inclinations

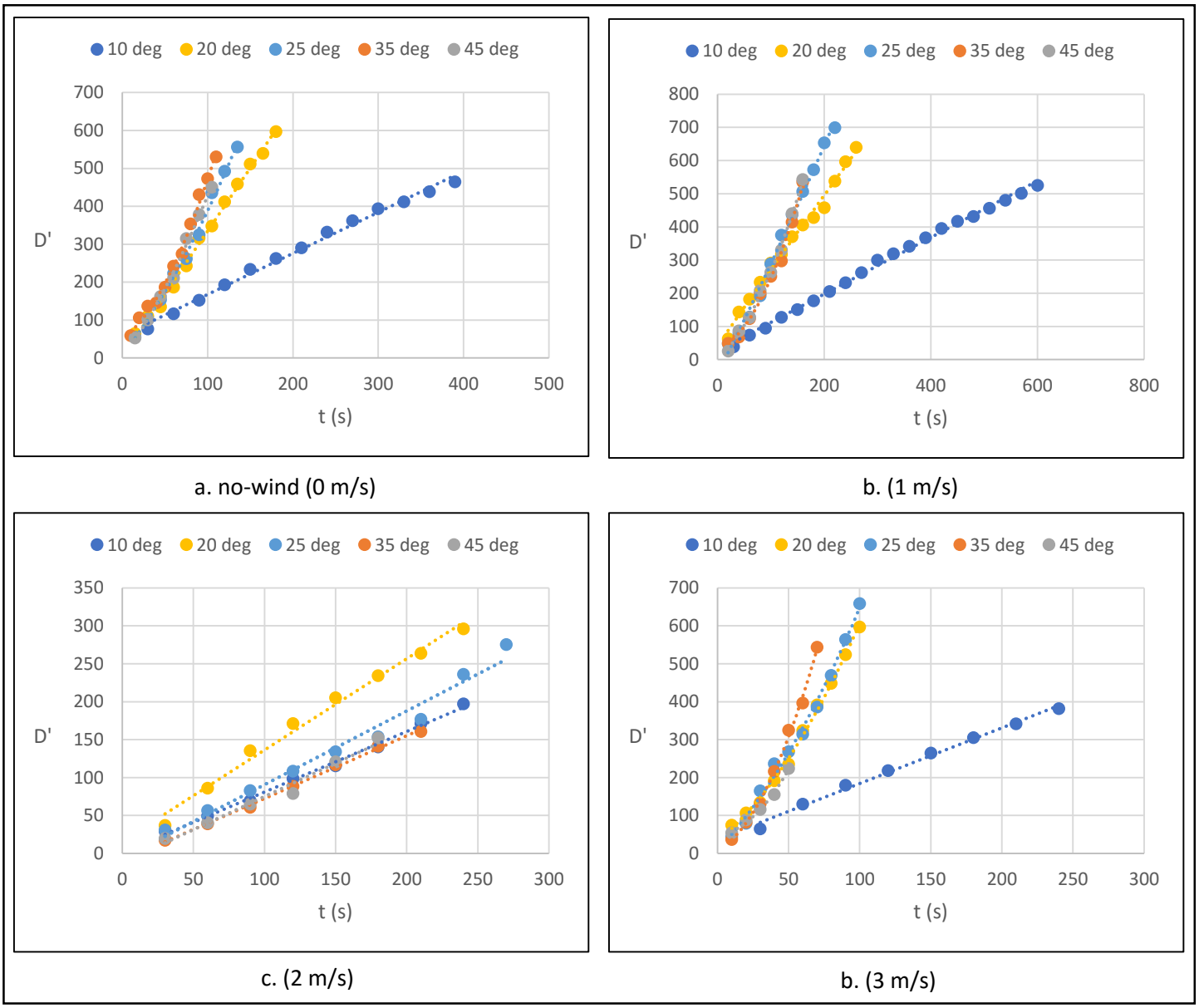

Fig 6-11 the non-dimensional distance versus the time representing the dynamic spread of the fire in the up ridge direction for different velocities

On Fig 6-9 we can see the behavior of the fire spread dynamically for the five inclinations each one with the different wind velocities, the fitted curves are always from second order degree except for the no-wind case the curve is linear, on these plots we can see there is a second order behavior for the spreading appearing and as mentioned before that there is a lateral spread happening in all the inclinations with all wind velocities except for the 10-deg inclination, indeed, the plots presenting this lateral spread happening on the up ridge direction except for the 10-deg where it's a normal spread happening on that direction, see Fig 6-25, Fig 6-28, Fig 6-30 and Fig 6-31 presenting the propagation map of the fire front on different tests showing it. On Fig 6-10 we can see also the same inclination presented with same wind velocities but with NDROS versus the time.

Starting from the 10-deg inclination we can find the ROS for the no-wind case is increasing with the time a little but we can consider it as constant, with wind we can see that the ROS is decreasing with time and the rate of this decreasing is higher as we increase the velocity but generally the values of the ROS is higher on the higher velocities. For the higher inclinations where the lateral spread started to happen we can see from the D-t plots that there is a second order behavior exist in most of the tests which means that ROS is increasing with time and it's clear on Fig 6-9 with R-t plots, this increase in the ROS we can see it starting to happen with 3 m/s at 20-deg inclination and then at 25-deg inclination it happened with 2 and 3 m/s, for higher inclinations, 35 and 45-deg it happened with all the velocities, on Fig 6-10 (c, d and e) we can see how much is the ROS is increasing with the time, especially for the highest tested velocity (3m/s) we can find the ROS when the fire reach the end of the fuel bed is about the double of the ROS when the fire started to propagate latterly.

For the R-t plots (Fig 6-10) we can see generally the ROS is oscillating randomly from time step to another but as an overall there is a trend in the values and we can get this trend from the linear fitted line between them. As comparison between the behavior of the fire on the different inclinations with the same wind velocity we can deduce from Fig 6-11 that for the same wind velocity the behavior doesn't change a lot and the values of the ROS are close except for the10-deg inclination as we can see the values are much less, actually, this 10-deg inclination can show us clearly in a comparison to the others the dramatic change in the ROS caused by the lateral spared phenomenon.

Down Ridge Direction

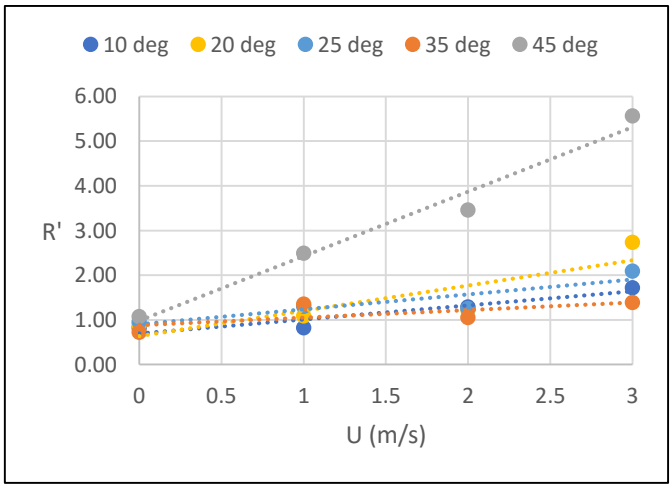

Fig 6-13The average NDROS for the different inclinations with different wind velocities in the down ridge direction on the leeward face

Fig 6-12 Image showing the fire front shape on the up ridge direction, image from (3D2)

From Fig 6-13 we can see the average NDROS for the different inclinations with different wind velocities in the down ridge direction and it shows us that the values are very close to each other even for 2 m/s we can see a match almost between the values of the ROS, it's very important to mention that there is no lateral spread behavior happening on this direction as the up ridge direction, so in a comparison between the up ridge and down ridge spreads we will see the down ridge is less, for 2 m/s as an example, the NDROS varying between 4 and 6 on the up ridge direction and mean while it's varying between 1 and 2 on the down ridge direction. For 45-deg inclination we can see that it has high values of ROS relatively, this spread actually didn't happen because of the fire dynamics on the leeward face but it's because there is an extreme behavior happening on the windward face has a high flame height and propagating on that direction, this extreme behavior dragged the fire front on the leeward face and as a result we had relatively high ROS. In a matter of fact, the same behavior was noticed also for 35-deg inclination but it was less intense and didn't appear on the average ROS but we will see it on following dynamic behavior results.

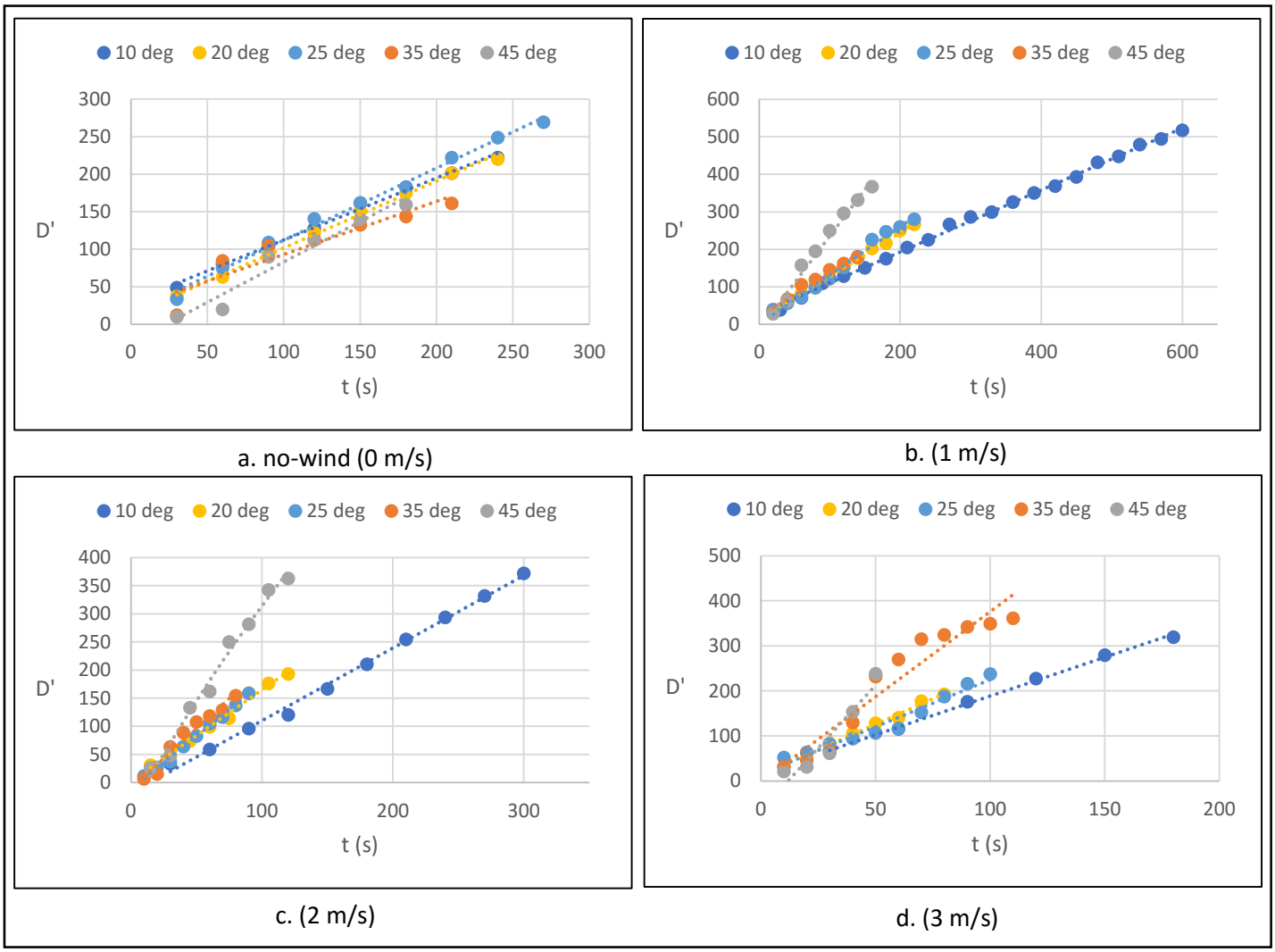

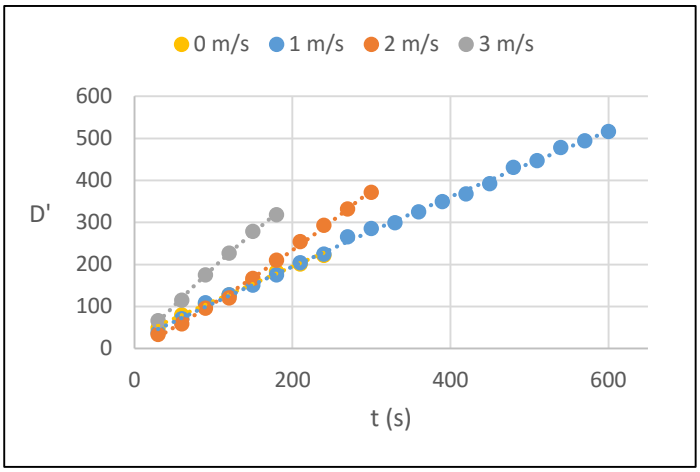

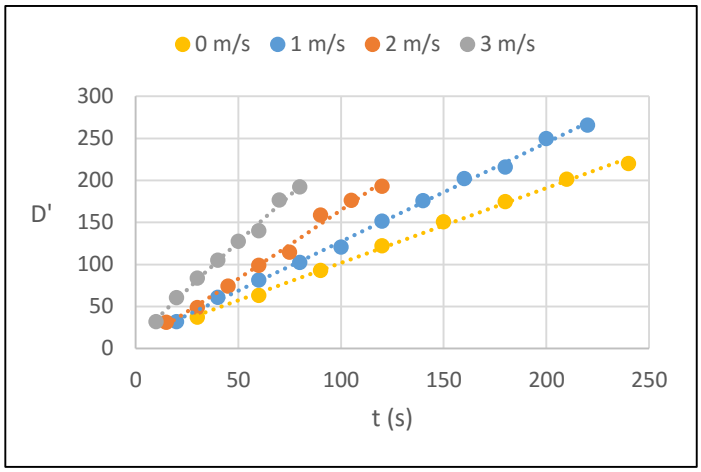

Fig 6-14the non-dimensional distance versus the time representing the dynamic spread of the fire in the up ridge direction for different velocities

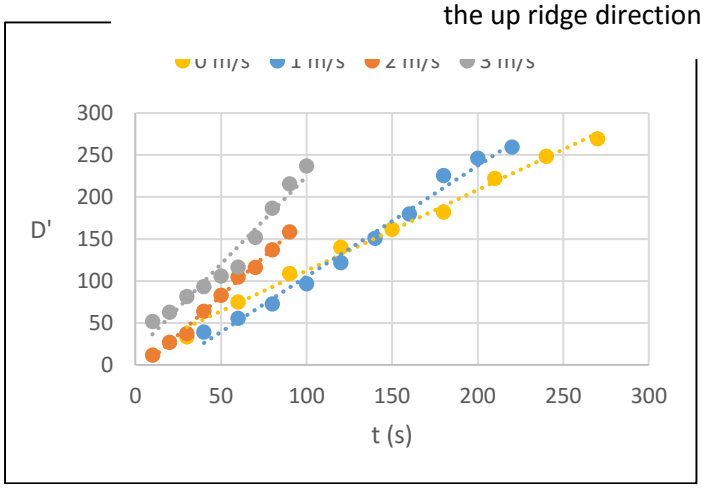

c. 25-degree inclination

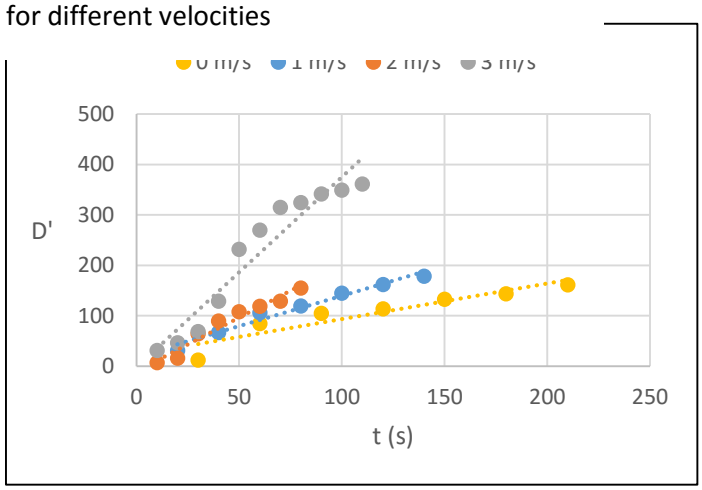

d. 35-degree inclination

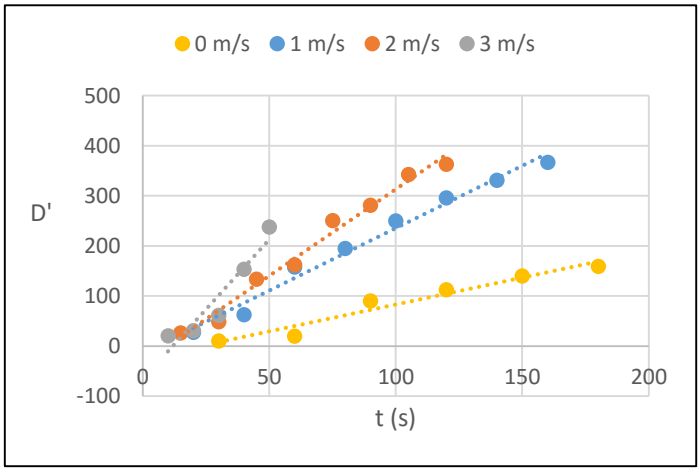

d. 45-degree inclination

Fig 6-15the non-dimensional distance versus the time representing the dynamic spread of the fire in the down ridge direction for different inclinations

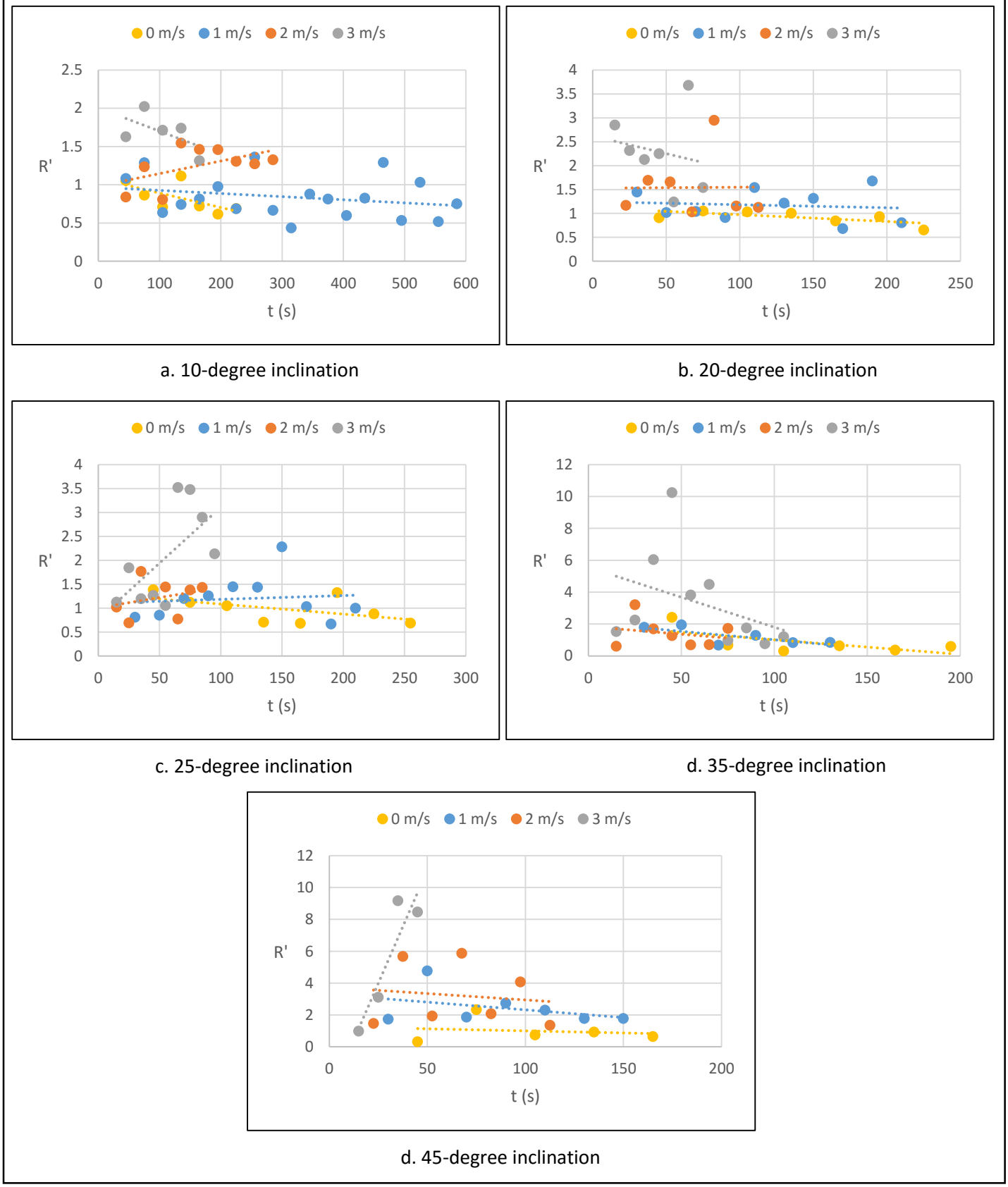

a. 10-degree inclination

b. 20-degree inclination

c. 25-degree inclination

d. 35-degree inclination

d. 45-degree inclination

Fig 6-16the NDROS versus the time representing the dynamic ROS of the fire in the down ridge direction for different inclinations

For the dynamic behavior of the fire that we can see through the plots on Fig 6-15 and Fig 6-16, we can notice that the data is fitted with a linear curve where we can see it's the general behavior of the fire since the linear fitting describing the values quit good except for some tests like with the 35 and 45-degree inclinations with high wind velocities where the fire front have been dragged by the fire front on the windward face as we mentioned before, the dragging behavior appeared clearly on the 35-deg inclination with 3 m/s wind speed (Fig 6-15 (d)) where the spread started to increase with relatively normal slope and then there is a four continues point have a slope much higher and this is where the dragging was happening exactly, then the slope becomes normal again as the slope in the beginning, these three stages didn't appear in the 45-deg inclination since this dragging behavior was happening from the beginning till the end of the fuel bed so it appeared with a normal behavior (slope) but we saw that the average ROS has high values and we can see it also in Fig 6-16 where there is a comparison between the inclinations for each velocity.

For the R'-t plots on Fig 6-16 we can see the slopes on most of the test showing that the ROS's have trend either constant or decreasing a little with the time except the cases when the fire front was dragged. For the comparison between the inclinations plots for each velocity (Fig 6-14) the values of ROS for the same velocity is generally close as we saw on the up ridge direction except again for the dragged fire fronts or for the 10-deg inclination as we saw also on the up ridge direction

Downslope Direction

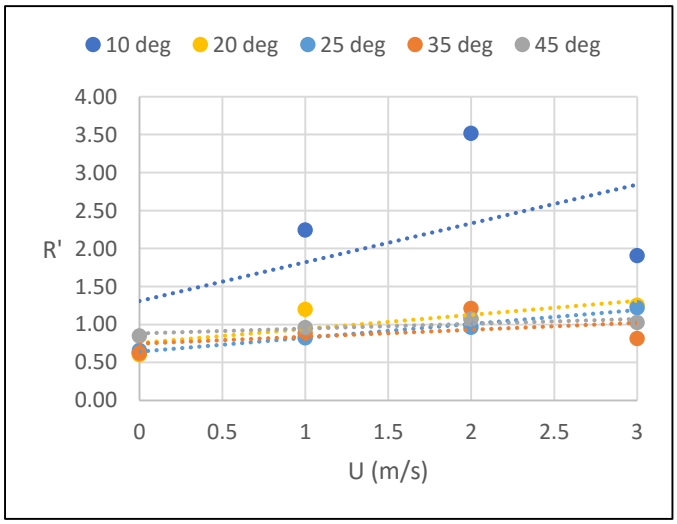

Fig 6-18The average NDROS for the different inclinations with different wind velocities in the down slope direction on the leeward face

Fig 6-17Image showing the intense fire behavior on the windward face caused by the wind sliding effect, image from (3D12)

On the downslope direction in Fig 6-18 we can see as an overall there is no big variation between the values either if we changed the slope or the velocity except for 10-deg inclination, in all the inclination with no-wind case we can see the effect of the slope alone, so the values of NDROS are less than one which means the spread is slower than the basic ROS (R_o) with no-wind and no-slope conditions, with the wind, we can see the ROS is almost independent of the wind velocity or the inclination and it's around 1, this is happening since we have a conical vortex as we saw before on the wind tunnel and the CFD simulation, this vortex makes a wind draft to up slope as it rotates and it's against the fire spread direction (downslope), the vortex change its intensity with the change of the wind velocity and as a result of that we had an independent ROS on the down slope direction. For the 10-deg inclination the conical vortex as we saw before dosn't exist and the fire front on the down slope direction is subjected directly to the free stream of the wind and as a result it behaves as a spread on a flat plane (no-slope condition).

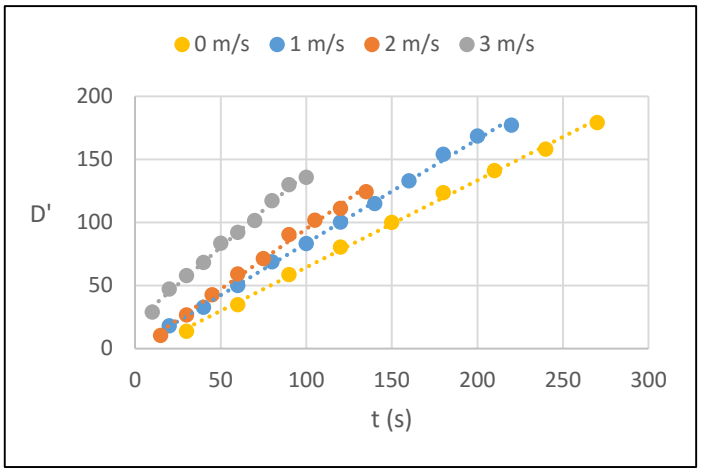

Fig 6-20The D'-T plot for 25-deg inclination as the dynamic spread in the down slope direction

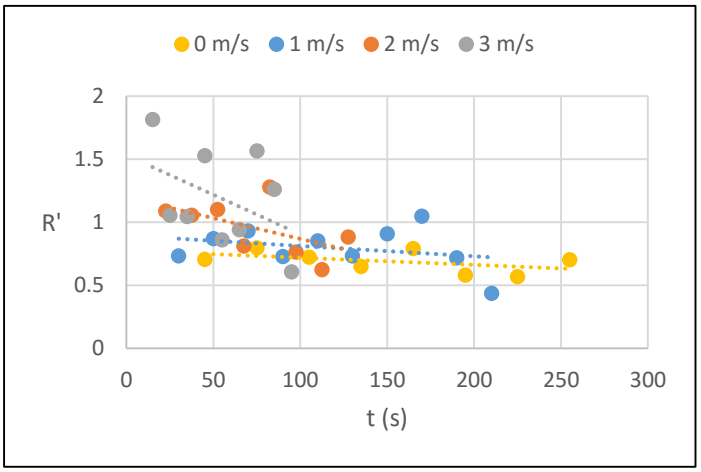

Fig 6-19The R'-T plot for 25-deg inclination as the dynamic ROS in the down slope direction

To analyze the dynamic spread of the fire front on the down slope direction we presented above only one case of 25-deg inclination since the other cases are quite similar and there is no any extreme behavior of the fire on this direction. For the D-t plot on Fig 6-20 we can see the values have linear evolution and can be fitted with a linear line and for the different velocities we have almost the same slope of this line with a small increasing in the values from velocity to another, on Fig 6-19 we can see the R-t plot where there is small decreasing in ROS values with time where the ROS starts on the leeward face with a maximum value and decreasing as we are going downslope, but as an overall the ROS is about 1. On Fig 6-21 we can see a 3D representation of the ROS over the whole leeward face where we can see the difference in the ROS's in the different directions.

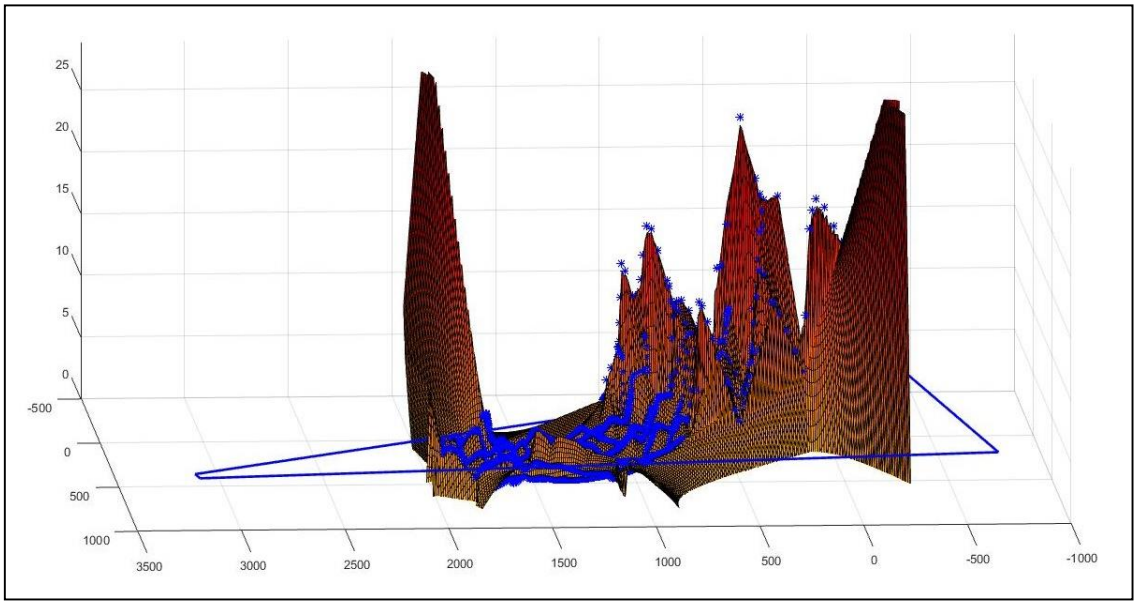

Fig 6-21 An iso-surface presentation of the NDROS for test 3D3 which and identical behavior on the leeward face. The ROS is on mm/s

6.2.1.2. The Windward Face

A common behavior of fire on the leeward face for inclinations lower than 35 that the fire starts to spread from the ignition point in upslope direction and once it reached the ridgeline it starts to propagate in the up and down ridge directions for a small distance and then distinguish leaving a burned area with a typical V shape (See Fig 6-22), however in the cases where the fire have distinguished we will not present its ROS's in the up and down ridge directions since it only propagated for a relatively very small distance.

Up ridge direction

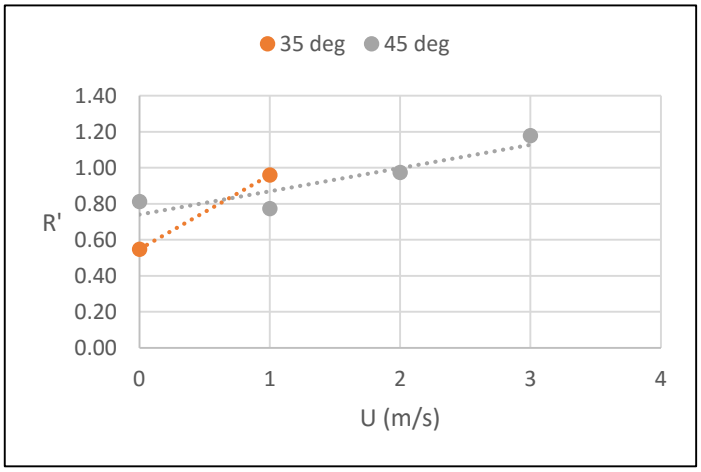

Fig 6-23 The average NDROS for the different inclinations with different wind velocities in the up ridge direction on the windward face

Fig 6-22 a typical shape of burned area on the windward face for inclinations less than 35-deg, the image is from test (3D3)

On Fig 6-23 we can see the average ROS for the up ridge direction for 45-deg with all the velocities and 35-deg with 1 m/s only since the fire was distinguished with 2 and 3 m/s and as well for the lower inclinations, however, we can see that the values of the ROS for no-wind case that it's lower than 1 or lower than the basic ROS (R_o) so the effect of the slope on the up ridge direction is not very strong, with applying the wind the values starts to increase slightly as we increase the wind velocity but generally it's also around 1 also.

As the fire have distinguished in most the cases and even if it didn't we don't have any extreme behavior or effect so we will not present the dynamic spread of the fire on this direction.

Down slope direction

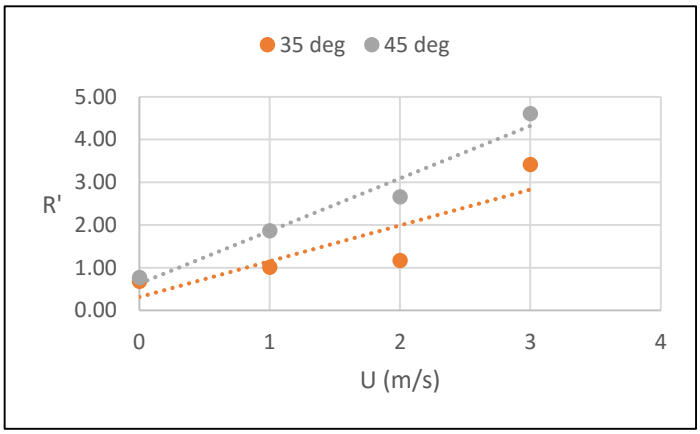

Fig 6-24 The average NDROS for the different inclinations with different wind velocities in the down ridge direction on the windward face

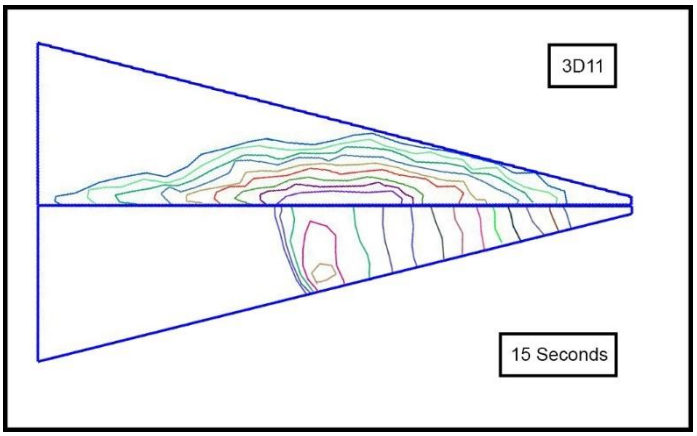

Fig 6-25 Fire front propagation map for test 3D11 (45-deg, 2m/s)

On the down slope direction as we see on Fig 6-24 the fire didn't distinguish on the 35-deg inclination with 2 and 3 m/s as on the up ridge direction but it did with the lower inclinations than 35-deg, however, generally we can see much higher ROS than the up ridge direction noticing that this direction is considered to be down slope not up slope as the up ridge direction. With no-wind we can see the values are less than 1 as usual and with the wind the ROS is increasing with the velocity and the inclination. On these two inclination and on this direction the fire have relatively high ROS that we can call it even extreme behavior since it's spreading with this ROS's on direction different than the wind direction, this behavior is taking place because of the so called "wind sliding" effect on this area that we have saw and discussed before on the wind tunnel and the CFD simulation sections, now we can see its result where the whole fire front propagated with high ROS on the down ridge direction and we should notice that it's not only a part of the fire front near the ridgeling as it's happening on the lateral spread on the leeward face. See Fig 6-25 for the propagation map of 45-deg with 2 m/s.

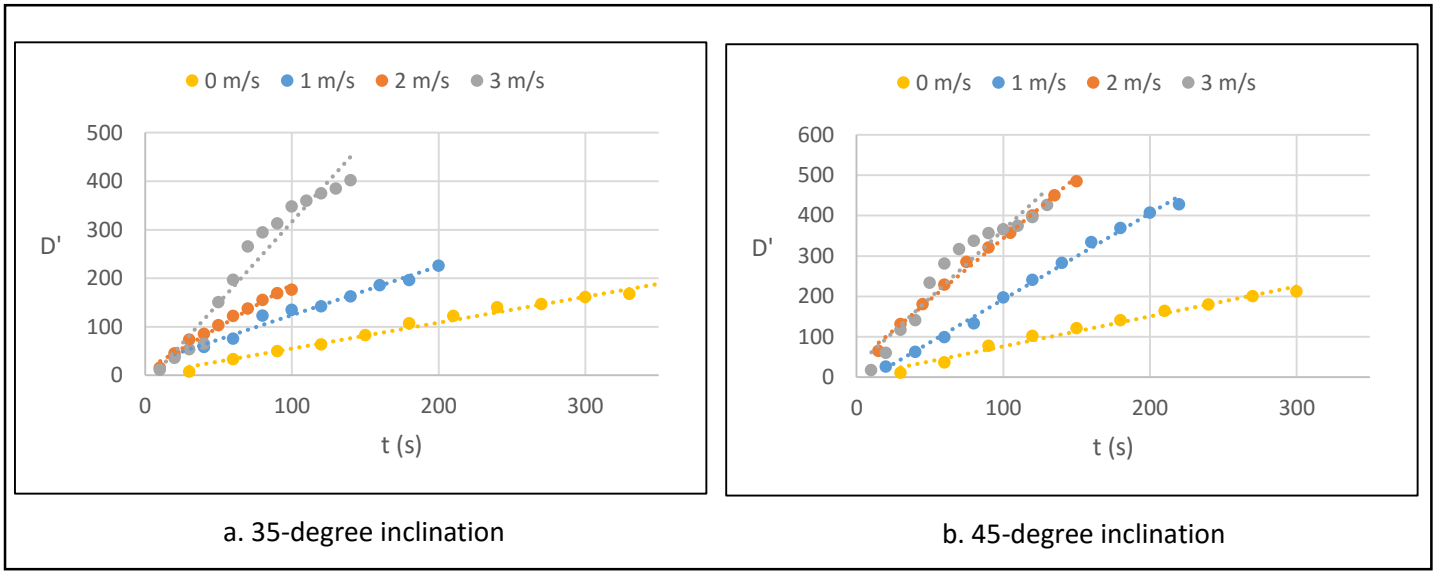

a. 35-degree inclination

b. 45-degree inclination

Fig 6-26 the non-dimensional distance versus the time representing the dynamic spread of the fire in the down ridge direction for different inclinations

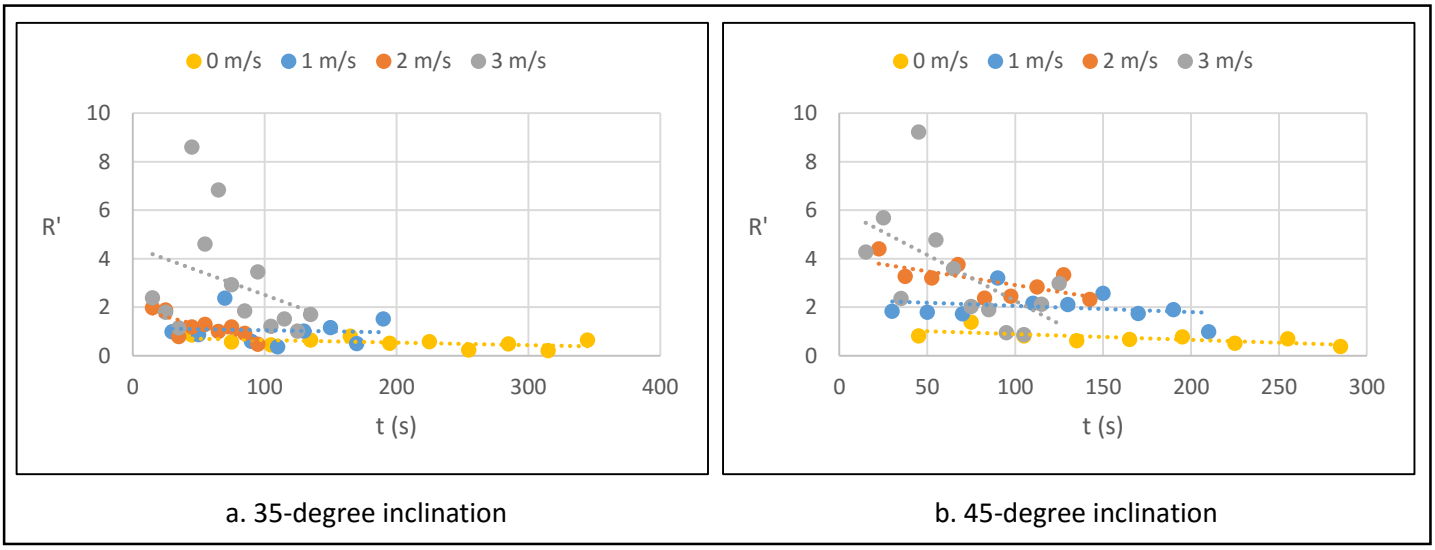

a. 35-degree inclination

b. 45-degree inclination

Fig 6-27 the NDROS versus the time representing the dynamic ROS of the fire in the down ridge direction for different inclinations

In a dynamic description of the fire spread from Fig 6-26 we can see it's taking generally a linear behavior and on Fig 6-27 we can see the ROS is higher for higher velocities, from the D-t and R-t plots we can see that with 3 m/s there is a behavior on the two inclinations 35 and 45-degree where a peak in the ROS is happening in the middle, this is the clear result of the wind sliding effect that mentioned before on the dynamic representation, however the overall trend of the ROS is decreasing with the time since the wind sliding effect is getting lower as we are approaching more the end of the ridge on the down ridge direction.

Up Slope Direction

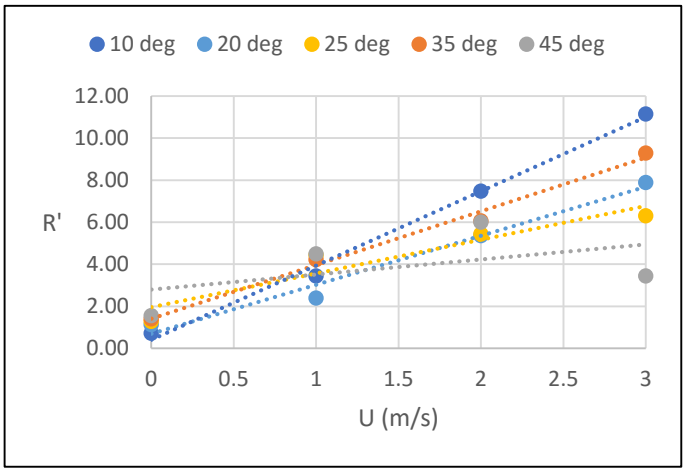

Fig 6-29 The average NDROS for the different inclinations with different wind velocities in the up slope direction on the windward face

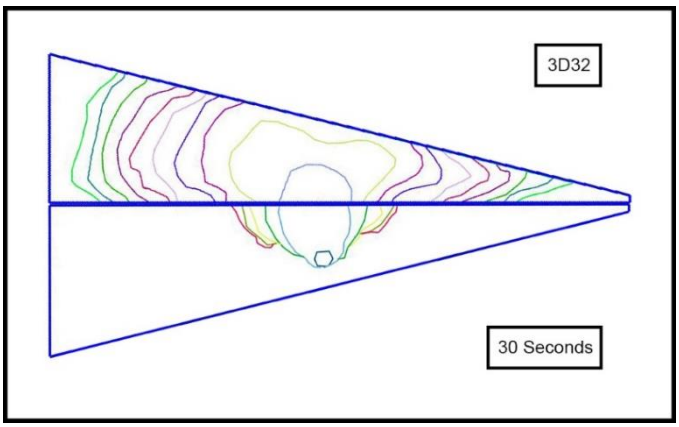

Fig 6-28 Fire front propagation map for test 3D32 (10-deg, 3m/s)

On the up slope direction from Fig 6-29 we can see the average ROS where the fitted lines have similar slope except for the 45-deg inclination where we have a drop on the ROS for 3 m/s, in fact it's an expected behavior since the wind's total velocity component has a direction more parallel to the ridgeline in down ridge direction as we saw on the wind tunnel results and this parallel component is stronger than the perpendicular component of the velocity, and as a result for this particular case (45-deg, 3m/s) we have an average NDROS on the up slop direction about 4 while it's about 5 on the down ridge direction.

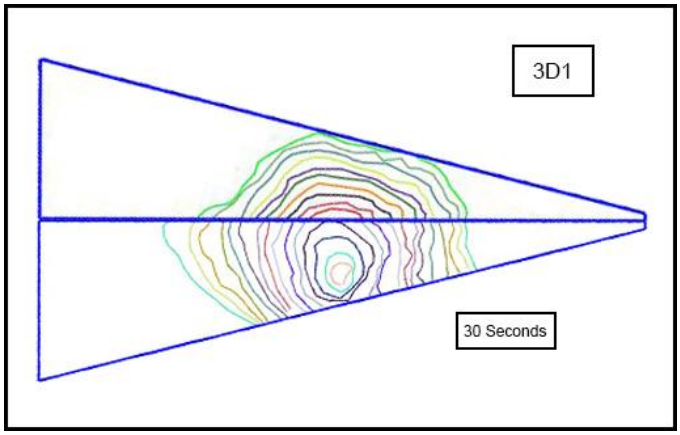

Fig 6-31 Fire front propagation map for test 3D1 (25-deg, 0m/s)

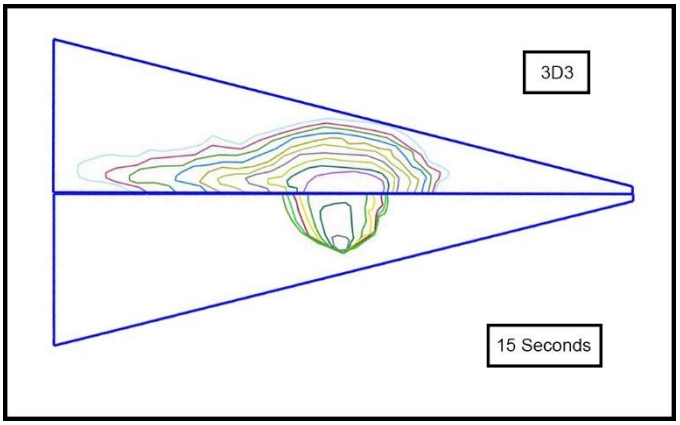

Fig 6-30 Fire front propagation map for test 3D3 (25-deg, 2m/s)

6.2.2. Second Group of Tests

On this group of tests, we are changing the orientation of the ridge between (-20, -10, 10, 20) and for each one a test with no-wind condition and another with wind condition (2 m/s) was carried out, all the tests have fixed inclination at 35-deg

6.2.2.1. Leeward face

Up ridge direction

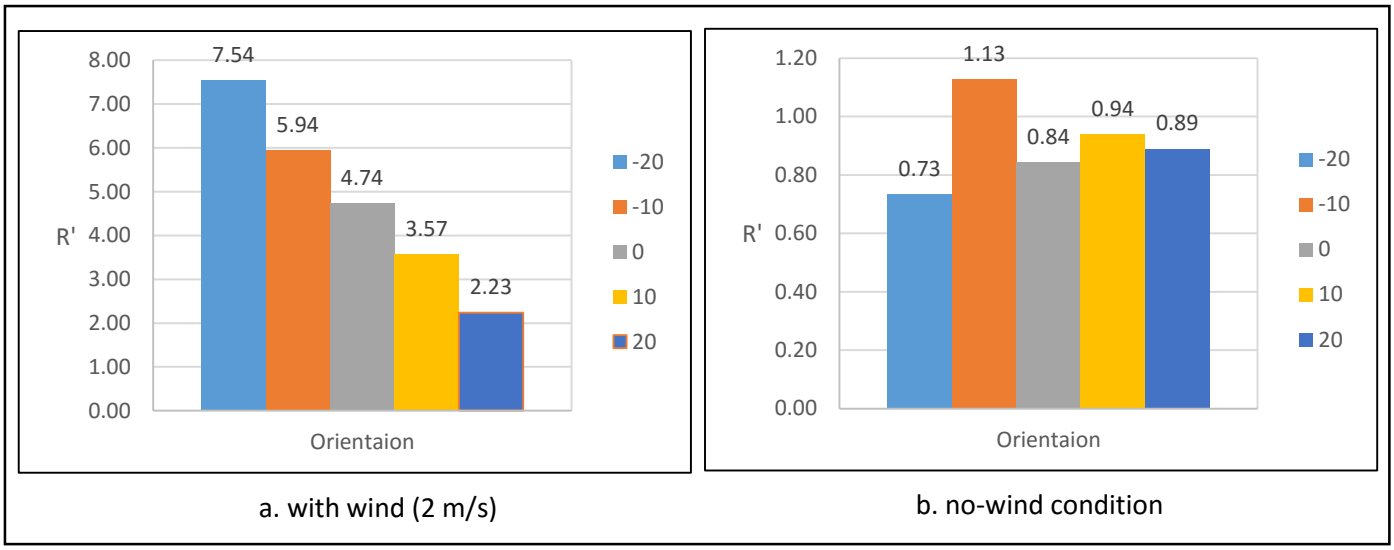

a. with wind (2 m/s)

b. no-wind condition

Fig 6-32 The average NDROS for the different Orientations with wind and no-wind conditions in the up ridge direction on the leeward face

On Fig 6-32 we can see a representation of the average ROS on the up ridge direction with and without wind for the different orientations, starting with no-wind condition we can that there is a slight difference between them which is a result of the changes happening in the air entrance conditions to the fire as we change the ridge orientation, with wind we can see an almost constant difference happening between the different orientations where if we ordered the tested orientation's form the highest negative to the highest positive we can see the ROS has the highest value at -20-deg and decreasing gradually until we reach the 20-deg orientation. This is showing us that the lateral spread or the "fire channeling" is more extreme if we tilted the triangle ridge to the negative direction (CW) and less extreme if we tilted the ridge to the positive direction (CCW).

On Fig 6-33 and Fig 6-34 we can see the dynamic behavior of the fire on this direction, we can notice a relativley low values for 20-deg orientaion, but for the 0, -10 and -20 we can see the values are increasing respectively and having the second order behavior on the D-t plot, on the 10-deg orientation there is realitvly a stange behavior where the values of NDROS is dereasing with time, it's worth to mention that for this orinetiona we will have the ground edge of the windward face almost perpendicular to the wind direction.

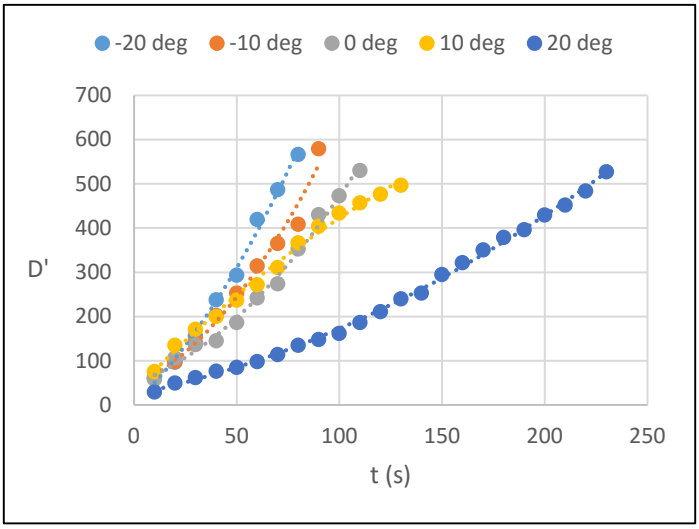

Fig 6-33 The D'-T plot for different orientations with wind as the dynamic spread in the up slope direction

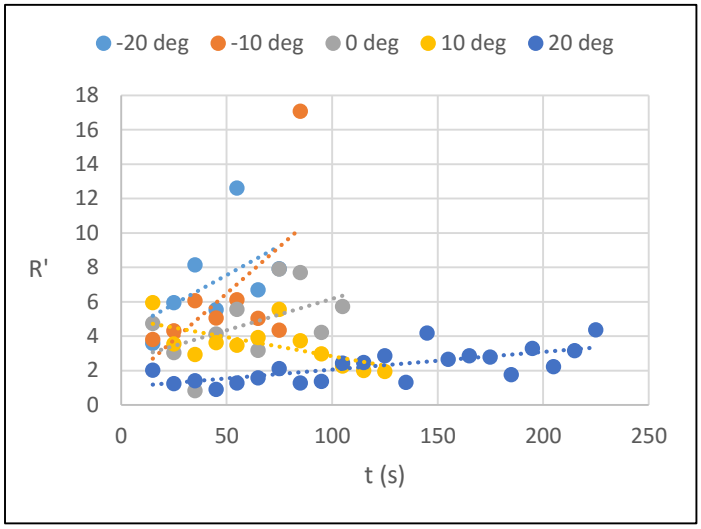

Fig 6-34 The R'-T plot for different orientations with wind as the dynamic ROS in the up slope direction

Down Ridge Direction

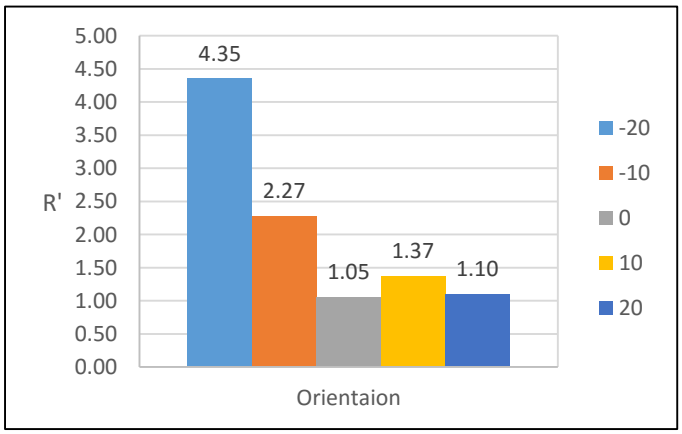

Fig 6-36 The average NDROS for the different Orientations with wind condition in the down ridge direction on the leeward face

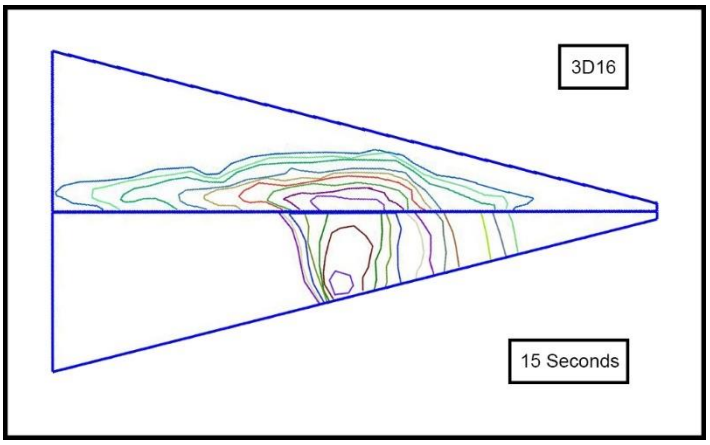

Fig 6-35 Fire front propagation map for test 3D16 (35-deg, -20-deg, 2m/s)

On the down ridge direction, we can see from the representation of the average ROS on Fig 6-36 that the ROS values are increasing form 0 to -20-deg orientation, this increasing is due to the dragging of the fire front by the fire front on the windward face as it propagates fast on the down ridge direction (Fig 6-35) as will be seen on the next point, we have saw also the same behavior before with 45-deg inclination, for the positive orientations we find a slight increase with 10-deg and then for 20-deg we have almost the same value as the 0-deg orientation, however the positive ordinations doesn't have any extreme behavior since its ROS values are around one. (Fig 6-37)

Down Slope direction

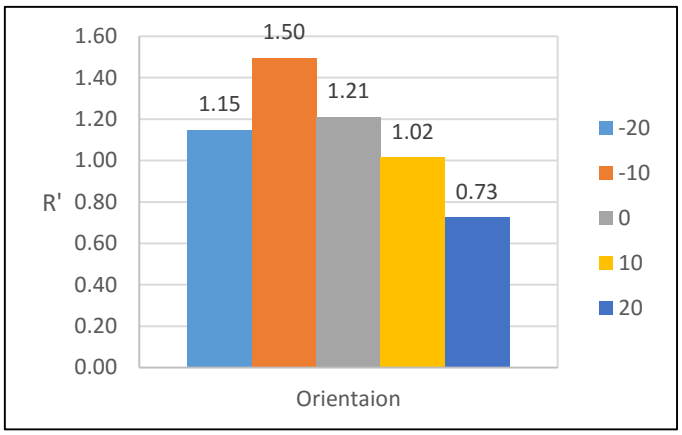

Fig 6-38 The average NDROS for the different orientations with wind condition in the down slope direction on the leeward face

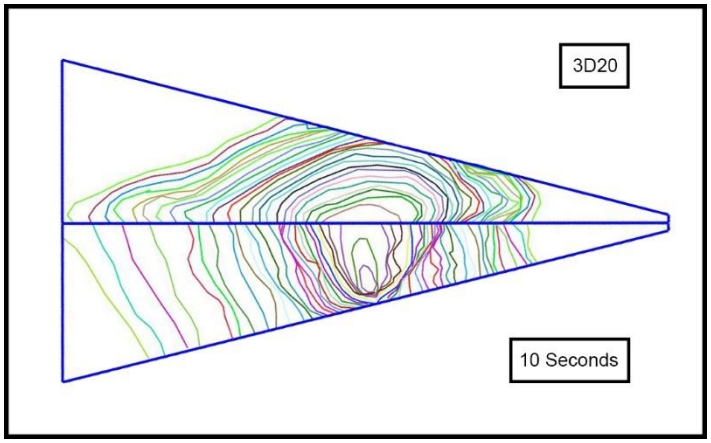

Fig 6-37 Fire front propagation map for test 3D20 (35-deg, 20-deg, 2m/s)

For the down slope direction, we can see with different orientations under wind that we have a high value at the -10-deg and decreasing until 20-deg, while for -20-deg we have a value very close to the 0-deg orientation. This behavior is very hard to explain since we have a complex flow on the leeward face that is not easy to be interpreted, the conical vortex is getting deflected with change of the orientation but we had an idea about that from the CFD simulation.

6.2.2.2. The Windward Face

Up Ridge Direction

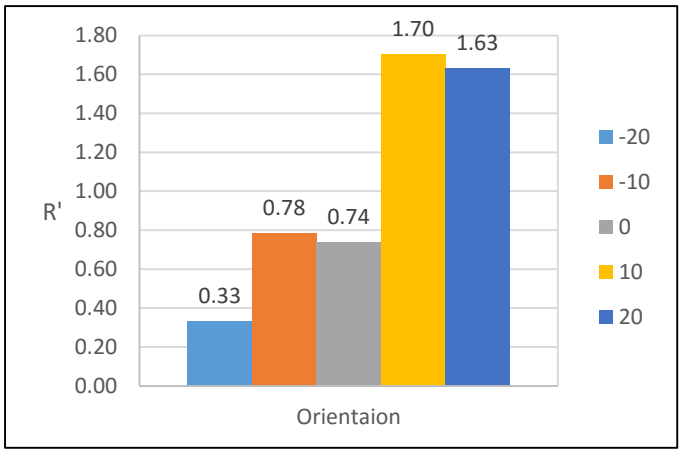

Fig 6-40 The average NDROS for the different orientations with wind condition in the up ridge direction on the windward face

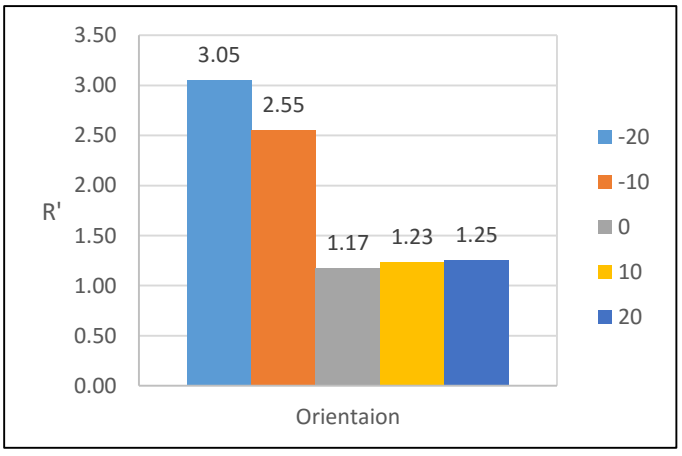

Fig 6-39 The average NDROS for the different orientations with wind condition in the down ridge direction on the windward face

From Fig 6-40 we can see the positive orientations are having a high values of ROS and the negatives have lower values of ROS comparing to the 0-deg orientation, the negatives have low values since the wind sliding behavior is happening toward down ridge direction and as we increase the angle on the negative the result of the behavior is more clear where the ROS is lower, for the other orienting direction, the positive, the ROS is higher is the wind sliding behavior doesn't exist and even the wind may slid on the up ridge direction as we saw on the wind tunnel tests.

Down Ridge Direction

On the down ridge direction as we see from Fig 6-39 that we have almost the reversed behavior of the up ridge direction where the negative orientations have higher values because the wind sliding behavior and for the positive orientations we have almost the same ROS as the 0-deg orientation, for the negative direction we find as the angle value is increasing the ROS increase also.

From the dynamic behavior showed on Fig 6-41 and Fig 6-42 we deduce that the fire is spreading on down ridge direction with increasing trend on the ROS with the time for the negative orientations, although that it starts with relatively low values and then a peak is happening followed by decreasing in the ROS as we are approaching the end of the ridge. For the positive orientations we have generally lower values and the fire is spreading with almost a constant ROS.

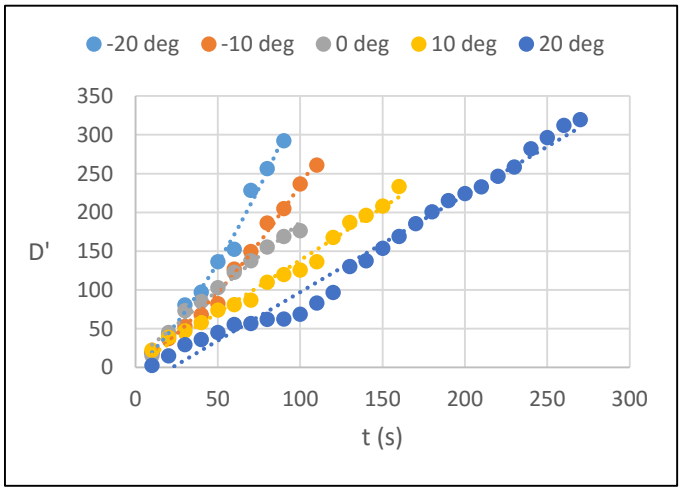

Fig 6-41 The D'-T plot for different orientations with wind as the dynamic spread in the down slope direction

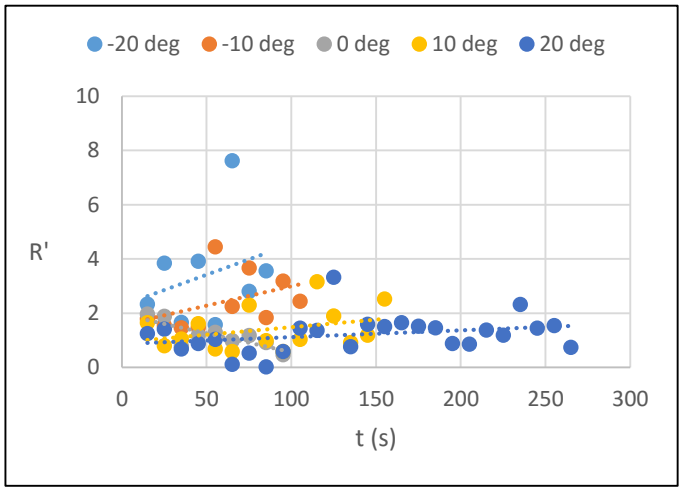

Fig 6-42 The R'-T plot for different orientations with wind as the dynamic ROS in the down slope direction

Up Slope Direction

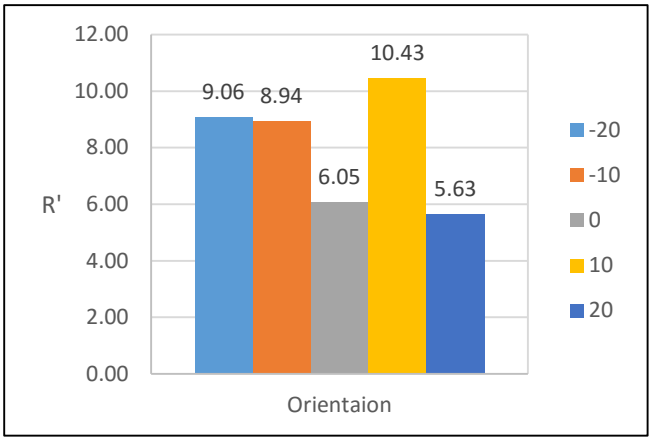

Fig 6-44 The average NDROS for the different orientations with wind condition in the up slope direction on the windward face

Fig 6-43 Image showing the extreme fire behavior on the down ridge direction and the height of the flame on the windward face, image from (3D18)

On the up slope direction we have generally a higher average ROS as we see on Fig 6-44 for the negative orientations than the no-oriented case and we have almost the same value for both of them (-10, -20), the value of the 10-deg is also close to them but for 20-deg it's the lowest between all of them. We should mention also that the propagation direction was effected by the orientation it become more to the down ridge direction for the negative orientations instead of being exactly perpendicular to the ridgeline, for the other orienting direction (the positive) the propagation direction was tilted a little also to the up ridge direction. see on Fig 6-44.

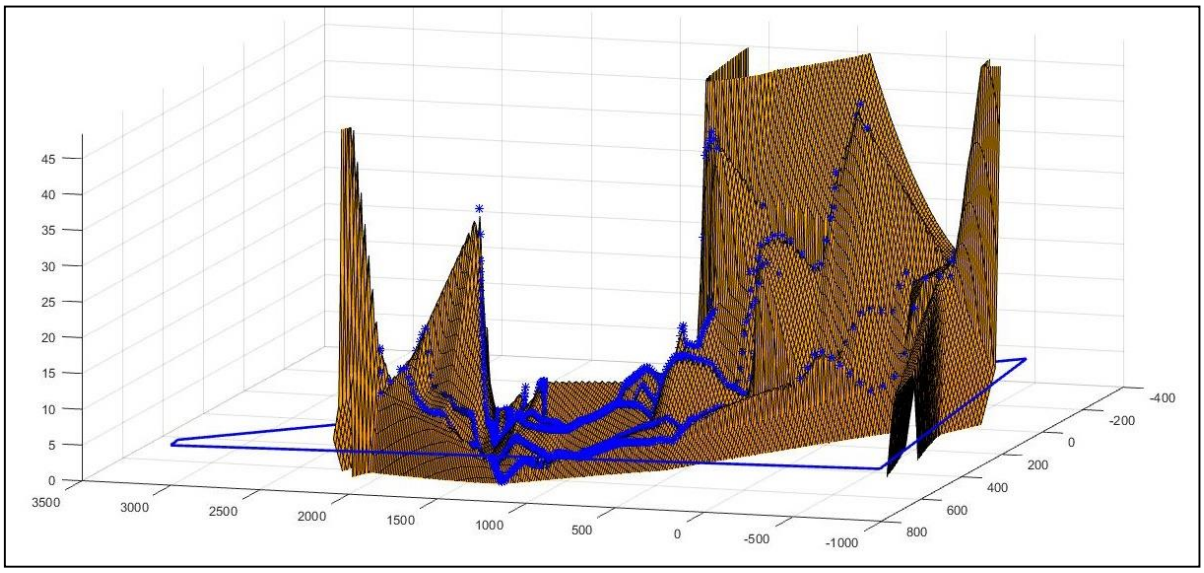

Fig 6-45 An iso-surface presentation of the NDROS for test 3D16 on the leeward face.

6.2.3. Third Group of Tests

On this group we are changing the ignition point location where we have three locations: A, B and C (Fig 6-2), for the three locations a test with no-wind condition and another with wind (2 m/s) have been performed, all the tests have 35-deg inclination.

We should notice that we have for the ignition C one propagation direction only to the up ridge and for the ignition B also one propagation direction only to the down ridge.

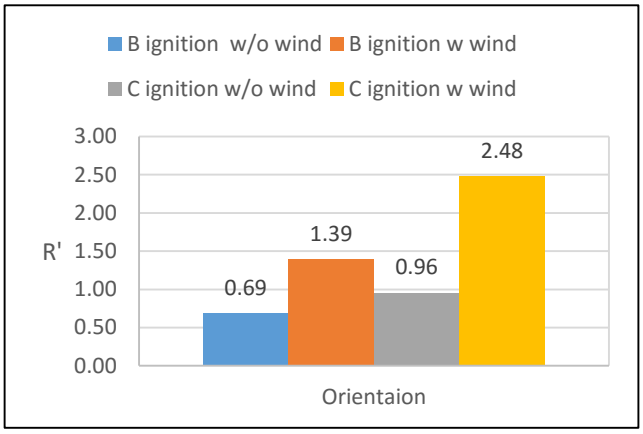

Fig 6-46 The average NDROS for the different ignition locations with and without wind condition on the leeward face

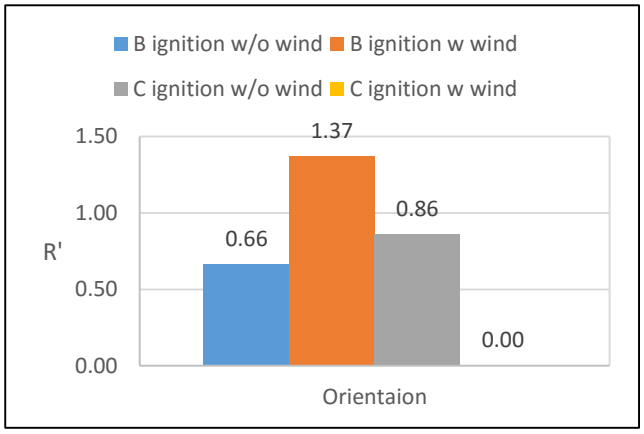

Fig 6-47 The average NDROS for the different ignition locations with and without wind condition on the windward face

On Fig 6-46 we can see the average NDROS for ignition C is higher than ignition B either with or without wind, from the difference between the two ROS without wind we can see the effect of the ridge slope where the fire have higher ROS on the up ridge propagation, with wind the difference is due to two effects, the ridge slope effect and the lateral spread effect where it happened in the case of ignition C (see Fig 6-51) but only after the fire front pass the middle of the ridgeline.

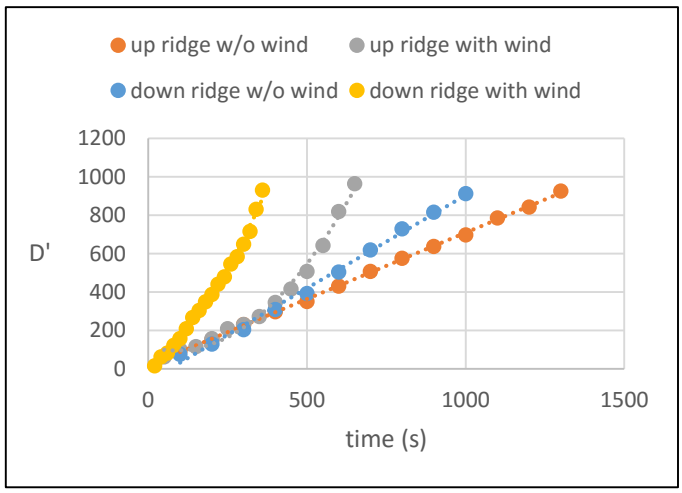

Fig 6-48 The D'-T plot for different ignition locations with wind and without wind as dynamic spread

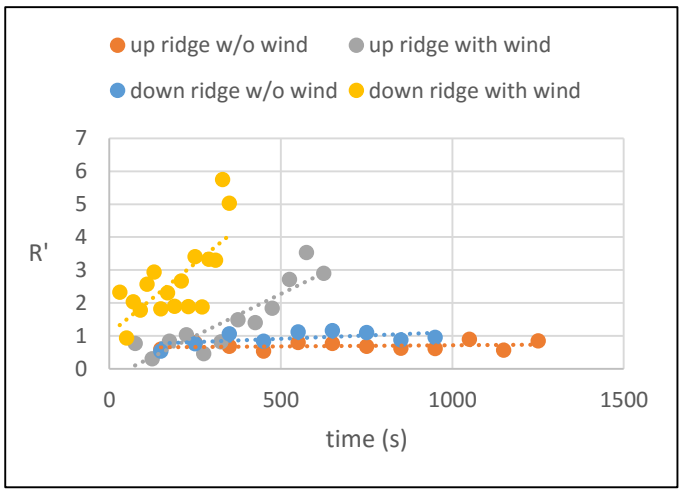

Fig 6-49 The R'-T plot for different ignition locations with wind and without wind as dynamic ROS

On the windward face (Fig 6-47) we can find the average NDROS are quite similar to the spreading ROS's on the leeward face but there is a slight decrease in all of them, for the case where the ignition was on C with wind the fire distinguished on the windward face once the fire reaches the ridgeline and it's a very small distance, then the fire starts to propagate on the leeward face.

From the D-t and R-t plots on Fig 6-48 and Fig 6-49 we can find the difference between a fire propagating up ridge and another propagating down ridge in a dynamic form, in a case of no-wind we can find the pure effect of the ridgeline slope where the starting of the propagation is similar but then the down ridge ignition where the fire is propagating up ridge is start to have higher ROS relatively. With the wind as we showed before on the average ROS that there is also the difference of the lateral spread where it will happen on the up ridge propagation but not on the down ridge propagation, we can see that on the R-t plot the last values of the R' is relatively very high when the lateral spread happened.

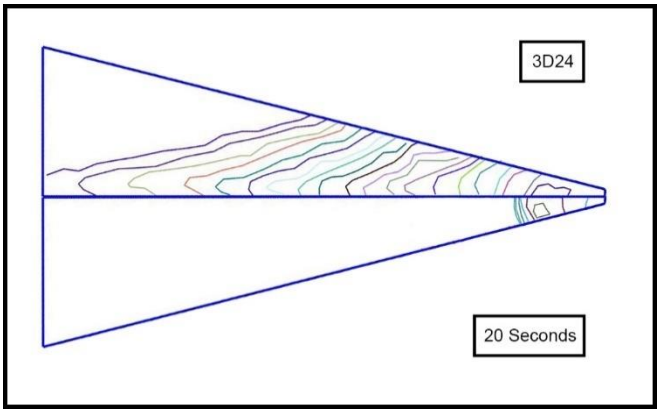

Fig 6-51 Fire front propagation map for test 3D24 (35-deg, C , 2m/s)

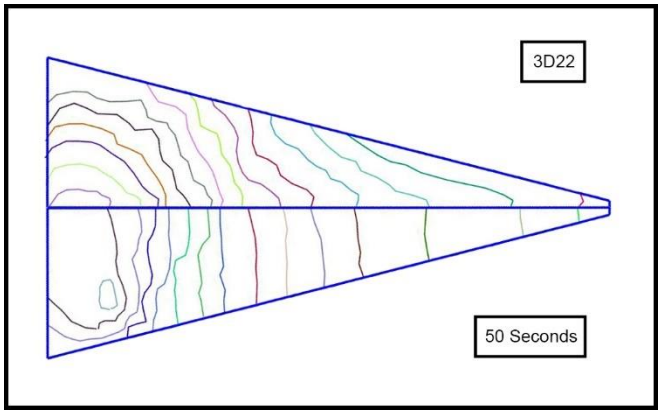

Fig 6-50 Fire front propagation map for test 3D22 (35-deg, B , 2m/s)

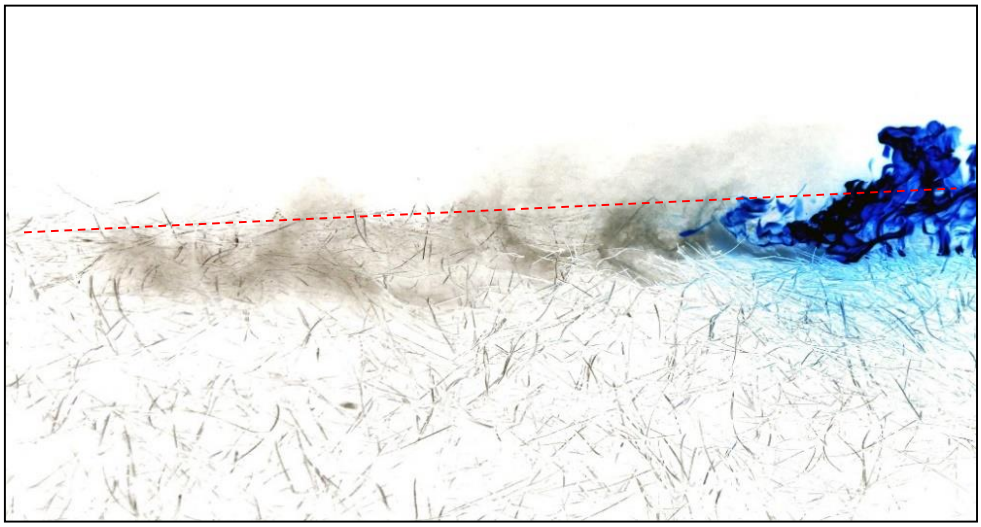

Fig 6-52 Processed image showing the smoke movement to up ridge direction (in gray), the fire is in blue and the red line is the ridgeline, image taken during test 3D28

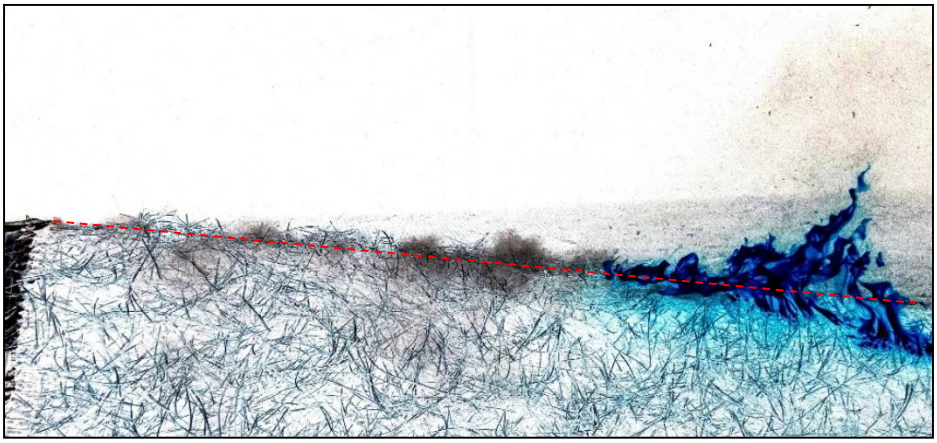

Fig 6-53 Processed image showing the smoke movement to up ridge direction (in gray), the fire is in blue and the red line is the ridgeline, image taken during test 3D6

On Fig 6-52 and Fig 6-53 we can see processed images from different tests showing the movement of the smoke on a direction parallel to the ridgeline, indeed, this movement was noticed almost on all the performed tests and the smoke wasn't moving just in a straight line to the up ridge but it was moving forming a vortex and translating in the up ridge direction, this vortex is the reason behind the extreme behavior (Fire Channelling) where the fire spreads laterally. The images showing also a wider smoke plum for the 20-deg inclination and thinner for the 45-deg inclination.

An important two observations also about the lateral spread, the first one is the shape of the fire front where it takes a form of an arrow with a sharp angle, we can see this shape on Fig 6-12 and on all the propagation maps like in Fig 6-35 and Fig 6-30. The second observation is that the formed arrow shapes or peaks if we connected them from their tips by a line we will find this line is parallel to the ridgeline and away from with some distance, in fact by studying this distance and how it changes with different inclinations and velocities we found the results in Fig 6-54

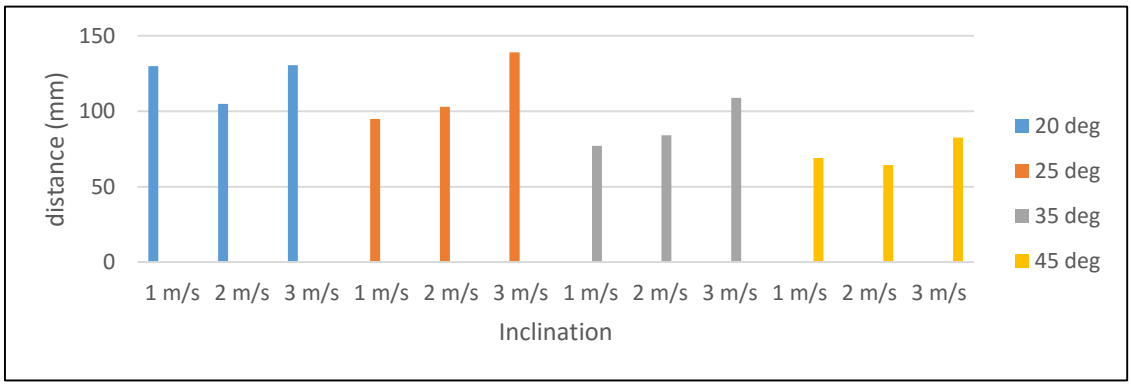

Fig 6-54 the distance between the fire front peaks on the lateral spread and the ridgeline for different inclinations and velocities

We can see that the distance generally decreases with increasing the inclination and increasing with increasing the velocity for the same inclination, however, we interpret these distances as they are presenting the radius of the horizontal vortex since the fire is getting dragged to its core forming the mentioned peaks before.

7. Conclusion

The conclusion is divided into two main sections, one concluding the study of the flow around the 3D ridge, and another concluding the fire behavior over the ridge.

7.1. The Flow Around the Ridge

As a conclusion of the flow on the windward face, it was found that the flow accelerates as it's heading in the up slope direction approaching the ridgeline and with changing the inclination of the ridge the flow has lower velocities for higher inclinations, as overall for the same inclination and wind velocity it was found that the flow has the heist velocity at the down ridge and get decreased gradually as we are heading up ridge along the ridgeline.

On the leeward face we have a conical vortex, this vortex changes its diameter with the inclination where it has wider diameter with the high inclinations and get smaller with the lower inclination until we reach 10-degrees where it will disappear, this vortex is also effected by changing the orientation of the ridge where on the positive direction orientations it starts to disappear as we increase the orientation and another vortex is generated from the top corner of the ridge, on the negative direction there is a slight increase in its diameter as we increase the orientation.

7.1.1. The Sliding Wind

An important behavior was noticed on the windward flow and it was called the sliding wind, this behavior is happening on the lower half of the ridge where the total component of the velocity changes its direction instead of being perpendicular to the ridgeline it becomes more parallel to it forming a flow draft toward the down ridge direction, this flow draft is more strong on the higher inclinations and it starts to disappear as we lower the inclination until we reach 25-deg where it disappears, with changing the orientations it gets stronger on the negative orientations and almost disappear with the positive orientations. The draft is happening because the flow takes a path where it will dissipate less energy and that's why it was called the sliding wind since it slides on the face until it gets caught by free stream near the tip of the ridge.

7.1.2. The Horizontal Vortex

Another important behavior was notices on the leeward face in the area just after the ridgeline where there is a flow draft directed parallel to the ridgeline, if we splitted the ridgeline to two half, it was found that the direction of this draft is toward up ridge on the upper half of the ridgeline where on the lower half it's directed toward down ridge (the other direction), this flow was interpreted as a horizontal vortex happening directly after the ridge pushing the flow to the edges of the ridge from both sides, the generation of this vortex is referred to a flow coming from the windward side and gets trapped from up by the high velocity flow passing over the ridgeline and from the sides by the conical vortex structure or the circulation zone generally and the face of the ridge itself, Fig 7-1 showing an illustration of the stream lines. However, this suggested flow stream lines topography is not very correct and there must be some secondary flows to make it possible.

On the following we have addressed some remarks about this vortex existence and its characteristics concluded from the whole work:

- On the wind tunnel tests, a line of wool strings was attached just after the ridgeline and it showed clearly the existence of the flow draft in both directions and with almost all the tested configuration. The strings also showed sometimes that the draft is not very strong in the middle of the ridgeline and gets stronger as we approach the edges.
- On the CFD simulation the area of the vortex had the lowest pressure on the leeward face and also showed a line parallel to the ridgeline with almost zero magnitude vorticity along it which is the core vortex and relatively high vorticity around it. However, a simulation and a wind tunnel test made by Ferreira AD (1995) on a 2D ridge where the horizontal vortex also exists, the results showed a drop in the pressure after the flow pass the ridgeline in both the simulation and wind tunnel tests.
- During the fire tests a plume of smoke was noticed on this area in almost all the tests moving in a vortex movement and was translating parallel to the ridgeline in the up ridge direction. Also this plume was wider for the low inclinations (20-deg) and thinner for the high inclinations (45-deg).
- This horizontal vortex is causing a lateral fir spread in the up ridge direction where the fire front is pulled by the low pressure at the vortex core and takes a shape of a sharp angle arrow directed toward the core, by connecting this arrows from its tip on each time step on the fire front propagation map, we will find that it's forming a line parallel to the ridgeline and away from it by some distance which is the vortex core, by studying this distance from the ridgeline it was found that it gets increased by decreasing the inclination and for the same inclination it gets increased also by increasing the wind velocity. An important observation also about this, that the fire front doesn't start to spear laterally until it reaches this core vortex and then the lateral spread will start to take place.
- Since the line connecting the peaks was interpreted as it's the core vortex so it means that the vortex changes its diameter with the inclination, this change is referred to the changes on the gap area between the face of the ridge and the conical vortex, the area increases with increasing the inclination, we saw on the CFD simulation that the conical vortex diameter or the circulation zone gets less wider with decreasing the inclination and leaving a bigger gap where the horizontal vortex is formed.
- In the fire tests, the lateral spread which is a direct result of this vortex didn't happen on the down ridge direction, this is happened because the horizontal vortex is interrupted by the free stream near the tip of the ridge, also before the tip we have the conical vortex generation near the ridgeline which effecting the horizontal vertex also, that's why the vortex in that direction is not strong enough to pull the fire but however on the past studies on the 2D ridge the lateral spread and the horizontal vortex do exit on that direction.

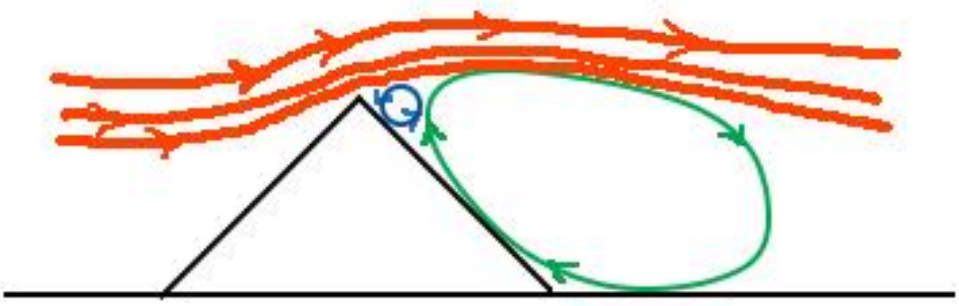

Fig 7-1 An illustration for the suggested flow structures on the windward of the ridge, the free stream is in red, the conical vortex is in green and the horizontal vortex is in blue

7.2. The Fire Behavior

From the rate of spread (ROS) analysis of the fire spread along different direction over the ridge we can find two extreme fire behavior happening, one is the lateral spread on the leeward face in the up ridge direction and the other is a lateral spread also on the windward face but in the down ridge direction. The fire behavior along the other directions is considered to be a normal behavior as it has relatively low rate of spread (0 to 3 times the basic rate of spread (Ro) in average). Since the fire extreme behaviors are the main interest on this study so it's concluded on the following:

7.2.1. Leeward Lateral Spread (fire channelling)

The lateral spread on the leeward face of the ridge is a direct result of the horizontal vortex happening just after the ridgeline, in fact, this extreme behavior was one of the main motivations to make this study as a continuation of the experimental studies made on the 2D ridge by Raposo et al. (2015), in the 2D ridge the lateral spread was found happening in both direction, right and left, with balanced characteristics, however, on the 3D ridge the lateral spread was found happening on the up ridge direction only and it didn't happen in down ridge since the horizontal vortex is not strong enough to pull the fire on that direction with a high ROS. By studying the inclination (45, 35, 25, 20 and degrees) and the wind velocity (0, 1, 2 and 3 m/s) parameters effects on the lateral spread it was found that the lateral ROS is increasing with increasing the inclination and in an overall the ROS also increases with increasing the wind velocity for the same inclination, for the 10-deg inclination the lateral spread didn't happen since there is no any complex flow happening. In a study of the orientation parameter (-20, -10, 0, 10, 20) it was found that the ROS had the highest values with the most negative orientation tested (-20-deg) and decreasing gradually in the positive direction for the same inclination (35-deg) and wind

velocity (2 m/s). In a study of the ignition point location it was found that the lateral spread is happening as expected only if the fire is propagating in the up ridge direction and it happened after the fire front reaches the middle of the ridgeline, for the other case where the fire is propagating in the down ridge direction it was very slow without any extreme behaviors.

In a dynamic analysis of the ROS for each time step in the lateral spread direction it was found that from the distance versus the time plot that the values are following a second order behavior and increasing its rate with the increase in the inclination or the velocity.

7.2.2. Windward Lateral Spread

This extreme behavior was found happening on the windward face with the high inclinations (35 and 45 degrees) where the fire propagates in the down ridge direction parallel to the ridgeline with high ROS's, this propagation is happening with the entire fire front on the face not like the lateral spread on the leeward face where only a portion of the fire front near the ridgeline is propagating, however, this spread is a direct result of the sliding wind behavior that was explained before, with changing the orientation it was found that on the negative direction the ROS is increasing as we increase the orientation and on the positive direction the behavior disappears and even with increasing the orientation more than 10-deg, the ROS will start to increase a little in the other direction.

Finally, the extremist tested configurations ware two, one is the 45-deg inclination and the other is the 35-deg with -20-deg orientation, in these two configurations the both extreme behaviors happened on the leeward and windward faces with ROS's about 10 times the basic ROS (Ro) at some time steps.

References

J. R. Raposo, S. Cabiddu, D. X. Viegas, M. Salis, J. Sharples (2015) Experimental analysis of fire spread across a two-dimensional ridge under wind conditions International Journal of Wildland Fire 2015, 24, 1008–1022. doi:10.1071/WF14150

Viegas DX, Neto LP (1991) Wall shear-stress as a parameter to correlate the rate of spread of a wind-induced forest fire. International Journal of Wildland Fire 1, 177–188. doi: 10.1071/WF9910177

Viegas DX (2006) Parametric study of an eruptive fire behavior model. International Journal of Wildland Fire 15, 169–177. doi:10.1071/WF05050

McRae RHD (2004) Breath of the dragon – observations of the January 2003 ACT Bushfires. In 'Proceedings of the Conference Bushfire 2004: Earth, Wind and Fire – Fusing the Elements', May 2004, Adelaide. (CD-ROM) (South Australian Department of Environment and Heritage: Adelaide, SA)

Simpson C, Sharples J, Evans J, McCabeM (2013) Large-eddy simulation of atypical wildland fire spread on leeward slopes. International Journal of Wildland Fire 22, 599–614. doi:10.1071/WF12072

Sharples J, McRae RHD, Wilkes SR (2012) Wind–terrain effects on the propagation of wildfires in rugged terrain: fire channelling. International Journal of Wildland Fire 21, 282–296. doi:10.1071/WF10055

Ferreira AD, Lopes AMG, Viegas DX, Sousa ACM (1995) Experimental and numerical simulation of flow around two-dimensional hills. Journal of Wind Engineering and Industrial Aerodynamics 54–55, 173–181. doi:10.1016/0167-6105(94)00040-K

Schlichting HT (1968) 'Boundary-layer theory.' 6th edn (McGraw-Hill,Inc.: London) Meroney RN (1990) Fluid dynamics of flow over hills and mountains: insights obtained through physical modeling. In 'AMS Monograph on Current Directions in Atmospheric Processes Over Complex Terrain', AMS Monograph Vol. 23, No. 45, June 1990, pp. 145–172.

H. Kawai*, G. Nishimura (1992) Characteristics of fluctuating suction and conical vortices on a flat roof in oblique flow, Department of Civil Engineering, Tokyo Denki University, Hatoyama, Saitama 350-03, Japan

Autodesk® CFD simulation software overview
http://www.autodesk.com/products/simulation/overview

Mathworks® MATLAB® calibration functions manual
http://www.mathworks.com/help/vision/ref/generatecheckerboardpoints.html

Appendix 1

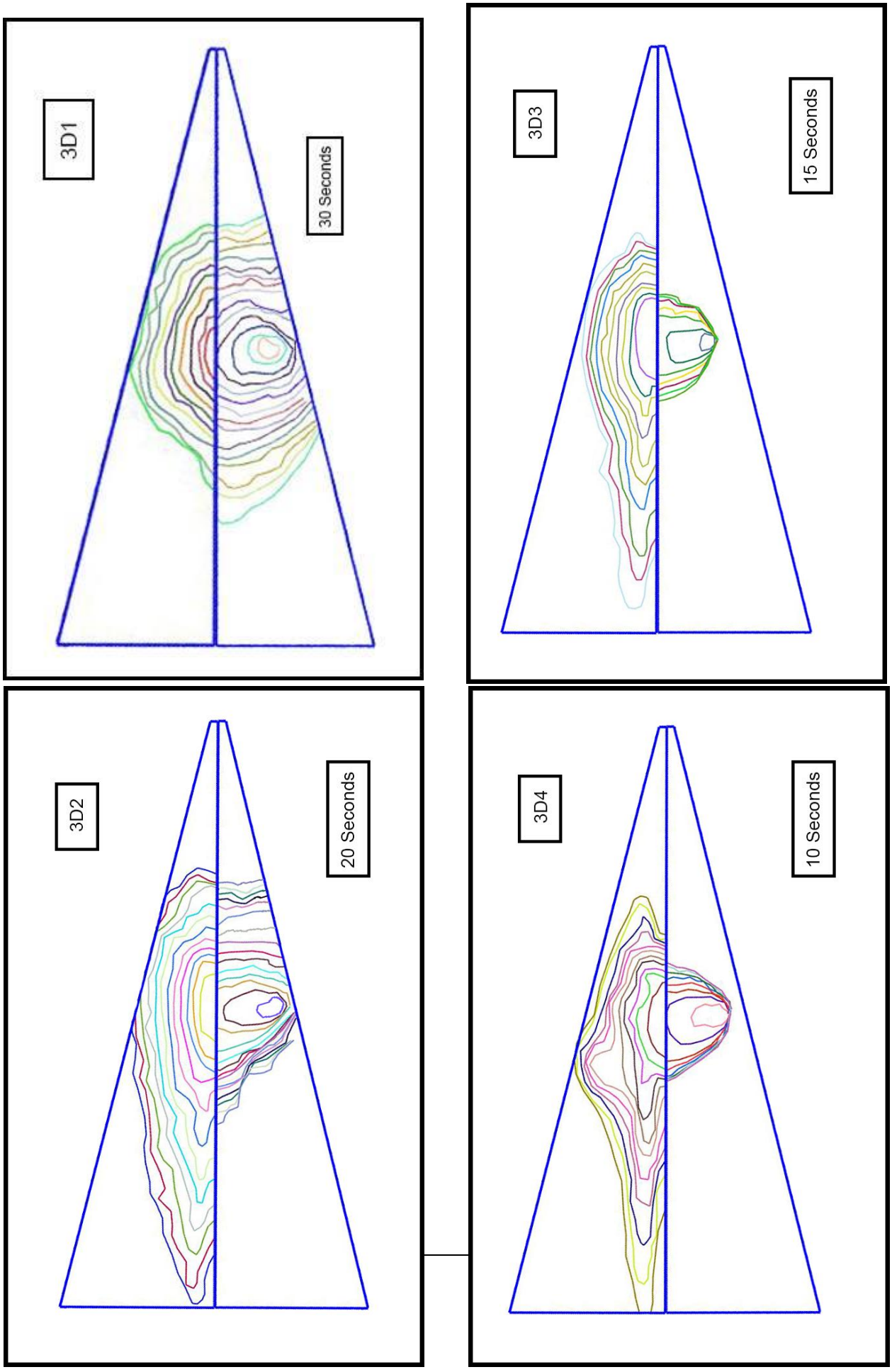

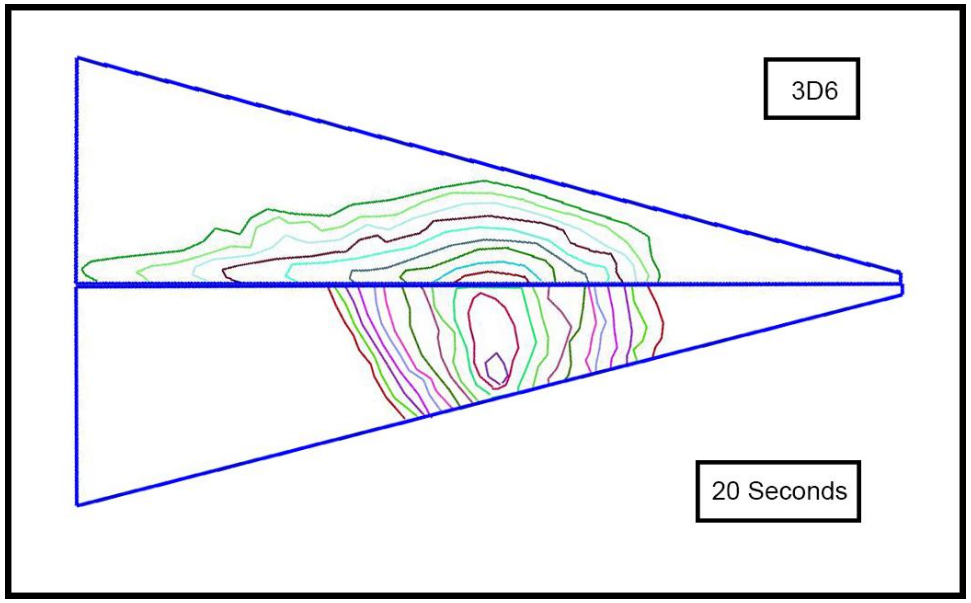
3D6
20 Seconds

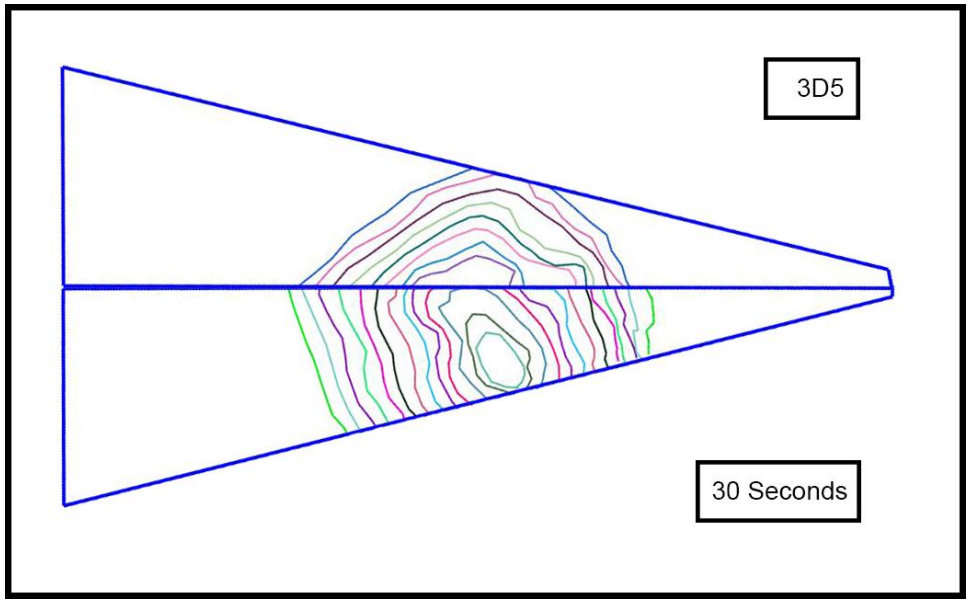
3D5
30 Seconds

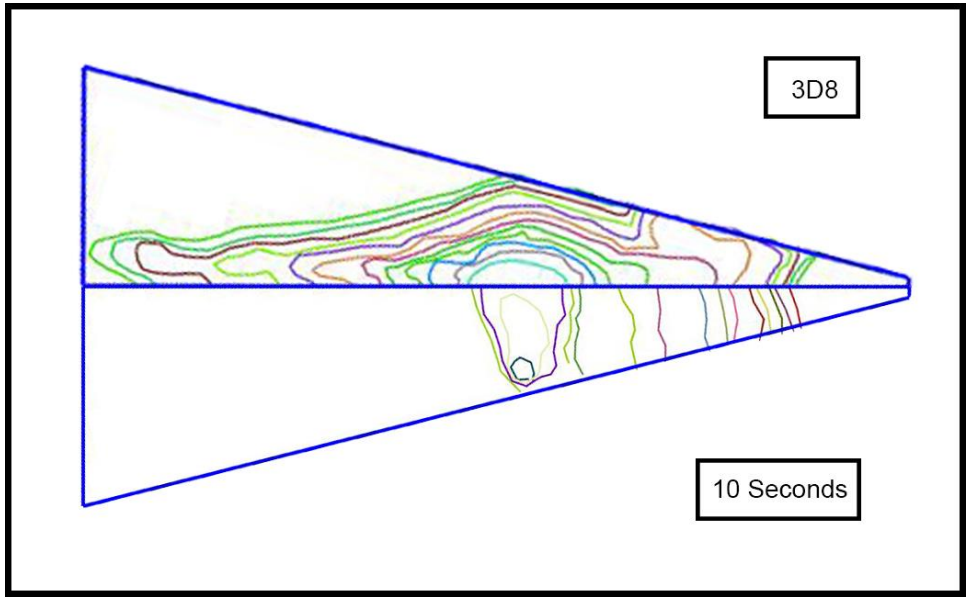
3D8
10 Seconds

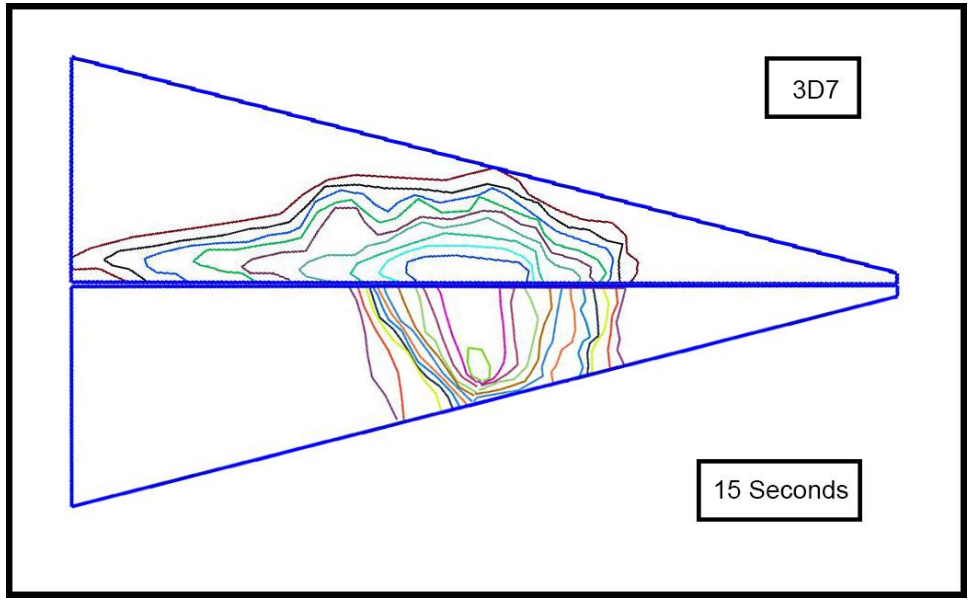
3D7
15 Seconds

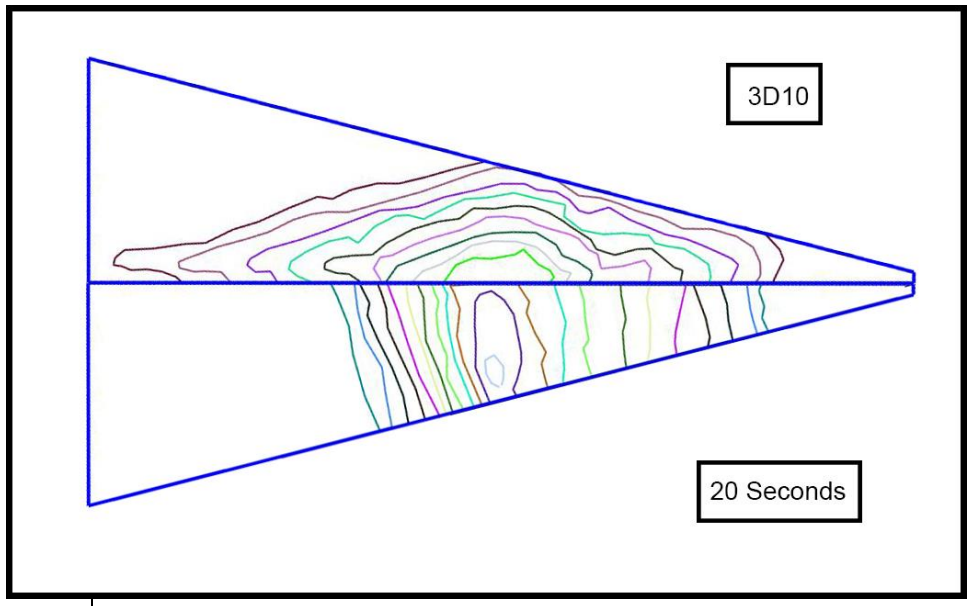
3D10
20 Seconds

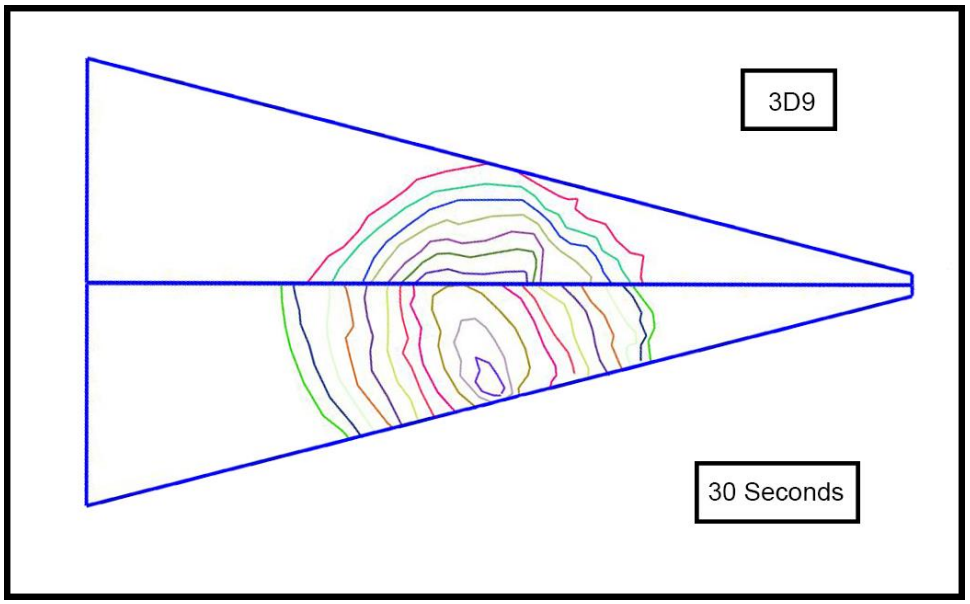
3D9
30 Seconds

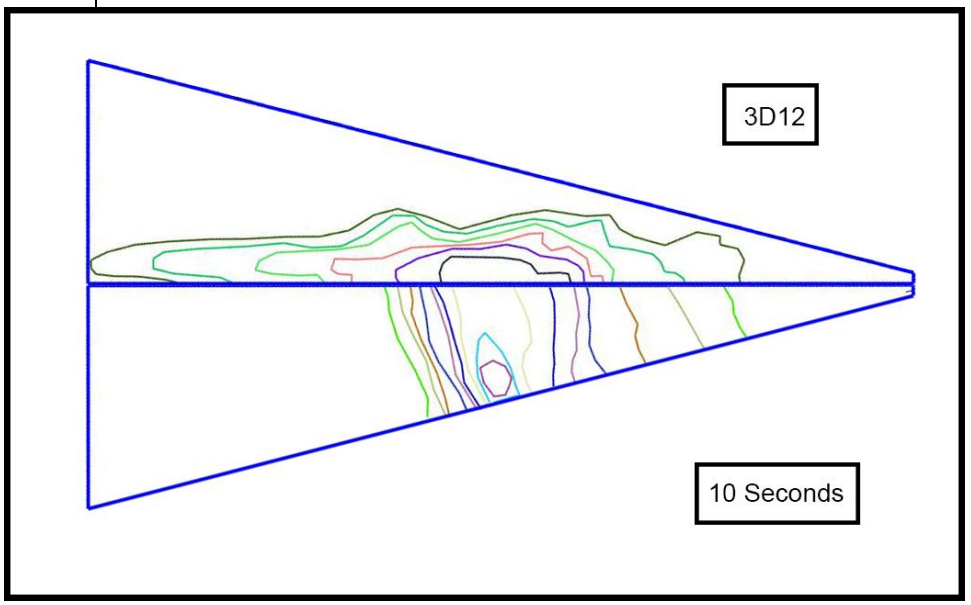
3D12
10 Seconds

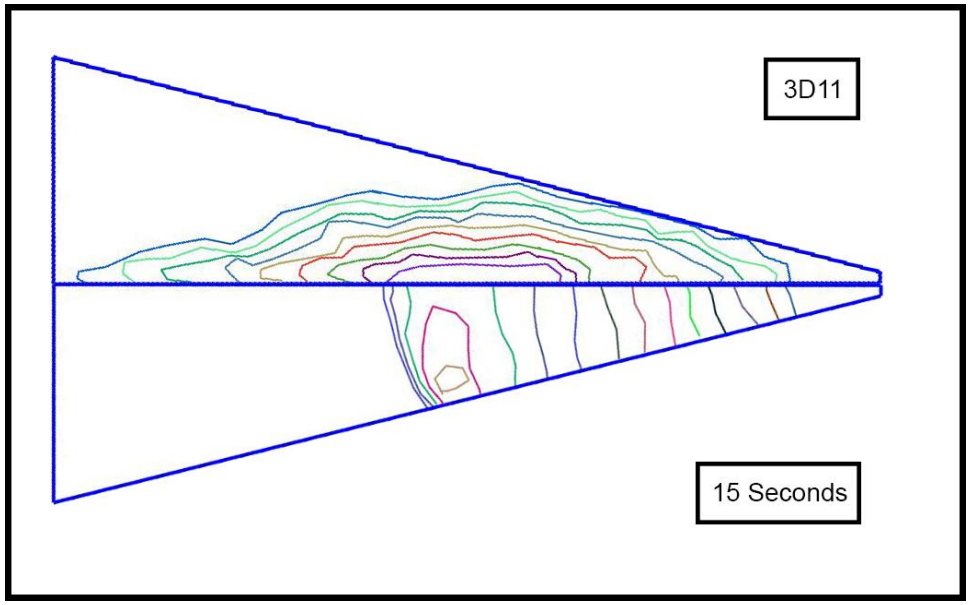
3D11
15 Seconds

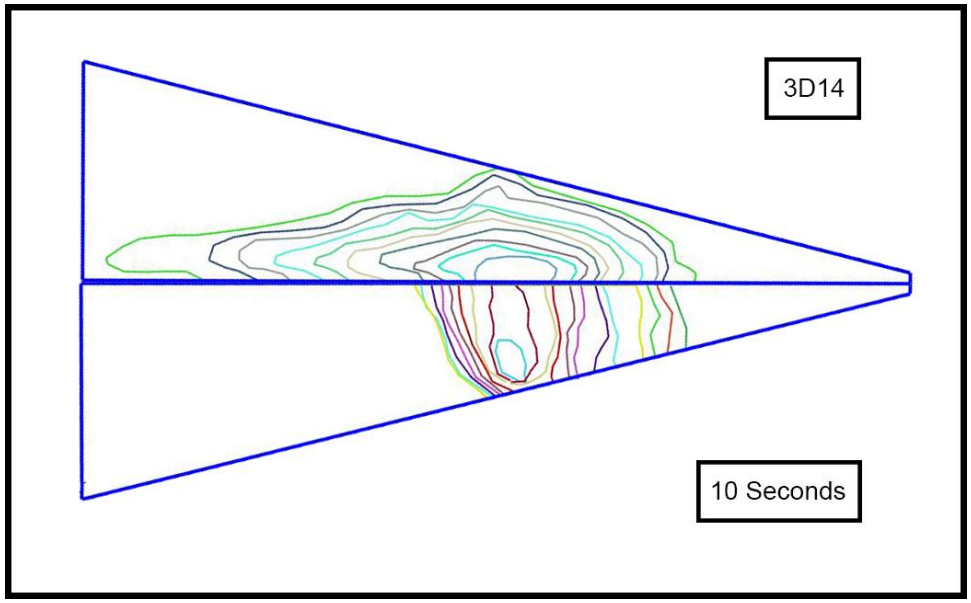
3D14
10 Seconds

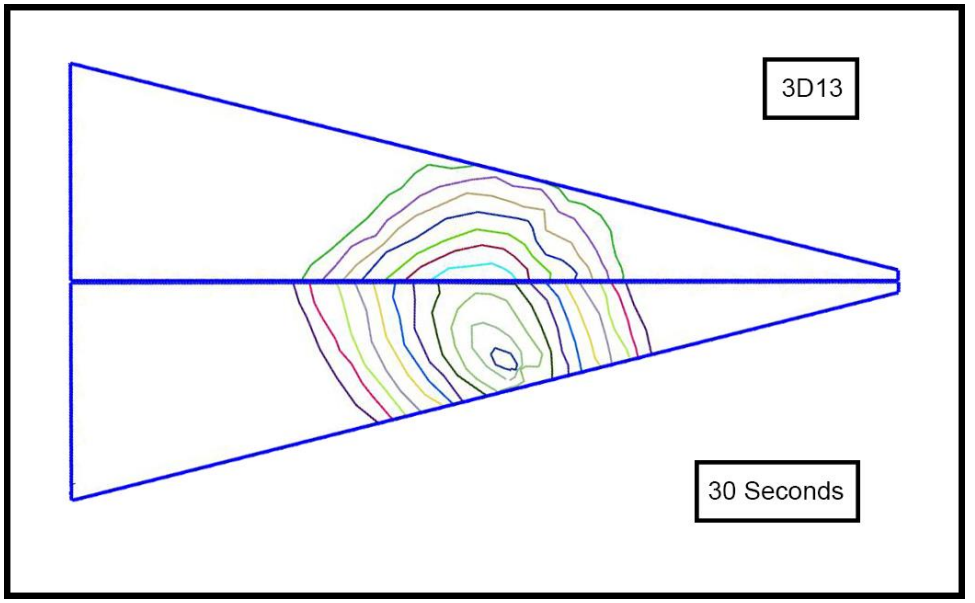
3D13
30 Seconds

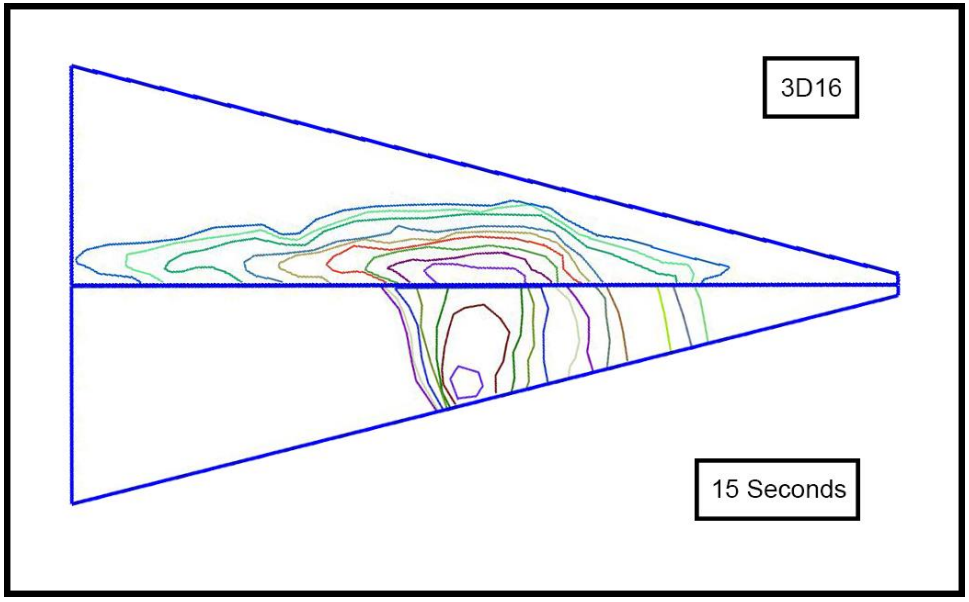
3D16
15 Seconds

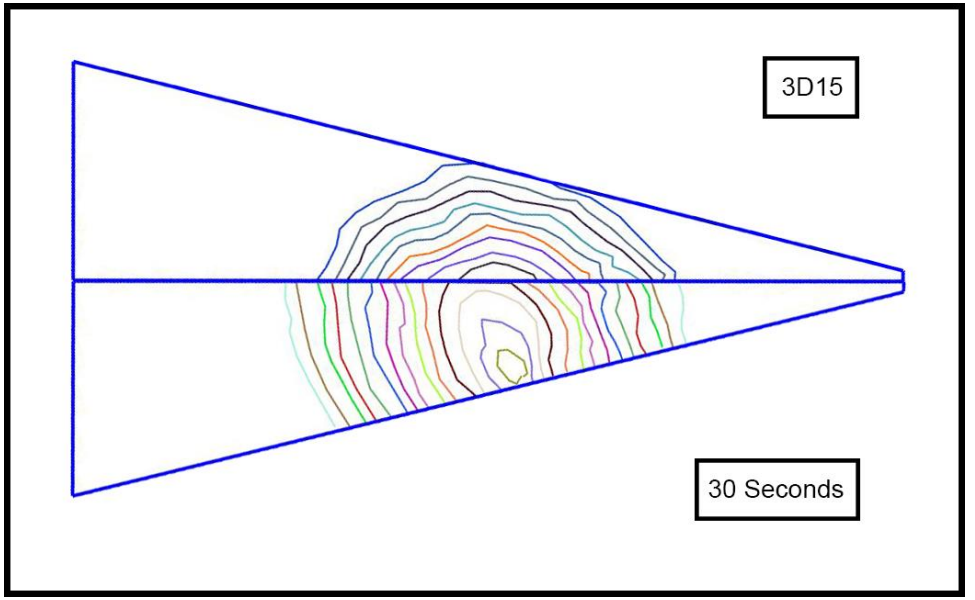
3D15
30 Seconds

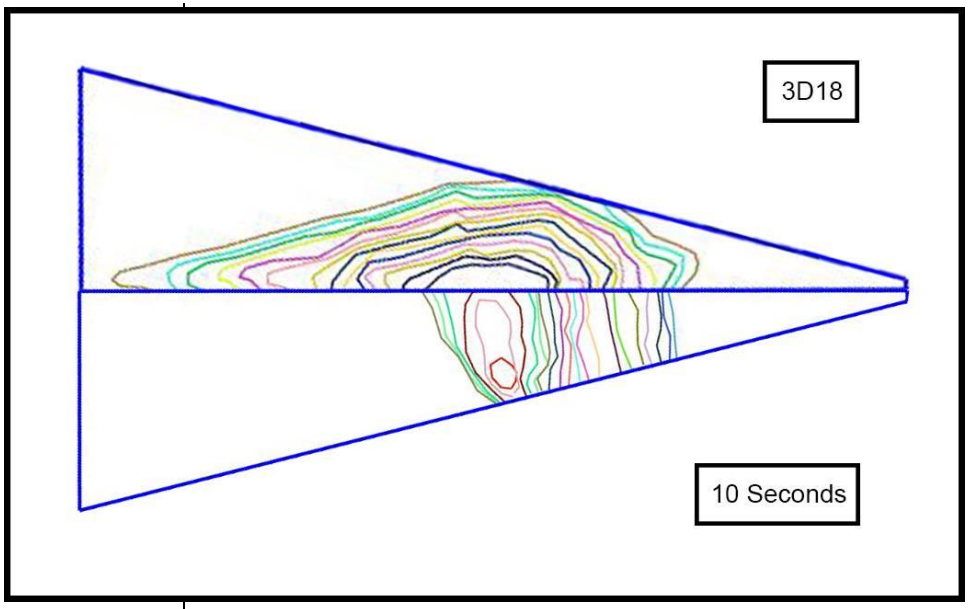
3D18
10 Seconds

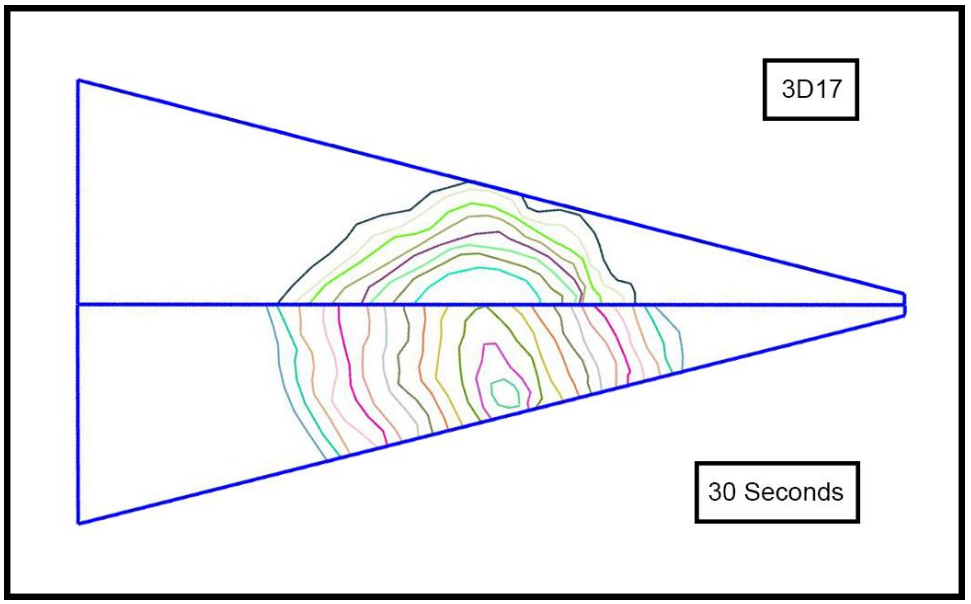
3D17
30 Seconds

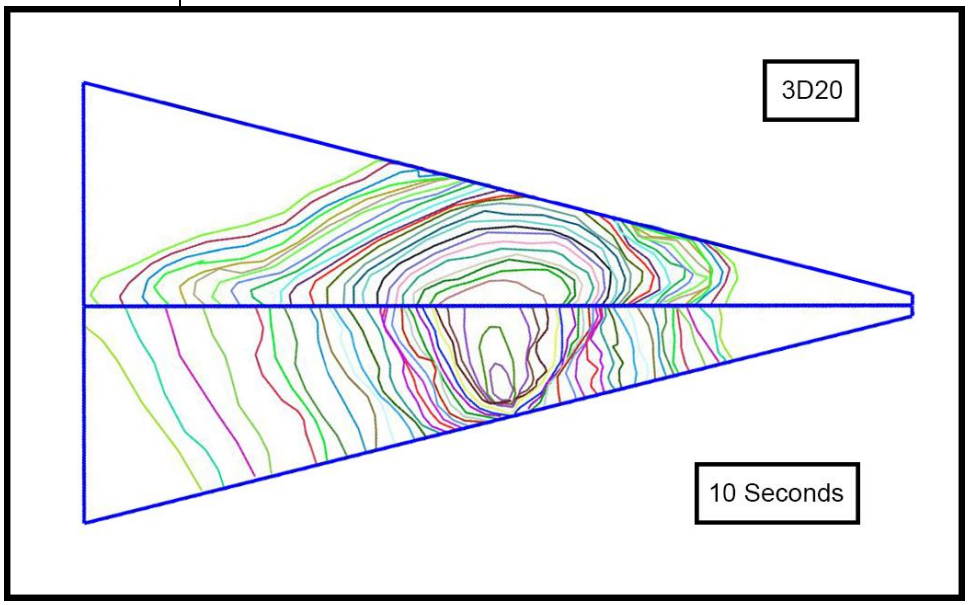
3D20
10 Seconds

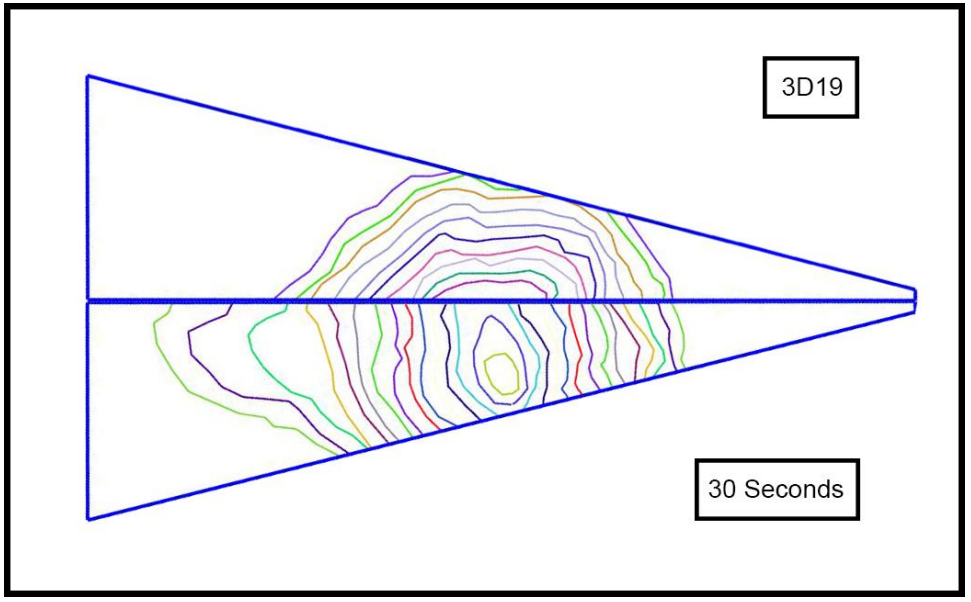
3D19
30 Seconds

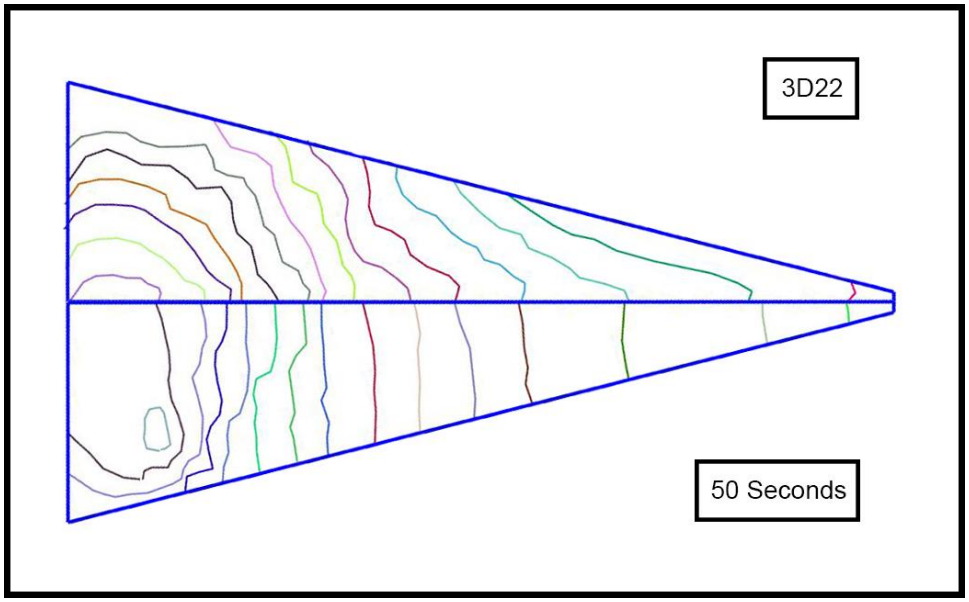
3D22
50 Seconds

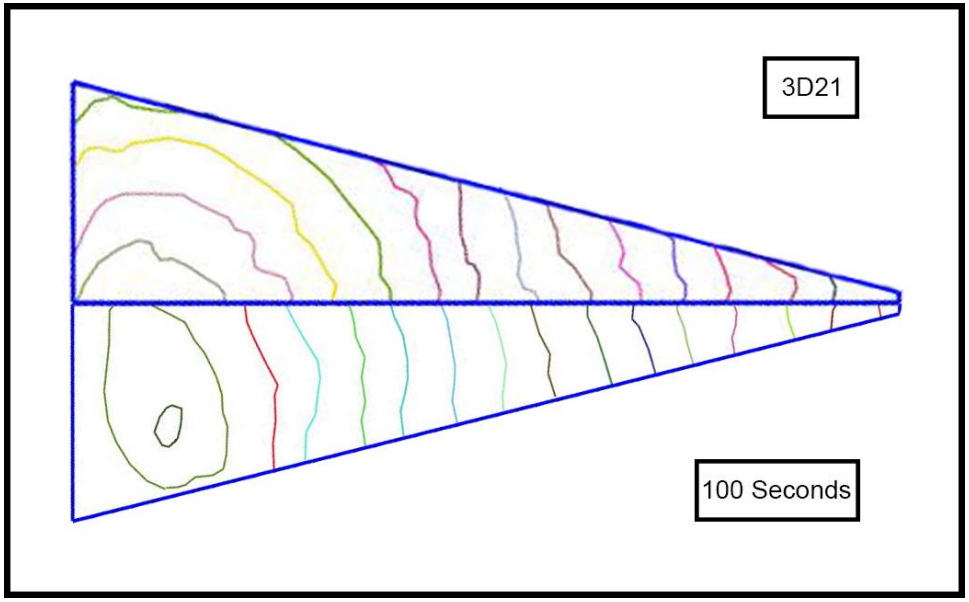
3D21
100 Seconds

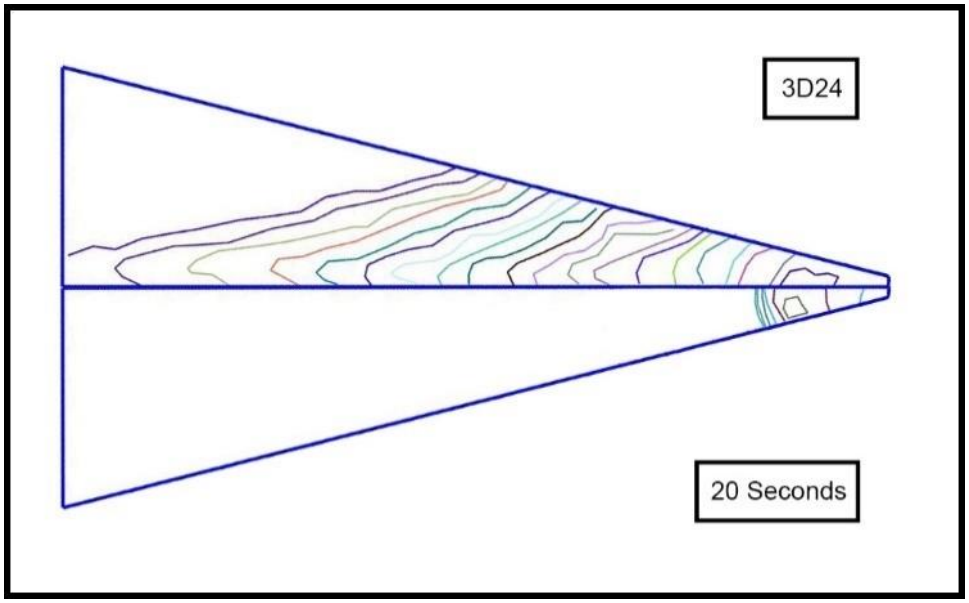
3D24
20 Seconds

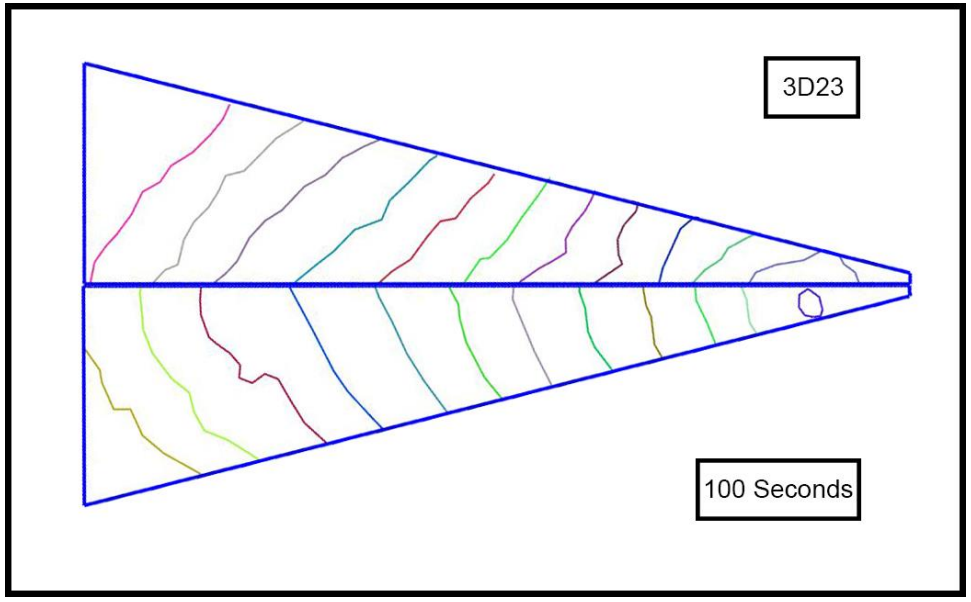
3D23
100 Seconds

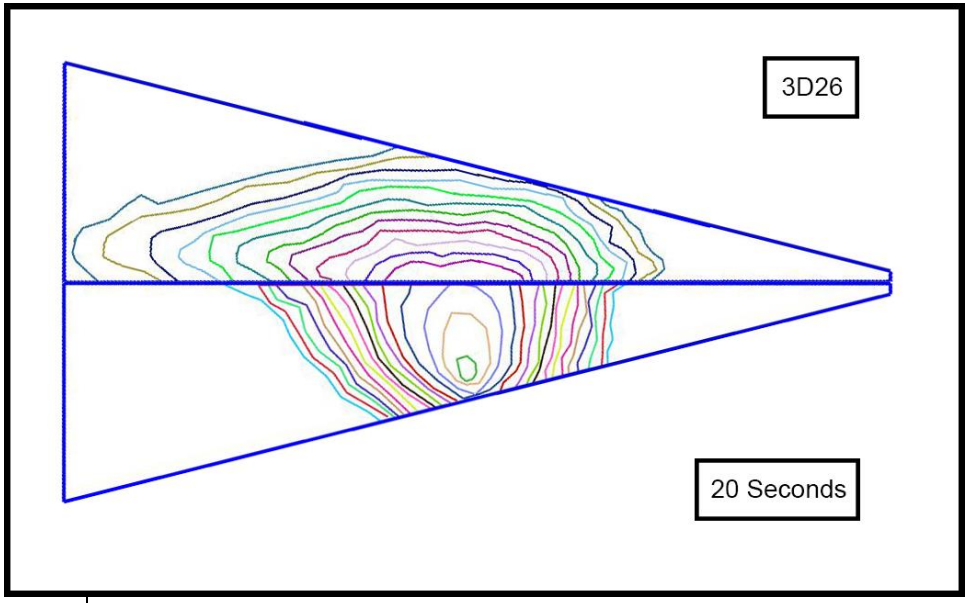
3D26
20 Seconds

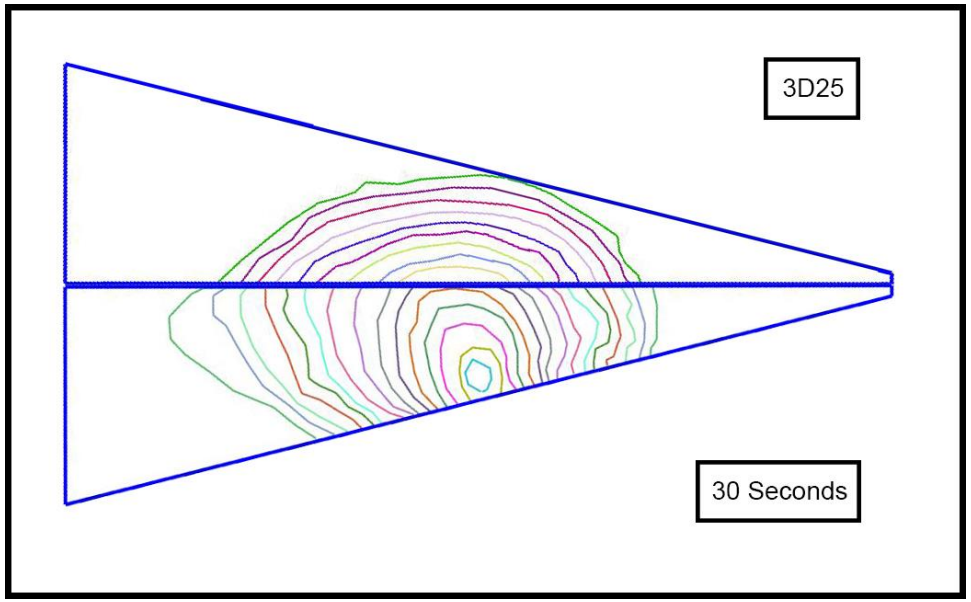
3D25
30 Seconds

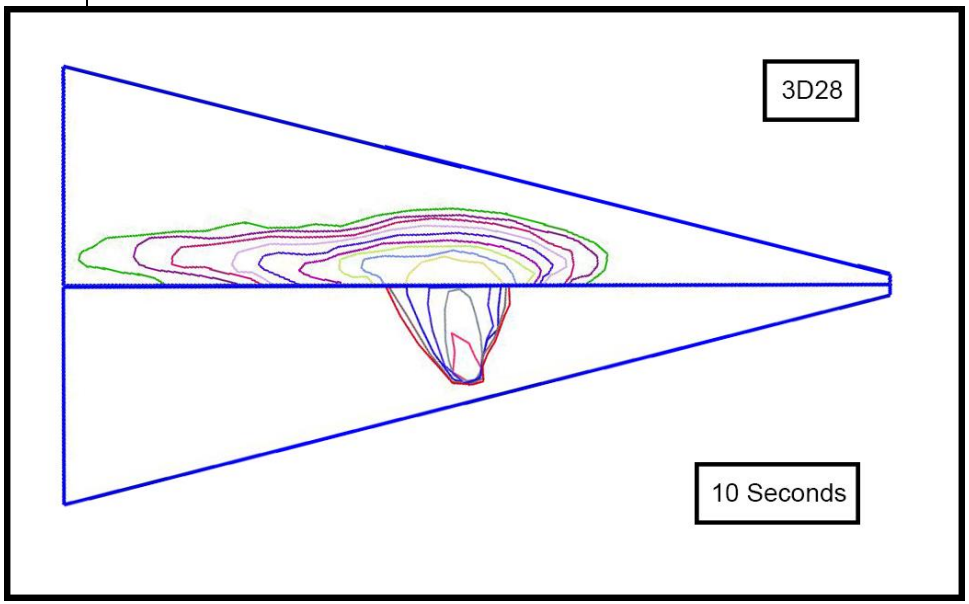
3D28
10 Seconds

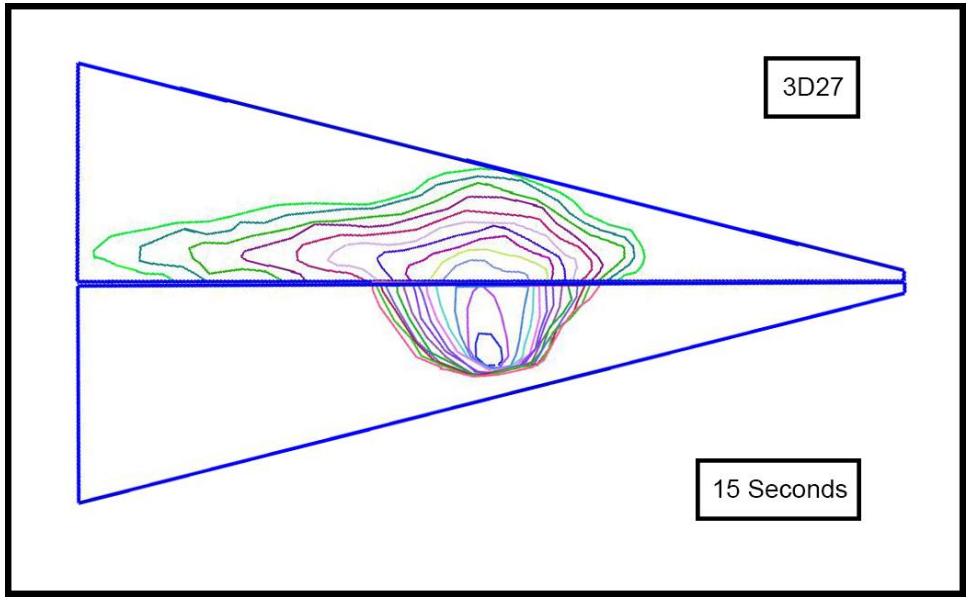
3D27
15 Seconds

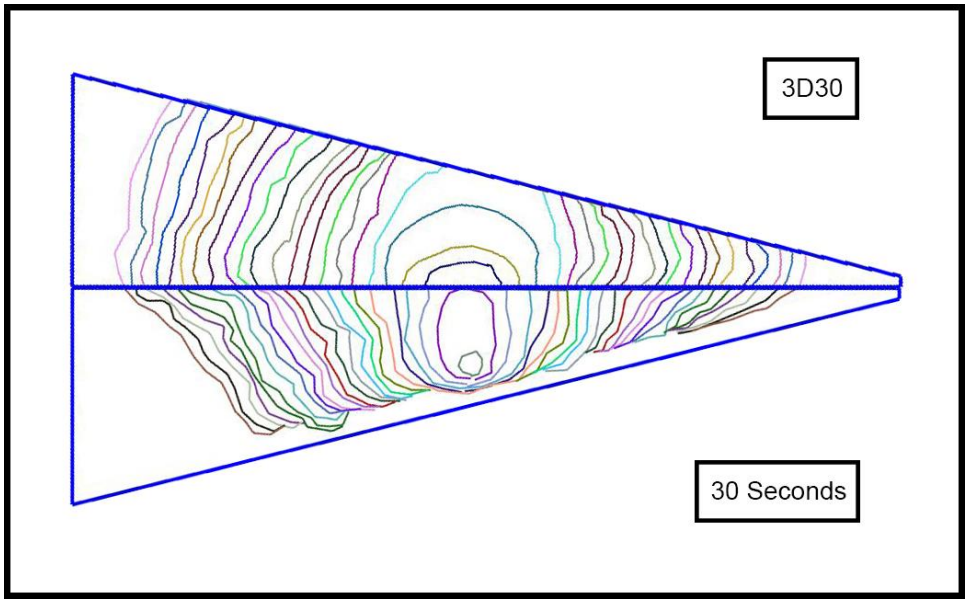
3D30
30 Seconds

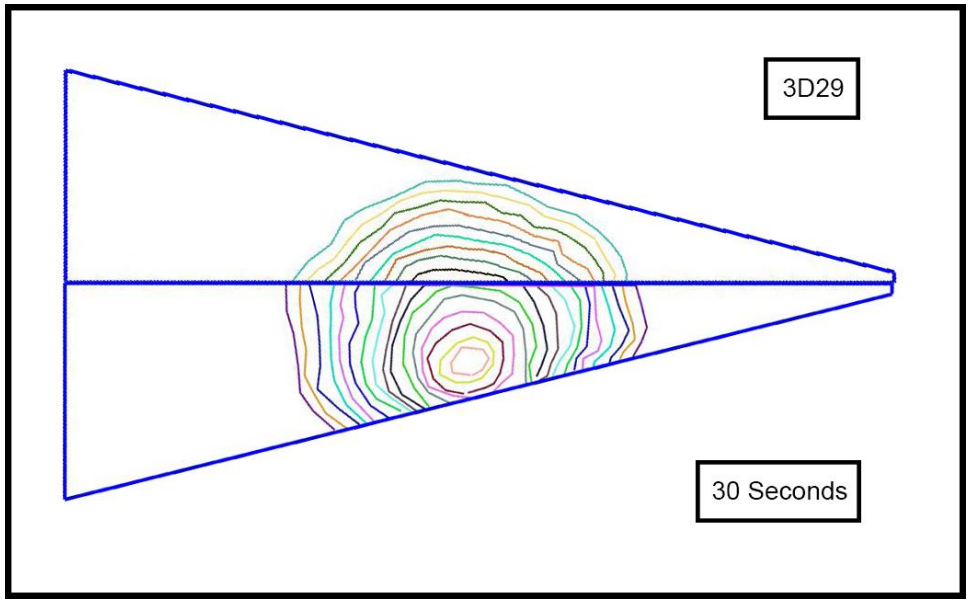
3D29
30 Seconds

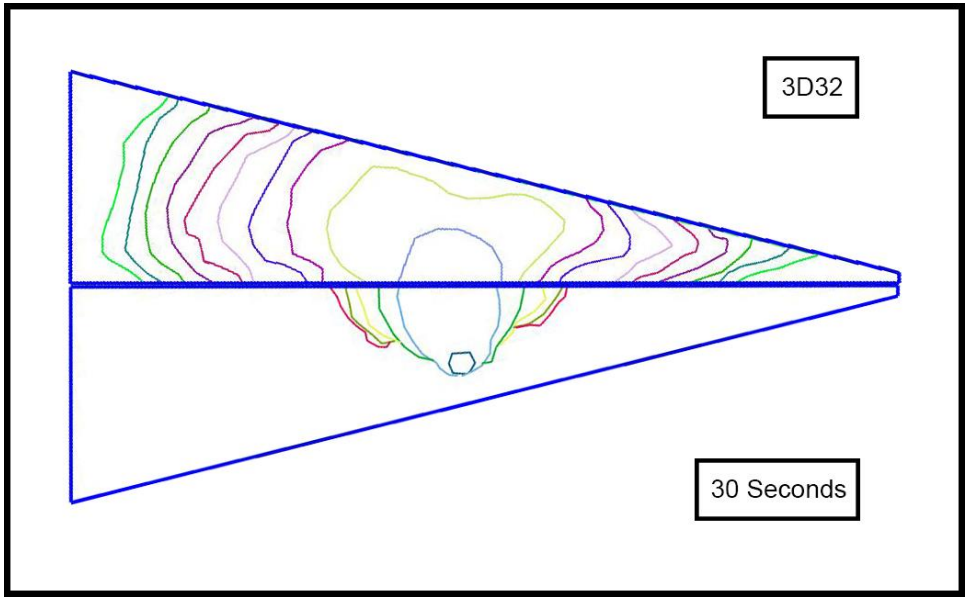
3D32
30 Seconds

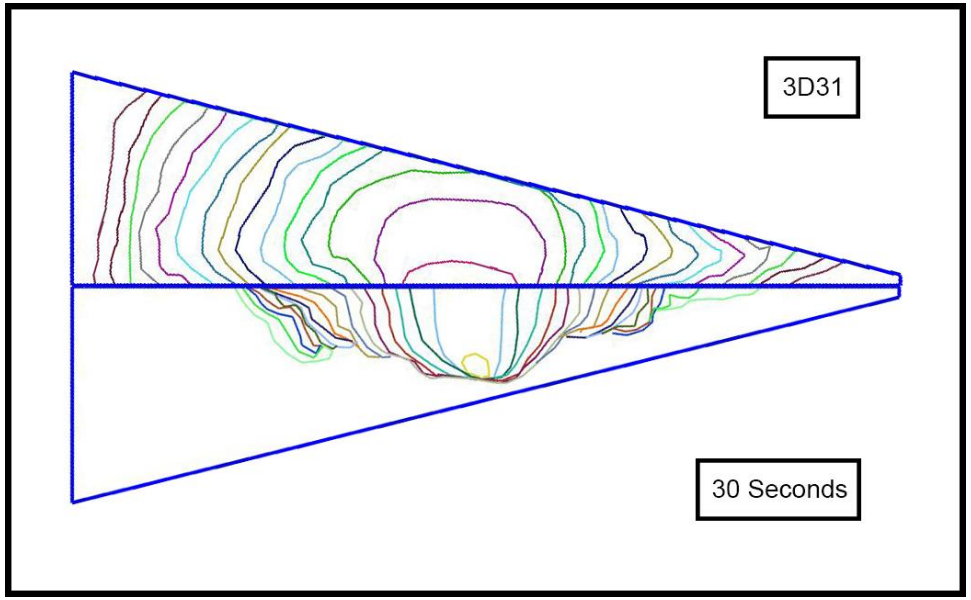
3D31
30 Seconds